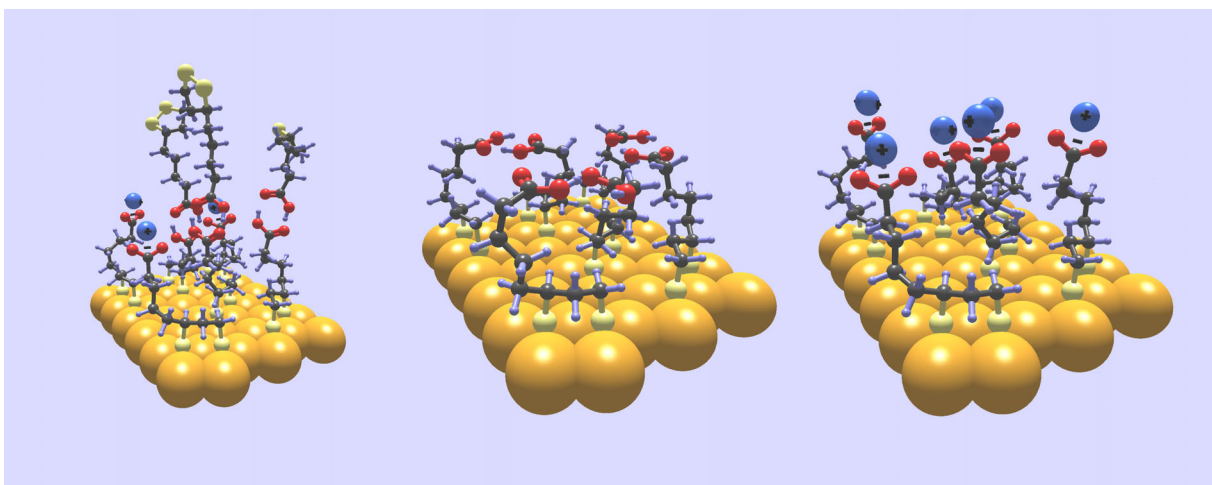


**Characterization of Functionalized Self-Assembled Monolayers
and Surface-Attached Interlocking Molecules
Using Near-Edge X-ray Absorption Fine Structure Spectroscopy**

Trevor M. Willey

April, 2004

Ph. D. Dissertation
University of California, Davis



University of California

This document was prepared as an account of work sponsored by an agency of the United States Government. Neither the United States Government nor the University of California nor any of their employees, makes any warranty, express or implied, or assumes any legal liability or responsibility for the accuracy, completeness, or usefulness of any information, apparatus, product, or process disclosed, or represents that its use would not infringe privately owned rights. Reference herein to any specific commercial product, process, or service by trade name, trademark, manufacturer, or otherwise, does not necessarily constitute or imply its endorsement, recommendation, or favoring by the United States Government or the University of California. The views and opinions of authors expressed herein do not necessarily state or reflect those of the United States Government or the University of California, and shall not be used for advertising or product endorsement purposes.

This work was performed, in part, under the auspices of the U.S. Department of Energy by University of California, Lawrence Livermore National Laboratory under Contract W-7405-Eng-48.

Characterization of Functionalized Self-Assembled Monolayers
and Surface-Attached Interlocking Molecules
Using Near-Edge X-ray Absorption Fine Structure Spectroscopy

by

TREVOR MICHAEL WILLEY
B.S. (Utah State University) 1997
M.S. (University of California, Davis) 1999

DISSERTATION

Submitted in partial satisfaction of the requirements for the degree of

DOCTOR OF PHILOSOPHY

in

PHYSICS

in the

OFFICE OF GRADUATE STUDIES

of the


UNIVERSITY OF CALIFORNIA

DAVIS

Approved:



Charles S. Fadley



Louis J. Terminello



Shirley Chiang

2004

Acknowledgements

I am thankful to Chuck Fadley, for being my advisor, for his help in pointing out the LLNL Student-Employee Graduate Research Fellowship (SEGRF) program and introducing me to Lou Terminello, and for his timely comments and suggestions. Both his love of science and attention to detail have given me a pattern to follow in my career.

Lou Terminello graciously accepted me into his group at Livermore, and allowed me to develop and grow as a scientist through my own successes and mistakes. I am grateful for his encouragement, ideas, and help in obtaining funding for a large portion of these projects. He has allowed me to directly interact with the scientific community by attending and presenting at many conferences, from Stanford to Sweden and many places in between.

Tony van Buuren in many ways has been my day-to-day supervisor with “hands-on” help, and I’m grateful to him for allowing me to barge into his office at any time with questions concerning our projects.

This thesis would not have been possible without Andy Vance, and his Laboratory Directed Research and Development (LDRD) funding to produce surface-attached interlocking molecules. He was the driving force behind many of the ideas for this work, synthesizing various “custom-designed” molecules. He was also patient in explaining elementary chemistry concepts to a physics graduate student. Brad Hart was also a lifesaver in stepping in with synthesis during final experiments.

Christoph Bostedt kept me sane through crazy hours of beam time at the ALS and SSRL, and has been a supportive friend and example during our tenure together at Livermore.

Others who must be mentioned for their support include Barry Cheung, Nicolas Franco, Rob Meulenberg, Julie Perkins, and Sergei Kruscheyev. Thanks to Art Nelson and Cheryl Evans of LLNL, as well as Mark Engelhard and Don Baer of the Environmental Molecular Science Laboratory, Pacific Northwest National Laboratory, for the acquisition of XPS spectra on their PHI Quantum 2000 instruments. Curtis Troxel of SSRL was an invaluable asset at beamline 8.2, especially in ensuring the Io grid was spotlessly clean with a fresh gold coating at each beam time. Jan Luning gave helpful advice to a synchrotron “newbie” with discussions on measuring the polarization of the beam and auger-yield detection schemes. I am appreciative to Christof Wöll (Univ. of Bochum, Germany) for discussion regarding carboxyl-terminated SAM formation.

There are many other mentors not directly involved with the research in this dissertation that have encouraged me and helped me in the pursuit of a career in physics from Steve Jackson at Viewmont High School, Bountiful, UT, to M. Riffe, J. R. Dennison, J. Marshall, C. Torre, F. Edwards, D. Lind, and others at Utah State University, as well as S. Chiang, C.Y. Fong, and R. Zieve and others at U. C. Davis.

My wife Lisa, my parents, in-laws, and children, and other family have been supportive, kind and loving in helping me through graduate school. I am thankful to them.

Lawrence Livermore National Laboratory provided funding support through a Student-Employee Graduate Research Fellowship.

This work was performed under the auspices of the U. S. Department of Energy by University of California Lawrence Livermore National Laboratory under Contract W-7405-ENG-48.

Work was conducted at the Stanford Synchrotron Radiation Laboratory, which is supported by the U.S. Department of Energy under contract DE-AC03-76SF00515.

The Advanced Light Source is supported by the U. S. Department of Energy under contract DE-AC03-76SF00098, Lawrence Berkeley National Laboratory.

Work was also conducted at the Environmental Molecular Sciences Laboratory, a national scientific user facility sponsored by the Department of Energy's Office of Biological and Environmental Research and located at Pacific Northwest National Laboratory, Richland WA.

UCRL-TH-203310

Dedication

I dedicate this work to my wife Lisa and my children, Adam and Anna, who have all come into my life since I embarked on the journey to a Ph.D. in physics. I am thankful for their love, patience, understanding, and support.

Abstract

Quantitative knowledge of the fundamental structure and substrate binding, as well as the direct measurement of conformational changes, are essential to the development of self-assembled monolayers (SAMs) and surface-attached interlocking molecules, catenanes and rotaxanes. These monolayers are vital to development of nano-mechanical, molecular electronic, and biological/chemical sensor applications. This dissertation investigates properties of functionalized SAMs in sulfur-gold based adsorbed molecular monolayers using quantitative spectroscopic techniques including near-edge x-ray absorption fine structure spectroscopy (NEXAFS) and x-ray photoelectron spectroscopy (XPS).

The stability of the gold-thiolate interface is addressed. A simple model SAM consisting of dodecanethiol adsorbed on Au(111) degrades significantly in less than 24 hours under ambient laboratory air. S 2p and O 1s XPS show the gold-bound thiolates oxidize to sulfinates and sulfonates. A reduction of organic material on the surface and a decrease in order are observed as the layer degrades.

The effect of the carboxyl vs. carboxylate functionalization on SAM structure is investigated. Carboxyl-terminated layers consisting of long alkyl-chain thiols vs. thioctic acid with short, sterically separated, alkyl groups are compared and contrasted. NEXAFS shows a conformational change, or chemical switchability, with carboxyl groups tilted over and carboxylate endgroups more upright.

Surface-attached loops and simple surface-attached rotaxanes are quantitatively characterized, and preparation conditions that lead to desired films are outlined. A

dithiol is often insufficient to form a molecular species bound at each end to the substrate, while a structurally related disulfide-containing polymer yields surface-attached loops. Similarly, spectroscopic techniques show the successful production of a simple, surface-attached rotaxane that requires a “molecular riveting” step to hold the mechanically attached crown ether rings in place until disulfides in the molecules adsorb onto the gold. Finally, by introducing an aldehyde into the crown ether portion of this well-characterized surface-attached rotaxane, conformational changes are directly measured when the aldehyde is reacted with aniline. These fundamental results have implications for the creation of nanoscale functional surfaces using molecular monolayers.

Table of Contents

Chapter 1: Introduction.....	1
Self-Assembled Monolayers.....	1
Interlocking Molecules – Catenanes and Rotaxanes.....	3
Surface-attached Interlocking Molecules.....	5
Issues to Be Addressed.....	7
Summary.....	9
References.....	11
 Chapter 2: Experimental Techniques	 14
Monolayer Formation.....	14
Near Edge X-ray Absorption Fine Structure (NEXAFS).....	16
NEXAFS Polarization Dependence and its Connection to Orientation.....	18
Measuring NEXAFS	31
X-ray Photoelectron Spectroscopy.....	39
Reflection-Absorption Fourier Transform Infrared Spectroscopy.....	43
Summary.....	44
References.....	46
 Chapter 3: Rapid Degradation of Alkanethiol-Based Self-Assembled	
Monolayers on Gold Under Ambient Laboratory Conditions.....	49
Introduction.....	49
Experimental.....	51
Results	53
Discussion.....	59
Conclusions.....	61
References.....	62
 Chapter 4: Chemically Transformable Configurations of	
Mercaptohexadecanoic Acid Self-Assembled Monolayers	
Adsorbed on Au(111).....	64
Abstract.....	64
Introduction.....	65
Experimental.....	66
Results and Discussion.....	68
Conclusions.....	78
References.....	81

Table of Contents (continued)

Chapter 5: Surface Structure and Chemical Switching of Thioctic Acid	
Adsorbed on Au(111) as Observed Using NEXAFS	84
Abstract	84
Introduction	86
Experimental	88
Results and Discussion	90
Conclusions	102
References	104
Chapter 6: XAS and XPS Characterization of Monolayers Derived	
from a Dithiol and Structurally Related Disulfide-containing	
Polyamides	108
Abstract	108
Introduction	109
Experimental Methods	111
Results and Discussion	112
Conclusions	116
References	120
Chapter 7: Characterization of a Simple Surface-attached Rotaxane	124
Introduction	124
Experimental Results and Discussion	126
Conclusions	134
References	136
Chapter 8: A Functionalized, Surface-attached Rotaxane	138
Introduction	138
Experimental	140
Experimental Results	142
Discussion	144
Conclusions	146
References	147
Chapter 9: Conclusions and Outlook	148
Conclusions	148
Outlook	151
Summary	154
References	155

List of Figures

1.1	Steps for SAM formation.....	2
1.2	Interlocking molecules: catenanes and rotaxanes	4
1.3	A model of a switching catenane	5
1.4	Surface-attached interlocking molecules.....	5
1.5	Surface-attached catenane.....	6
1.6	Surface-attached catenane.....	7
2.1	NEXAFS geometry for vector-like transition dipole moments	22
2.2	NEXAFS geometry for plane-like transition dipole moments	24
2.3	Regressions obtained from ratio method	30
2.4	Regressions obtained from difference method.....	30
2.5	Depiction of a bend-magnet beamline.....	32
2.6	Characterization of x-ray beam damage on a hexadecanethiol based SAM ...	33
2.7	HOPG π^* resonance for degree of linear polarization	35
2.8	Auger yield energy level diagram	37
2.9	Total electron yield energy level diagram	38
2.10	Inelastic mean free path of electrons.....	39
2.11	Oversimplified diagram of x-ray photoelectron spectroscopy.....	40
3.1	S 2p XPS for fresh/aged dodecanethiol adsorbed on Au(111)	54
3.2	S L-edge XAS for fresh/aged dodecanethiol adsorbed on Au(111)	56
3.3	O 1s XPS for fresh/aged dodecanethiol adsorbed on Au(111).....	57
3.4	C 1s XPS for fresh/aged dodecanethiol adsorbed on Au(111)	57
3.5	Carbon NEXAFS for the freshly prepared sample.....	58
3.6	Carbon NEXAFS for the air-exposed sample.....	59
4.1	Carbon K-edge TEY and AEY for mercaptohexadecanoic acid on Au(111)..	69
4.2	Oxygen K-edge AEY for mercaptohexadecanoic acid on Au(111).....	72
4.3	Carbon 1s for mercaptohexadecanoic acid on Au(111)	75
4.4	RA-FTIR of mercaptohexadecanoic acid on Au(111)	77
4.5	Unbound thiol % as a function of solution molecular concentration.....	78
4.6	Schematic representation of terminating endgroup orientation	79
5.1	Thioctic acid.....	87
5.2	C NEXAFS of thioctic acid on Au using EtOH only.....	91
5.3	C NEXAFS of thioctic acid on Au prepared with 5% acetic acid in EtOH	91
5.4	C NEXAFS of thioctic acid on Au rinsed in KOH	92
5.5	O K-edge spectra for thioctic acid on Au(111).....	95
5.6	FTIR spectra of thioctic acid films produced with and without acetic acid	96
5.7	C 1s for thioctic acid layers prepared with and without acetic acid.....	97
5.8	S 2p XPS of thioctic acid films with and without acetic acid in solution	98
5.9	Three dimensional model of thioctic acid on Au(111).....	101

List of Figures (continued)

6.1	The monomer dithiol and disulfide-containing polyamide	110
6.2	C K-edge absorption for the monomer and polyamide monolayers	114
6.3	Deconvoluted S 2p spectra for the monomer and polyamide monolayers	116
6.4	Model of the monomer and polyamide films.....	117
S.1	Starting materials and anticipated monolayers	125
7.1	Carbon K-edge absorption on precursor powders.....	127
7.2	Carbon K-edge XAS of monolayers on gold	129
7.3	Carbon K-edge polarization dependence of thiol stopper only film	129
7.4	Carbon K-edge polarization of the layer formed from the [3] rotaxane.....	130
7.5	C 1s XPS spectra of monolayers on gold	131
7.6	S 2p XPS of the stopper only monolayer	133
7.7	S 2p XPS of the pseudorotaxane	133
7.8	S 2p XPS of the [3] rotaxane	134
8.1	The aldehyde functionalized surface-attached rotaxane.....	139
8.2	The aniline-exposed, aldehyde functionalized surface-attached rotaxane	139
8.3	Carbon K-edge close-up of the aldehyde functionalized rotaxane	143
8.4	C K-edge for the aniline-exposed, aldehyde functionalized rotaxane.....	144
9.1	Potential carboxyl-functionalized rotaxane under development.....	152
9.2	Potential carboxyl-functionalized catenane under development	152
9.3	Potentially more atmospherically and biologically stable SAMs on Si	153

List of Tables

3.1	S 2p integrated intensities, pristine / air-exposed SAMs.....	55
4.1	Carbon tilt angles; alkyl chains and carboxyl groups.....	70
4.2	Oxygen tilt angles; carboxyl groups.....	74
5.1	Thioctic acid angles derived from C K-edge NEXAFS	94

Chapter 1

Introduction

Self-Assembled Monolayers

Self-assembled monolayers consist of organic, hydrocarbon-containing molecules that are bound to a surface and spontaneously form ordered monolayers through van der Waal's interactions between molecules (Fig. 1.1). The most elegant methods for SAM formation consist of dissolving molecules in a suitable solution as in Fig. 1.1 a), and exposing an appropriate metal or substrate to this solution. A specific group such as a disulfide[1.1, 2], thiol[1.3], carboxyl[1.4-7], etc. promotes adsorption of the molecules onto the substrate at one end as in Fig. 1.1 b). As the molecules adsorb on the surface, interactions between molecules cause the spontaneous formation of a crystalline, upright, ordered layer depicted in Fig. 1.1 c). Extensive reviews of this process exist, including two books referenced here[1.8, 9].

The most common types of SAMs are alkanethiols on gold or other noble metal substrates, due to the ease in substrate preparation and storage. The phenomenon that sulfur would interact strongly to gold as an anchor for organics was first reported by Nuzzo and Allara[1.1]. Later, Porter, Chidsay, et al. investigated alkanethiols on gold[1.3, 10] and found that alkyl-chain interactions between molecules were sufficient to form well-ordered, crystalline monolayers with increasingly crystalline films as the alkyl-chain length was extended. They reported that the transition from marginally-

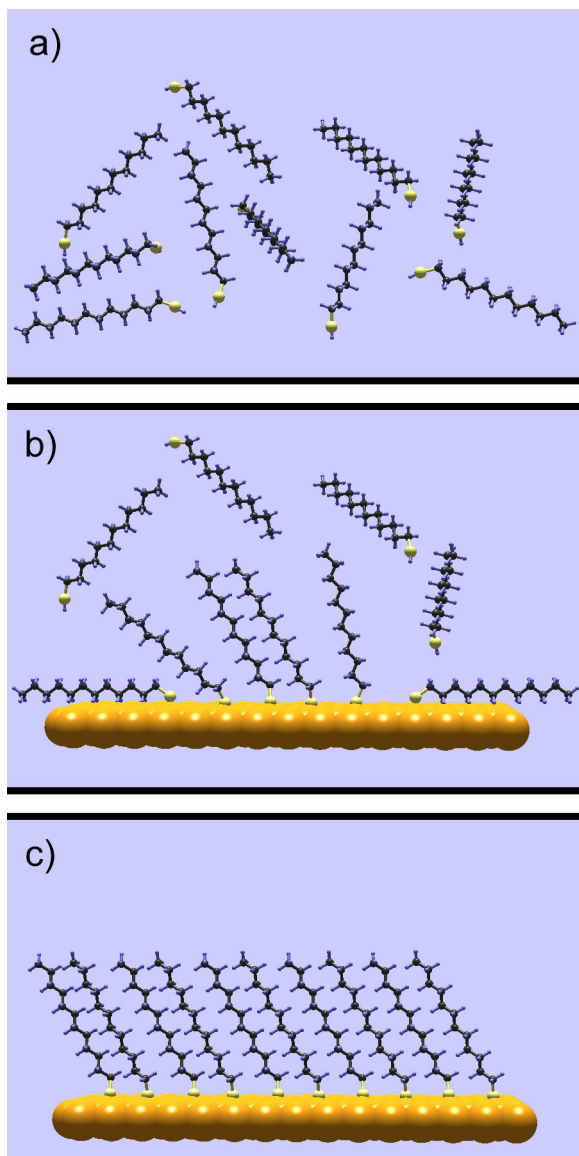


Fig. 1.1. Steps for SAM formation. a) molecules are dissolved in a suitable solvent, b) substrate exposed to solution and molecules begin to adsorb on surface, and c) molecules form a well-packed layer through van der Waal's interactions between them.

ordered to well-ordered layers occurs at chain lengths of about 10-11 alkyl units. These alkyl chains order in an upright manner, often tilted at some polar angle that depends on the sulfur-sulfur distances between neighboring molecules due to variations in substrate composition and the preferred binding site of the sulfur.

Alkanethiols are often functionalized – that is, the terminating methyl-group away from the substrate is replaced with a useful moiety. Carboxyl and amine groups lend themselves nicely to subsequent chemistry that can be of interest for chemical and biological functionality. For example, they are used in biosensor applications for surface-attachment and/or surface-immobilization of DNA, proteins, antigens and antibodies, viruses, and cells[1.11-13]. Carboxyl groups, in particular, are often used in biosensor applications[1.14-16]. One of the thrusts of this work is to investigate carboxyl end-group morphology and its effect on monolayer structure.

In another related community, SAMs and other organic monolayers are explored for their molecular electronic applications and nanotechnological possibilities. Recently, a carboxyl-terminated alkyl-thiol dilute SAM was “switched” using electrochemistry[1.17]. The carboxylic acid was deprotonated to a negatively charged carboxylate, and then by applying a positive bias on the electrode, the end-groups could be attracted and bent towards the substrate. This was observed through changes in wetting properties and sum-frequency generation of C-H vibrations. This and other schemes for integrating SAMs into molecular electronic devices continues to blossom as an active area of nanoscience and technology. Often, these systems depend on conformational changes (i.e. mechanical switching of molecules) in models and descriptions. However, conformational changes are rarely directly measured.

Interlocking Molecules – Catenanes and Rotaxanes

Along with SAMs, interlocking molecules also show promise for nanoscience and technology, and are a second thrust of this work. Catenanes and rotaxanes are

interlocking molecules that are not covalently bound to each other. Catenanes consist of interlocking rings, while rotaxanes are like rings on dumbbells. Both are depicted in Fig. 1.2.

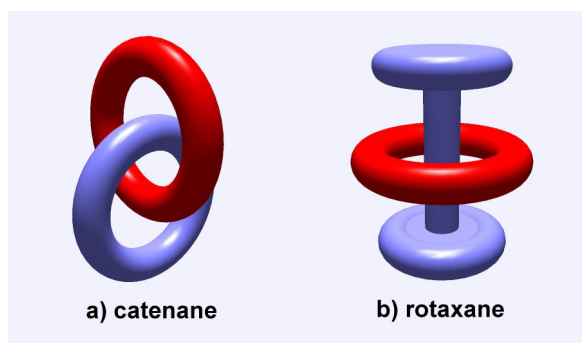


Fig. 1.2. Interlocking molecules: a model of a catenane in a) and a rotaxane in b).

This field of supramolecular chemistry has grown rapidly in recent years with the advent of templated synthesis and other techniques for creating interlocking molecules pioneered by Busch, Sauvage, Leigh, Stoddart, and others[1.18, 19]. These molecules show promise as the ultimate nano-machines and switches.

Prior to this work, electrical circuits depending upon conformational switching of interlocking molecules had been reported[1.20, 21]. These molecules are based upon one of the rings being charged, and the other having two points on the ring, one of which can be charged or discharged in metastable states. The electric gradient induced in this ring causes the switching, illustrated in Fig. 1.3. Upon switching of the molecules, large resistivity changes occur. However, the conformational changes have not been directly measured, and results based on mechanical switching within the molecules have now been called into question[1.22]. Thus, direct measurement of the

morphology of molecules that depend on conformational switching is necessary to ensure observed physical property changes are not entirely due to other phenomena.

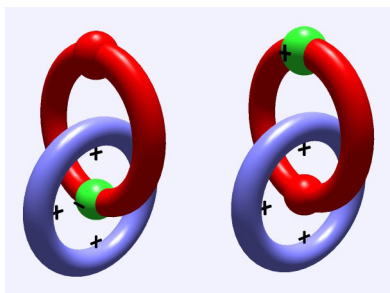


Fig. 1.3. A model of a switching catenane. A functionalization within the ring can be charged/discharged, inducing an electrical polarization in the ring and conformationally switching the molecule.

Surface-Attached Interlocking Molecules

Our goals were to develop methods to covalently link these molecules to surfaces – creating surface-attached catenanes and rotaxanes[1.23-25] as depicted in Fig. 1.4. Such surface-attachment is the natural progression towards building single molecule detectors and/or devices and integrating them with conventional electronics.

Additionally, quantitative techniques used in this work such as x-ray

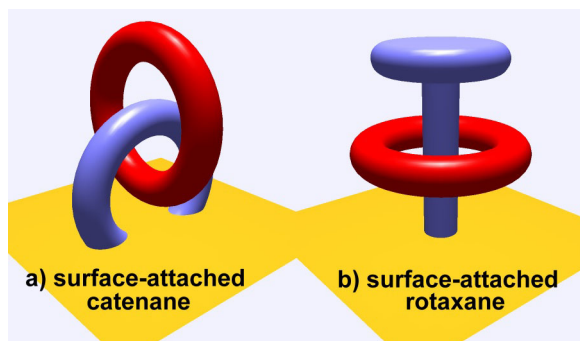


Fig. 1.4. Surface attached interlocking molecules.

photoelectron spectroscopy (XPS), Fourier-transform infrared (FTIR) spectroscopy, and especially near-edge x-ray absorption fine structure (NEXAFS) deliver direct observation of chemical composition, substrate binding, and even conformational orientation. Unlike indirect techniques such as resistivity measurements or electrochemistry, these techniques can show whether molecules are bound to a surface in monolayer fashion, and can potentially directly measure conformational changes in surface-attached interlocking molecules for molecular electronic applications.

Some initial experiments with such molecules (which came to us from UCLA) containing interesting chemistry in their switching molecules (Fig. 1.5, Fig. 1.6)[1.20, 21] were only marginally productive. Although spectra from the molecule presented in Fig. 1.5 showed features consistent with the full catenane, standard SAM formation techniques led to more than a monolayer on the surface, and included fragments of the molecules. The “surface-attached” molecule in Fig. 1.6 most likely was only attaching on one end. The nitrogen signal was not present, indicating that the adsorbate species did not have the aromatic, nitrogen-containing ring. These results inspired our work in characterizing simple surface-attached loops and rotaxanes on surfaces.

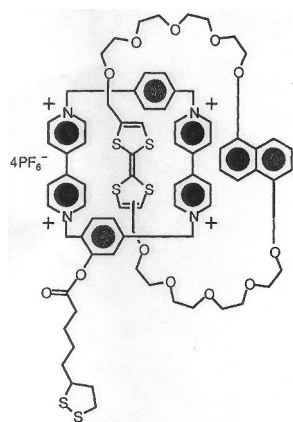


Fig. 1.5. A surface-attached catenane investigated in the early stages of this work. Molecule and figure courtesy of UCLA.

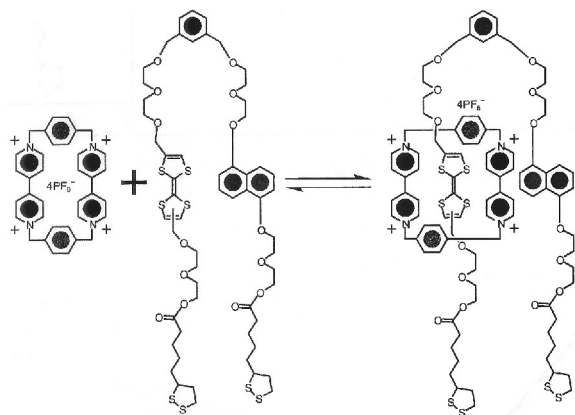


Fig. 1.6. A functionalized, switchable, surface-attached catenane investigated in the early stages of this work. Molecule and figure courtesy of UCLA.

Issues to be Addressed

Many open questions exist on fundamental binding and structure of SAMs and interlocking molecules introduced above. This work addresses a number of relevant issues. SAMs are increasingly used in chemical and biological functionalization of surfaces. Chapter 3 addresses the stability of alkanethiols on gold under ambient atmospheric conditions, which is crucial to biological, chemical, and molecular electronic applications.

- Are SAMs truly stable in air?
- Can a SAM survive, and if so...
- Will a molecule anchored by a gold-thiolate bond remain intact?

In Chapters 4 and 5, questions of carboxyl functionalization are addressed for formation, structure, and nanomechanical functionality.

- How does a carboxyl termination affect SAM formation and order?
- What is the orientation of the end-group on the surface?

- Carboxyl terminated SAMs are commonly used, however a controversy exists as they have been reported to form both ordered and disordered films[1.26, 27].
Is there a means that produces well-ordered SAMs consistently?
- What effect does the alkyl-chain play on carboxyl-terminated SAM structure?
- Are there more robust carboxyl-terminated surface-anchoring molecules such as disulfide-containing thioctic acid?
- Do films formed from thioctic acid, with a large footprint, disulfide containing base and a short alkyl chain show any SAM-like behavior?
- What happens when the alkyl-chain interactions are reduced and the carboxyl groups are free to interact as in monolayers of thioctic acid?
- What happens to monolayer structure if the terminating carboxylic acid is deprotonated to a highly charged carboxylate?
- If these films do change in a nanomechanical fashion, is the switching reversible?

Such potential switching leads to a central question:

- Can simple interactions be utilized to conformationally switch a surface-attached rotaxane?

Chapters 6, 7, and 8 address novel molecules and precursors for functionalized, surface-attached interlocking molecules.

- As a precursor to a surface-attached catenane, and based on the initial failure to create the intended functionalized surface-attached interlocking species pictured in Fig. 1.6, can one manipulate the synthesis of organics to form surface-attached loops?

- To actually form molecular scale devices, forming surface-attached, molecular monolayers could be an important step. Can one form surface-attached rotaxanes, and how?
- With simple, functionalized, surface-attached rotaxanes, can the actual conformational switching be measured?
- Can the orientation on the surface be directly determined?

Quantitative answers to these questions are presented in the coming chapters, furthering knowledge of binding, orientation, chemical switchability, and the ability to directly measure conformational changes for nanomechanical systems based on molecular monolayers. Chapter 2 introduces NEXAFS in detail, with its ability to determine both chemical composition and conformation in ultra-thin organic films. XPS is also introduced, emphasizing its ability to determine chemical composition with atomic sub-monolayer sensitivity and to give an estimate of monolayer thickness. The chapter concludes with a brief overview of FTIR spectroscopy and its ability to distinguish chemical environments and compositions.

Summary

This work uses the quantitative spectroscopic and structural techniques of near-edge x-ray absorption fine structure spectroscopy (NEXAFS) and x-ray photoelectron spectroscopy (XPS) to resolve questions in carboxyl functionalized self-assembled monolayers and in surface-attached interlocking molecules. These techniques elucidate the extent of substrate-molecule binding, the chemical composition of the films, and also provide a direct measurement of film structure. Through the analysis of such data,

we gain a fundamental understanding of film morphologies for improved SAMs, thus leading to more robust, higher efficiency chemical and biological systems. We also characterize formation conditions that lead to surface-attached monolayer species, and their orientations on surfaces in simple rotaxanes. The ability to directly measure claimed conformational changes that presumably are accompanied by physical property changes (e.g. resistivity) is paramount to understanding and development in this area of nanoscience. This research furthers our fundamental understanding of surface-attached catenanes and rotaxanes for incorporation into monolayer nanomechanical systems.

References:

- 1.1. R. G. Nuzzo and D. L. Allara, *Adsorption of Bifunctional Organic Disulfides on Gold Surfaces*. Journal of the American Chemical Society, 1983. **105**(13): p. 4481-4483.
- 1.2. R. G. Nuzzo, F. A. Fusco and D. L. Allara, *Spontaneously Organized Molecular Assemblies. 3. Preparation and Properties of Solution Adsorbed Monolayers of Organic Disulfides on Gold Surfaces*. Journal of the American Chemical Society, 1987. **109**(8): p. 2358-2368.
- 1.3. M. D. Porter, T. B. Bright, D. L. Allara, and C. E. D. Chidsey, *Spontaneously Organized Molecular Assemblies. 4. Structural Characterization of Normal-Alkyl Thiol Monolayers on Gold by Optical Ellipsometry, Infrared-Spectroscopy, and Electrochemistry*. Journal of the American Chemical Society, 1987. **109**(12): p. 3559-3568.
- 1.4. Y. T. Tao, *Structural Comparison of Self-Assembled Monolayers of N-Alkanoic Acids on the Surfaces of Silver, Copper, and Aluminum*. Journal of the American Chemical Society, 1993. **115**(10): p. 4350-4358.
- 1.5. Y. T. Tao, G. D. Hietpas and D. L. Allara, *HCl vapor-induced structural rearrangements of n-alkanoate self-assembled monolayers on ambient silver, copper, and aluminum surfaces*. Journal of the American Chemical Society, 1996. **118**(28): p. 6724-6735.
- 1.6. D. L. Allara and R. G. Nuzzo, *Spontaneously Organized Molecular Assemblies. 1. Formation, Dynamics, and Physical-Properties of Normal-Alkanoic Acids Adsorbed from Solution on an Oxidized Aluminum Surface*. Langmuir, 1985. **1**(1): p. 45-52.
- 1.7. D. L. Allara and R. G. Nuzzo, *Spontaneously Organized Molecular Assemblies. 2. Quantitative Infrared Spectroscopic Determination of Equilibrium Structures of Solution-Adsorbed Normal-Alkanoic Acids on an Oxidized Aluminum Surface*. Langmuir, 1985. **1**(1): p. 52-66.
- 1.8. A. Ulman, *An Introduction to Ultrathin Organic Films: from Langmuir-Blodgett to Self-Assembly*. 1991, San Diego, CA, U.S.A.: Academic Press, Inc. 442.
- 1.9. R. H. Tredgold, *Order in Thin Organic Films*. 1994, Cambridge, U. K.: Cambridge University Press. 199.
- 1.10. C. E. D. Chidsey, M. D. Porter and D. L. Allara, *Electrochemical Characterization of N-Alkyl Thiol, Sulfide, and Disulfide Monolayers on Gold*. Journal of the Electrochemical Society, 1986. **133**(3): p. C130-C130.

- 1.11. J. M. Brockman, A. G. Frutos and R. M. Corn, *A multistep chemical modification procedure to create DNA arrays on gold surfaces for the study of protein-DNA interactions with surface plasmon resonance imaging*. Journal of the American Chemical Society, 1999. **121**(35): p. 8044-8051.
- 1.12. D. G. Castner and B. D. Ratner, *Biomedical surface science: Foundations to frontiers*. Surface Science, 2002. **500**(1-3): p. 28-60.
- 1.13. M. Tirrell, E. Kokkoli and M. Biesalski, *The role of surface science in bioengineered materials*. Surface Science, 2002. **500**(1-3): p. 61-83.
- 1.14. F. Frederix, K. Bonroy, W. Laureyn, et al., *Enhanced performance of an affinity biosensor interface based on mixed self-assembled monolayers of thiols on gold*. Langmuir, 2003. **19**(10): p. 4351-4357.
- 1.15. V. P. Y. Gadzekpo, K. P. Xiao, H. Aoki, et al., *Voltammetric detection of the polycation protamine by the use of electrodes modified with self-assembled monolayers of thioctic acid*. Analytical Chemistry, 1999. **71**(22): p. 5109-5115.
- 1.16. Y. Z. Dong and C. Shannon, *Heterogeneous immunosensing using antigen and antibody monolayers on gold surfaces with electrochemical and scanning probe detection*. Analytical Chemistry, 2000. **72**(11): p. 2371-2376.
- 1.17. J. Lahann, S. Mitragotri, T. N. Tran, et al., *A reversibly switching surface*. Science, 2003. **299**(5605): p. 371-374.
- 1.18. C. O. Dietrick-Buchecker and J.-P. Sauvage, *Interlocking of Molecular Threads: From the Statistical Approach to the Templated Synthesis of Catenanes*. Chemical Reviews, 1987. **87**(4): p. 795-810.
- 1.19. S. Anderson, H. L. Anderson and J. K. M. Sanders, *Expanding Roles for Templates in Synthesis*. Accounts of Chemical Research, 1993. **26**(9): p. 469-475.
- 1.20. C. P. Collier, E. W. Wong, M. Belohradsky, et al., *Electronically Configurable Molecular-Based Logic Gates*. Science, 1999. **285**: p. 391-394.
- 1.21. C. P. Collier, G. Mattersteig, E. W. Wong, et al., *A [2]Catenane-Based Solid State Electronically Reconfigurable Switch*. Science, 2000. **289**: p. 1172-1175.
- 1.22. R. F. Service, *Next-Generation Technology Hits an Early Midlife Crisis*. Science, 2003. **302**: p. 556-558.
- 1.23. T. B. Lu, L. Zhang, G. W. Gokel, and A. E. Kaifer, *The First Surface-Attached Catenane - Self-Assembly of a 2-Component Monolayer*. Journal of the American Chemical Society, 1993. **115**(6): p. 2542-2543.

- 1.24. A. L. Vance, *Lawrence Livermore National Laboratory Lab-wide LDRD*. 1999.
- 1.25. C. De Nadia, C. M. Whelan, C. Perollier, et al., *Self-assembly of mechanically interlocked and threaded rings: a HREELS and XPS study of thiol-functionalised catenane and rotaxane molecules on Au(111)*. *Surface Science*, 2000. **454-456**: p. 112-117.
- 1.26. R. Arnold, W. Azzam, A. Terfort, and C. Wöll, *Preparation, Modification, and Crystallinity of Aliphatic and Aromatic Carboxylic Acid Terminated Self-Assembled Monolayers*. *Langmuir*, 2002. **18**(10): p. 3980-3992.
- 1.27. O. Dannenberger, K. Weiss, H. J. Himmel, et al., *An orientation analysis of differently endgroup-functionalized alkanethiols adsorbed on Au substrates*. *Thin Solid Films*, 1997. **307**: p. 183-191.

Chapter 2

Experimental Techniques

Monolayer Formation

The substrates used were epitaxial films of gold on mica, or gold on Ti/Si(100). Gold on mica substrates, consisting of ~ 1500 Å Au evaporated on green, freshly cleaved mica were purchased from Molecular Imaging Inc. Gold on Si substrates were formed by evaporating a 5 nm Ti adhesion layer and then 1000 Å gold onto Si(100) substrates in high vacuum (10^{-8} to 10^{-9} torr).

Hydrogen-flame annealing maximized the Au(111) terrace size, and assisted in removing impurities from the gold substrates before exposure to SAM solutions[2.1]. Annealing was accomplished using purified hydrogen (99.99%), and a special torch (The Little Torch™, Smith Equipment, Watertown, SD). A #2 tip with a 0.15 mm aperture in a sapphire bead allowed for a very small flame size. Safety precautions were observed, including using a sufficiently small cylinder such that if the entire contents were released into the room, the concentration would be below 4% in air, the point at which dilute hydrogen will burn. Standard backflash arresters furthered safety precautions with this flammable and potentially explosive gas. The hydrogen regulator was set to about 2 PSIG (15% ATM) and the lines were purged with hydrogen for 10-15 sec. to prevent backflash in the torch lines. The burning torch was adjusted to have a flame length of about 1-2 cm, and burns a very dark blue color that is invisible under

standard room lighting conditions, but is visible in a darkened room against a black background. Substrates were placed face-up on a 2 cm thick, 10 cm diameter fused-quartz plate. (As an added cautionary note, when 0.75 cm plate glass was initially used, local heating from the torch was sufficient to cause the glass to burst!) The quartz was heated around the substrate with the torch. Initially, this created a visibly hazy layer of condensed water droplets on the cool quartz substrate, but as heating continued, the substrates became sufficiently warm to no longer retain water vapor. This assured even heating and annealing. The substrates were then annealed using the outer edge of the hydrogen flame with sweeping motions across the face of the substrate at a frequency of about 1 Hz for about 30 seconds. Care must be taken, especially with the mica samples. A visible, dark reddish glow often indicates the heating has been too high, which ruins the atomically flat surface as seen with subsequent AFM characterization. Si-based substrates take more heat for annealing, presumably due to the higher thermal conductivity in the Si. Flame annealed Au/mica can have (111) terraces up to 500 nm by 500 nm[2.1], but our samples typically had terraces estimated to be ~100 nm in width using AFM. Si-based substrates led to smaller domains, with terrace widths from ~10-50 nm in our samples.

Substrates were then immersed in ethanolic (or other) solutions of thiol or disulfide containing molecules. These solutions are prepared by simply dissolving a few mg of molecules into a few ml of solvent. In most cases, 1 μ mol to 1 mmol is an appropriate concentration that allows for a huge excess of molecules in solution. SAMs then form through gold-thiolate bonding and self-assembly as described in Chapter 1. Substrates were left immersed in solutions for ~24 hrs. to allow for compete monolayer

formation. Monolayers were then rinsed in the corresponding pure solvent to remove extraneous molecules. The much greater strength of the sulfur-substrate bond in the first monolayer as compared to the mostly van der Waals bonding between the first and subsequent monolayers then often leads to the clean formation of single molecular monolayer. The SAMs were finally carefully blown dry with nitrogen; the best monolayers result from carefully driving solvents to the edge and off of the sample with the N₂ stream, rather than allowing the solvent to evaporate on the surface, leaving behind trace solvent impurities or excess molecules. Samples were then immediately placed in the vacuum chamber for analysis to prevent degradation of the thiolate as discussed in Chapter 3.

Near-Edge X-ray Absorption Fine Structure Spectroscopy

Near-edge x-ray absorption fine structure spectroscopy (NEXAFS) can answer questions of the chemical state and orientational nature of molecules on surfaces, and is a part of a broad set of measurement techniques called X-ray absorption spectroscopy (XAS.) For XAS, one measures the absorption of a tunable source of x-rays as photon energy is scanned through the electronic core-level binding energy of an element present in the probed material. Thus, XAS has inherent elemental specificity, as one chooses the absorption edge of the core-level of interest, such as the K-edges for carbon at ~288 eV, nitrogen at ~399 eV, or oxygen at ~534 eV. The resultant spectrum is the absorbed x-ray intensity vs. photon energy. A steep absorption onset arises as the energy passes through the first allowed transitions from the core-level to unoccupied bound states, and as the energy is increased one reaches the core ionization potential or

binding energy. The ionization potential occurs at the point where x-ray energy is just large enough to excite electrons beyond the vacuum level, or into the continuum as photoelectrons, and, in the simplest picture of x-ray absorption, leads to a step-function-like feature in the spectrum. However, the energy position of this bound-to-continuum step edge, from x-ray absorption alone, is neither directly observable nor easy to obtain due to the many sharp, bound-to-bound excitations occurring at lower energies and overlapping this edge.

Two energy regions of interest with associated sub disciplines exist in XAS studies. Extended x-ray absorption fine structure (EXAFS) deals with the small oscillations of a few percent occurring at energies much higher than the absorption edge due to photoelectron scattering from the local atomic structure of the material probed, while the much stronger, partial unoccupied density of states features within 30-100 eV of the absorption edge are referred to as the x-ray absorption near-edge structure (XANES) or NEXAFS.

The synonyms XANES and NEXAFS are often used interchangeably within the literature. However, XANES is often used when dealing with absorption from deep core-levels and/or when used in conjunction with EXAFS[2.2]. Conversely, NEXAFS is nearly exclusively used when referring to experiments involving K-edges (absorption arising from 1s core levels) of light elements such as C, N, and O, with emphasis both on the chemical nature through partial density of states mapping, and bond orientation through polarization dependencies of these antibonding orbital states. Thus, NEXAFS is the descriptor of choice for this dissertation.

NEXAFS is very sensitive to bonding environment through the measurement of the partial unoccupied density of states or equivalently, the measurement of excitations into molecular antibonding orbitals. For C, N, and O, these orbitals are most often sp , sp^2 , or sp^3 hybridized, and are often designated as π^* or σ^* . In addition, atomic-like Rydberg (R^*) excitations occur and converge on the continuum near the ionization potential. NEXAFS easily identifies the π^* or σ^* nature of the empty electronic states, and exploits the associated symmetries. For many systems, fingerprinting based on spectra from well-characterized molecules, and/or a combination of theory and experiment are often necessary to unambiguously resolve chemical nature[2.3]. NEXAFS features also exhibit chemical shifts, for example, the carboxyl π^* appears at 288.7 eV in the C K-edge, roughly 3.3 eV higher than for the π^* resonance in benzene or graphite (~285.4 eV). The higher excitation energy of the C 1s core-level in the carboxyl group arises from the electron-density withdrawing effect of a single carbon atom bound to two oxygen atoms. Features within the partial density of states lead to not only chemical information, but spatial orientation of their associated orbitals, via measurements of the angular dependence of NEXAFS, as described in the next section.

NEXAFS Polarization Dependence and its Connection to Orientation

NEXAFS powerfully and quantitatively determines orientations of orbitals and hence bonds and even molecules. Consider, for example, the Hamiltonian \mathbf{H} for a single electron of charge e , mass m , and momentum \mathbf{p} in an electromagnetic plane-wave field with vector potential \mathbf{A} [2.4-7]:

$$\mathbf{H} = \frac{1}{2m} \left(\mathbf{p} + \frac{e}{c} \mathbf{A} \right)^2 - e\phi. \quad (2.1)$$

Using an incident plane wave in the coulomb gauge, expanding the square, and neglecting the higher-order \mathbf{A}^2 term, (2.1) becomes

$$\mathbf{H} = \frac{\mathbf{p}^2}{2m} + V_0(r) + \frac{e}{mc} \mathbf{A} \cdot \mathbf{p} \quad (2.2)$$

where $V_0(r)$ is the static potential of the nuclei and other electrons, and the first

perturbative term is $\frac{e}{mc} \mathbf{A} \cdot \mathbf{p}$. Next, look at the transition probability from an initial

state $|i\rangle$ to a final state $|f\rangle$ driven by this incident plane wave:

$$P_{if} \propto \left| \langle f | \frac{e}{mc} \mathbf{A} \cdot \mathbf{p} | i \rangle \right|^2 \quad (2.3)$$

where $\mathbf{A} = \mathbf{E} \frac{A_0}{2} \left(e^{i(\mathbf{k} \cdot \mathbf{x} - \omega t)} + e^{-i(\mathbf{k} \cdot \mathbf{x} - \omega t)} \right)$. The amplitude of the wave is A_0 , \mathbf{E} is a unit

vector in the direction of the electric field, \mathbf{k} is the wave-vector in the direction of propagation, and ω is the frequency of the radiation. As presented later in this chapter, radiation used for NEXAFS is often elliptically polarized, so \mathbf{E} is complex. The transition probability is then

$$P_{if} \propto \left| \langle f | \mathbf{E} \cdot \left(e^{i(\mathbf{k} \cdot \mathbf{x} - \omega t)} + e^{-i(\mathbf{k} \cdot \mathbf{x} - \omega t)} \right) \cdot \mathbf{p} | i \rangle \right|^2. \quad (2.4)$$

The operator $e^{i(\mathbf{k} \cdot \mathbf{x} - \omega t)}$ corresponds to the absorption of a photon while $e^{-i(\mathbf{k} \cdot \mathbf{x} - \omega t)}$ corresponds to the emission. Considering only absorption, and looking at the time average, the transition probability between i and f is

$$P_{if} \propto \left| \langle f | e^{i\mathbf{k} \cdot \mathbf{x}} \mathbf{E} \cdot \mathbf{p} | i \rangle \right|^2. \quad (2.5)$$

The dipole approximation now assumes $\mathbf{k} \cdot \mathbf{x} \ll 1$, or that the region over which this integral is non-zero is much smaller than the photon wavelength. This is well satisfied, as the photons used for C, N, and O K-edges are from 2.0 – 4.5 nm and the orbital radii of the 1s sub-shells are less than 1 Å. Upon application of this approximation, (2.5) becomes

$$P_{if} \propto \left| \langle f | \mathbf{E} \cdot \mathbf{p} | i \rangle \right|^2 \quad (2.6)$$

The momentum operator in this dipole matrix element can also be represented in “length” form[2.4, 8], which leads to the expression

$$P_{if} \propto \left| \mathbf{E} \cdot \langle f | \mathbf{r} | i \rangle \right|^2. \quad (2.7)$$

The final state, in the lighter, second row elements of interest, can be represented to good first approximation by a hybridized molecular orbital of mixed 2s / 2p nature.

This orbital may be represented as a linear combination of atomic orbitals:

$|f\rangle = a|2s\rangle + b|2p_x\rangle + c|2p_y\rangle + d|2p_z\rangle$ along with terms due to atomic orbitals on near-

neighbor atoms. The dipole selection rule immediately implies that the contribution

from 2s be zero. Near-neighbor terms will contribute very little to the matrix element.

Considering first the case where $b=1$ and $c=d=0$, the matrix element becomes

$\langle f | \mathbf{E} \cdot \mathbf{r} | 1s \rangle = \langle 2p_x | \mathbf{E}_x x | 1s \rangle$ which goes like x^2 , and is non-zero. The maximum

probability density of a more general final-state orbital will be along the vector

$\mathbf{O} = b\mathbf{e}_x + c\mathbf{e}_y + d\mathbf{e}_z$ and (2.7) can then be reduced to the heuristic form

$$P_{if} \propto |\mathbf{E} \cdot \mathbf{O}|^2 \quad (2.8)$$

Thus, the intensity of absorption is proportional to the dot product of the electric field vector and the direction of maximum probability density for the final-state orbital, which is collinear with the transition dipole moment. Orbital and hence molecular orientation may thus be obtained through the use of polarized x-rays.

Fortuitously, bend-magnet radiation generated at synchrotron light sources (described in the next section) is naturally highly polarized in the plane of the storage ring. One can define the degree of linear polarization as[2.4]

$$P = \frac{E_p^2}{E_p^2 + E_s^2} \quad (2.9)$$

where E_p is the electric field component in the plane of the storage ring, and E_s is the component orthogonal to the plane of the storage ring in the highly linearly yet elliptically polarized light. This is easily measured, with a method presented later in this chapter. The intensity of a resonance is proportional to the dot product of the electric field vector and the transition dipole moment. The transition dipole moment is commonly modeled as a vector for single bonds or linear molecular orbitals such as carbon-carbon σ^* in an alkyl chain[2.9], or as a number of coplanar resonances as in the case of alkyl C-H σ^* (R^*) moments which lie in a plane whose normal is perpendicular to the alkyl chain[2.3].

Roughly following the derivation by Stöhr in reference [2.4], the intensity of a transition into a vector orbital (or planar group of orbitals) can be derived as a function of x-ray incidence and polar angle of the orbital (or normal to the plane.)

Beginning with the vector case (Fig. 2.1) the intensity is simply proportional to the dot product of the electric field and the transition dipole moment from Eq. (2.8).

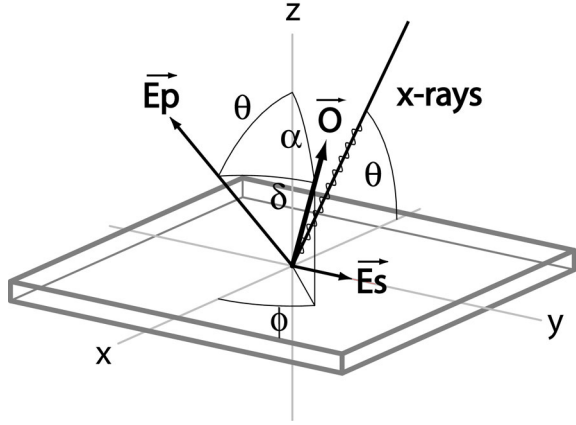


Fig. 2.1. NEXAFS geometry for vector-like transition dipole moments. See text for description.

This is:

$$I_v(E_p, E_s, \theta, \phi, \alpha) \propto \left[\begin{pmatrix} E_p \sin(\theta) \\ E_s \\ E_p \cos(\theta) \end{pmatrix} \cdot \begin{pmatrix} \cos(\phi) \sin(\alpha) \\ \sin(\phi) \sin(\alpha) \\ \cos(\alpha) \end{pmatrix} \right]^2 \quad (2.10)$$

Using Eq. (2.9), this is

$$I_v(P, \theta, \phi, \alpha) \propto \left(\sqrt{P} \sin(\theta) \cos(\phi) \sin(\alpha) + \sqrt{1-P} \sin(\phi) \sin(\alpha) + \sqrt{P} \cos(\theta) \cos(\alpha) \right)^2 \quad (2.11)$$

and gives the following six terms:

$$\begin{aligned}
& P \sin(\theta)^2 \cos(\phi)^2 \sin(\alpha)^2 \\
& 2\sqrt{P}\sqrt{1-P} \sin(\theta) \cos(\phi) \sin(\phi) \sin(\alpha)^2 \\
& 2P \sin(\theta) \cos(\theta) \cos(\phi) \sin(\alpha) \cos(\alpha) \\
& (1-P) \sin(\phi)^2 \sin(\alpha)^2 \\
& 2\sqrt{1-P}\sqrt{P} \cos(\theta) \sin(\theta) \cos(\alpha) \sin(\alpha) \\
& P \cos(\theta)^2 \cos(\alpha)^2
\end{aligned} \quad . \quad (2.12)$$

The symmetry of the molecules in the azimuthal direction will follow the symmetry of the substrate, and in this case, the Au(111) surface has threefold symmetry. Also, the beam spot is much larger than a single molecule, a domain of molecules, or even domains of the substrate. Threefold or higher symmetry can be thought of as averaging the molecules that lie in different azimuthal directions, so using

$$\begin{aligned}
& \int_0^{2\pi} \frac{d\phi}{2\pi} \sin(\phi) \cos(\phi) = 0 \\
& \int_0^{2\pi} \frac{d\phi}{2\pi} \sin(\phi)^2 = \frac{1}{2} \\
& \int_0^{2\pi} \frac{d\phi}{2\pi} \cos(\phi)^2 = \frac{1}{2} \\
& \int_0^{2\pi} \frac{d\phi}{2\pi} \sin(\phi)^2 \cos(\phi) = 0 \\
& \int_0^{2\pi} \frac{d\phi}{2\pi} \cos(\phi)^2 \sin(\phi) = 0
\end{aligned} \quad (2.13)$$

the intensity of the resonance becomes

$$I_v(P, \theta, \alpha) \propto \left(\frac{1}{2} \sin(\theta)^2 \sin(\alpha)^2 + \cos(\theta)^2 \cos(\alpha)^2 \right) P + \frac{1}{2} \sin(\alpha)^2 (1-P). \quad (2.14)$$

Finally, separating θ and α one obtains

$$I_v(\theta, \alpha) \propto \frac{1}{3} P \left(1 + \frac{1}{2} (3 \cos^2 \alpha - 1) (3 \cos^2 \theta - 1) \right) + \frac{1}{2} (1 - P) \sin^2 \alpha \quad (2.15)$$

where θ is the angle between the incident radiation and the surface, α is the angle between the surface normal and the transition dipole moment vector, and P is the polarization of the beam in the plane of incidence defined in (2.9) above. This is Eq. (9.16) in reference [2.4]. One can also model the transition dipole moment as a number of resonances in a given plane as depicted in Fig. 2.2.

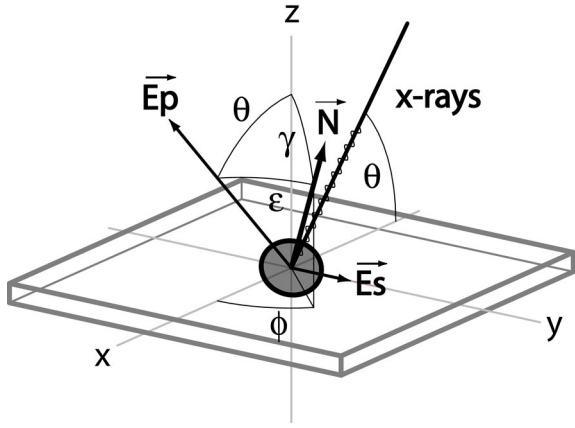


Fig. 2.2. NEXAFS geometry for multiple transition dipole moments which lie in a plane. See text for description.

For this plane model, the intensity is now proportional to the square of the projection of the electric field \vec{E} onto the plane whose normal is \vec{N} :

$$I_p(\vec{E}, \vec{N}) \propto \left| \vec{E} - (\vec{E} \cdot \vec{N}) \frac{\vec{N}}{|\vec{N}|^2} \right|^2 \quad (2.16)$$

Letting $|\vec{N}|=1$, and simplifying this equation,

$$I_p(\vec{E}, \vec{N}) \propto E^2 - (\vec{E} \cdot \vec{N})^2 \quad (2.17)$$

Using (2.9) and the geometry of (Fig. 2.2) and the intensity becomes

$$I_p(P, \theta, \phi, \gamma) \propto 1 - \left(\sqrt{P} \sin(\theta) \cos(\phi) \sin(\gamma) + \sqrt{1-P} \sin(\phi) \sin(\gamma) + \sqrt{P} \cos(\theta) \cos(\gamma) \right)^2 \quad (2.18)$$

and yields the following seven terms:

$$\begin{aligned} & 1 \\ & -P \sin(\theta)^2 \cos(\phi)^2 \sin(\gamma)^2 \\ & -2\sqrt{P}\sqrt{1-P} \sin(\theta) \sin(\phi) \cos(\phi) \sin(\gamma)^2 \\ & -2P \sin(\theta) \cos(\theta) \cos(\phi) \sin(\gamma) \cos(\gamma) \\ & -(1-P) \sin(\phi)^2 \sin(\gamma)^2 \\ & -2\sqrt{P}\sqrt{1-P} \cos(\theta) \sin(\phi) \sin(\gamma) \cos(\gamma) \\ & -P \cos(\theta)^2 \cos(\gamma)^2 \end{aligned} \quad (2.19)$$

Once again, integrating over ϕ , (2.13) these terms reduce to

$$I_p(P, \theta, \gamma) \propto 1 - \left(\frac{1}{2} \sin(\theta)^2 \sin(\gamma)^2 + \cos(\theta)^2 \cos(\gamma)^2 \right) P - (1-P) \frac{1}{2} \sin(\gamma)^2 \quad (2.20)$$

Separating θ and γ , and collecting on P and (1-P) one obtains

$$I_p(\theta, \gamma) \propto \frac{2}{3} P \left(1 - \frac{1}{4} (3 \cos^2 \gamma - 1) (3 \cos^2 \theta - 1) \right) + \frac{1}{2} (1-P) (1 + \cos^2 \gamma) \quad (2.21)$$

where θ is again the angle between the incident radiation and the surface, P is the polarization, and γ is the angle between the normal to the transition dipole moment plane and the normal to the surface. This is Eq. (9.17) in reference [2.4].

NEXAFS analyses based on variations of Eqs. (2.15) and (2.21) abound in scientific literature. The experimental angular variation of a given resonance is fit to

the appropriate theoretical expression, with estimated degree of linear polarization P . Often analysis proceeds by the ratio or difference method, while leaving functions in terms of θ only. The intensity curves are then plotted, and fits are estimated based on these curves. Although this is sufficient for estimating polar angles, leaving all angles as functions of \cos^2 greatly simplifies data and error analysis, and allows for greater precision through linear regression. As a part of this work, the description of a more elegant method of NEXAFS data analysis is presented.

To remove the proportionality, ratios are taken between spectra taken at different incident angles. In order to greatly simplify analysis, the intensities are left as functions of cosine squared. Thus, with $\Theta = \cos^2 \theta$, $A = \cos^2 \alpha$, and $\Gamma = \cos^2 \gamma$ the intensities from Eqs. (2.15) and (2.21) become:

$$\frac{I_v(\Theta_i, A)}{I_v(\Theta_j, A)} = \frac{P(3A-1)\Theta_i - A + 1}{P(3A-1)\Theta_j - A + 1} \quad (2.22)$$

and

$$\frac{I_p(\Theta_i, \Gamma)}{I_p(\Theta_j, \Gamma)} = \frac{P(3\Gamma-1)\Theta_i - \Gamma - 1}{P(3\Gamma-1)\Theta_j - \Gamma - 1} \quad (2.23)$$

These two equations are linear in Θ_i . A linear regression is then obtained from all spectra acquired at Θ_i vs. each incidence spectrum taken at Θ_j . For N spectra, this leads to N slopes and $N-1$ offsets that each return α (or γ .) One can then obtain a very precise angle from the average of $2N-1$ angles, and a precision error based on the standard deviation of these angles.

Another common method of determining orientation of bonds is through taking the difference of spectra taken at various incidence angles and comparing to a sample of a known orientation[2.4]. As a function of $\cos^2 \theta_i - \cos^2 \theta_j$ (or $\Theta_i - \Theta_j$) these equations are also linear:

$$I_v(\Theta_i, A) - I_v(\Theta_j, A) = SP \left(\frac{3}{2} A - \frac{1}{2} \right) (\Theta_i - \Theta_j) \quad (2.24)$$

and

$$I_p(\Theta_i, \Gamma) - I_p(\Theta_j, \Gamma) = SP \left(-\frac{3}{2} \Gamma + \frac{1}{2} \right) (\Theta_i - \Theta_j) \quad (2.25)$$

so linear regressions of all difference spectra taken at Θ_i and Θ_j can be made to determine angles relative to a sample with a known orientation. This reference sample with known orientation is needed to determine S , the transition dipole moment cross section, and P the polarization[2.4]. In this case, since all difference spectra are included in a single regression, errors are based on confidence limits of the linear fit.

Using these methods on a number of spectra, one can obtain a high degree of precision. Typical error bars for precision are less than 1.0° . However, these values of precision do not represent a number of other sources of systematic errors that lead to an estimated accuracy of $4\text{-}5^\circ$. These systematic errors come from manipulator beamline misalignment, estimated be a few degrees, and a number of approximations in the analysis such as the assumption that the dipole moment is simply a vector as in Eq. (2.8) rather than an orbital with spatial structure.

Peaks of polarization dependent NEXAFS resonances often overlap, and ride on a polarization independent background including the step-function-like absorption edge near the ionization potential. These two factors often make analysis using raw intensities of peaks through Eqs. (2.22) and (2.23) difficult. To resolve this issue, one can utilize Eqs. (2.24) and (2.25) with difference spectra to isolate polarization dependent peaks, but often these peaks both overlap and have opposite polarization dependence that eliminates accurate results by raw integration of difference spectra. In order to resolve these issues, as a part of this work, a custom code was written to more easily analyze polarization dependencies of overlapping peaks by simultaneously fitting spectra with appropriate peak shapes.

Peaks are fit in the following manner to obtain accurate positions, widths, and amplitudes. A series of N polarization dependent spectra will have $\sum_{i=1}^{N-1} N-i$ combinations of difference spectra. All raw and difference spectra are fit simultaneously. Peak positions and widths are held constant between all spectra, while amplitudes vary freely. Parameters for widths and positions are varied via Monte-Carlo, and all spectral fits are calculated with one new parameter. If the residual for all spectra is better with a new peak width or position, the new parameter is accepted. If not, the original parameter is retained and a different parameter is varied. For amplitudes, a new value is picked for a given peak and spectra. If the residual is better for the single spectra, it is retained, otherwise discarded. This procedure of randomly picking new parameters is repeated until the deviation of the fits vs. the experimental curves is acceptably small. Through careful analysis using this method one exploits the

peak position and width information primarily carried in raw spectra while retaining polarization dependent peak information within difference spectra. Peak positions, widths, and amplitudes return self-consistent angles using ratio (Eqs. (2.22), (2.23)) and difference (Eqs. (2.24), (2.25)) methods. This method of peak fitting was used extensively in the carboxyl-terminated self-assembled monolayer and thioctic acid systems presented in Chapters 4 and 5.

Examples of regressions obtained using the ratio and difference methods and peak fitting to deconvolute a polarization dependent resonance are presented in Fig. 2.3 and Fig. 2.4. These regressions were for the 0.001 mmol carboxyl terminated SAM investigated in Chapter 4 and are representative of regressions attainable with high quality, carefully acquired spectra, and the analysis methods presented above. Fig. 2.3 presents data points and linear regressions using the ratio method. Slopes of regressions used with Eq. (2.23) yielded angles 40.22, 40.22, 40.29, 40.36, 40.19, and 40.23 for an average of 40.25 and remarkable precision with standard deviation of 0.06. Offsets with (2.23) yielded angles 39.02, 39.21, 39.80, 40.72, and 38.89 for an average 39.52 and standard deviation of 0.67. The regression using all difference spectra is presented in Fig. 2.4. The upper and lower 95% confidence limits on the slope obtained in this regression through Eq. (2.25) yielded an error of ± 0.2 degrees. As stated earlier, the precise results do not account for a number of systematic errors. However, they greatly improve upon standard analysis techniques, and could be applied to systems in which analysis has been problematic without these methods as in reference [2.10].

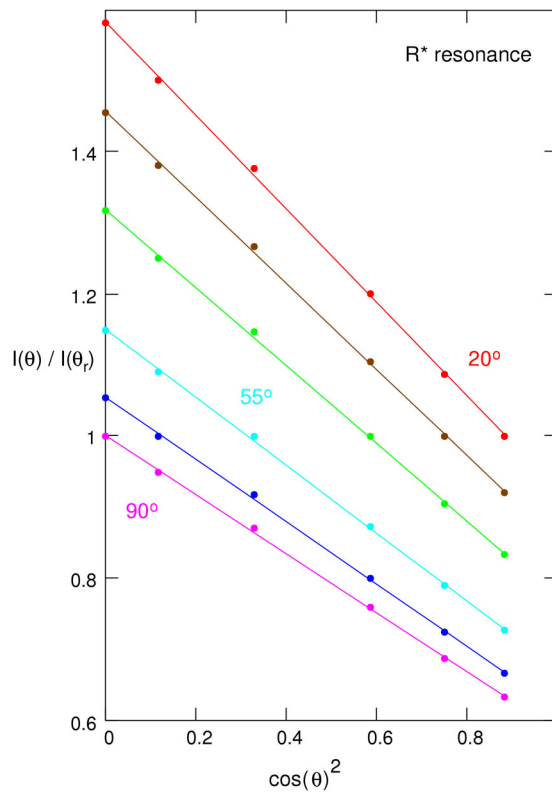


Fig. 2.3. An example of regressions obtained from the R^* resonance of one of the SAMs presented in Chapter 4 using the ratio method. The top line uses the spectra acquired at 20 degrees in the denominator, middle regressions use 30, 40, 55, and 70, while the bottom uses the spectra acquired at normal incidence.

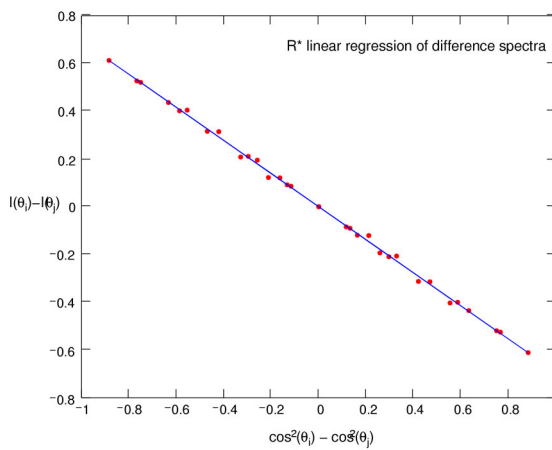


Fig. 2.4. An example of the regression obtained from difference spectra of the R^* region of one of the SAMs presented in Chapter 4.

Measuring NEXAFS

X-ray absorption requires an intense, collimated, monochromatic, and tunable source of x-rays. Well established through Maxwell's equations (as later adapted for special relativity effects) accelerating charges emit electromagnetic radiation[2.11]. Through the 1950's and 1960's, radiation emitted from particle accelerators began to be investigated as a novel source of x-rays for experimental condensed-matter physics, with this work being parasitic to high-energy physics experiments[2.12, 13]. X-rays emitted from relativistic charged particles in accelerators produce photons from the infrared to hard x-rays, including the otherwise inaccessible vacuum-ultraviolet and soft x-ray regime ($\sim 50\text{eV} - 2,000\text{ eV}$) with high brightness, flux and tunability of photon energy. Today, physics, chemistry, and biology exploit these properties of synchrotron radiation using many dedicated sources around the world.

The x-ray absorption spectra in Chapters 3 through 7 were acquired at VUV beamline 8.2 of The Stanford Synchrotron Radiation Laboratory (SSRL) using the SPEAR II storage ring at the Stanford Linear Accelerator Center. This beamline uses bend magnet radiation and a spherical grating monochromator[2.14] whose configuration is roughly depicted in Fig. 2.5.

The spot size within our chamber is roughly 1-2 mm in diameter. These factors contribute to make this beamline ideal for the ultra-thin, organic monolayers, as they degrade rapidly under high-brightness more strongly focused x-rays[2.15].

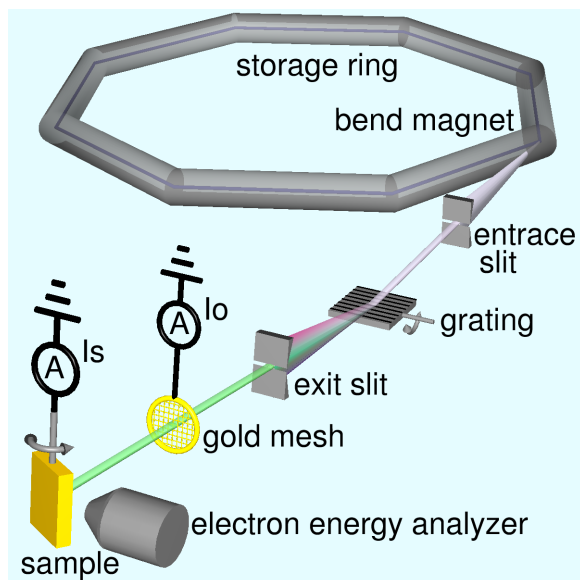


Fig. 2.5. Depiction of a bend-magnet beamline. The "white" bend magnet synchrotron radiation is monochromatized using a rotatable grating placed between entrance and exit slits. Flux is monitored using a gold grid (I_0). Absorption is measured through sample current (I_s). Auger yield is measured through an electron energy analyzer. Other optics present are not shown for brevity and clarity.

For this beamline, degradation of a simple hexadecanethiol monolayer on gold was investigated to ensure minimal damage to molecular monolayer films. The alkanethiolate C K-edge spectra acquired at normal incidence are presented in Fig. 2.6. Slits were opened above what was typically used to about 40-50 microns for the exit and entrance slits. This is an upper limit for reasonable resolution and beam intensity. As seen in the figure, minimal damage occurs over the acquisition time, which is typically 3-4 minutes. However, the first noticeable change in the spectra occurs through a decrease in the C-H σ^* / R* features at about 289eV, with increasing changes over time. After about 25 minutes in this test, pre-edge features, at around 285.5 eV associated with sp or sp² carbon bonding, depicted π^* , are clearly evident. The shape of the σ^* resonances above the absorption onset also changes. These features are all

emphasized with arrows in the final, lowest spectra, which had been exposed to x-rays in the 280-325eV range on this beamline for 42 minutes.

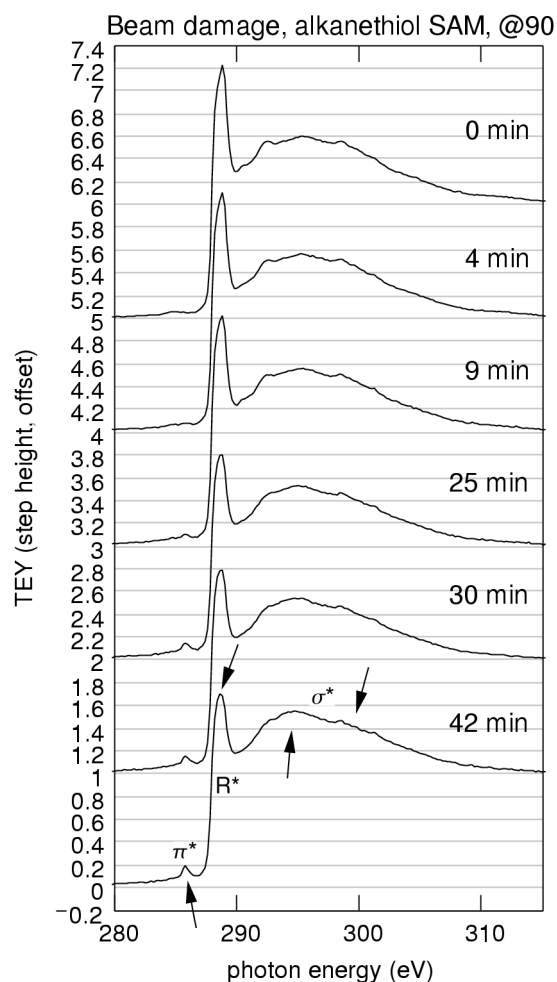


Fig. 2.6. A series of carbon NEXAFS spectra from hexadecanethiol on gold SAMs at normal incidence, under the x-ray beam. The top spectra is from the pristine film, while the bottom spectra has been in the beam ~45 minutes.

These features indicate the following changes and degradation. The spectra presented were all acquired at normal incidence to ensure the beam remained on the same spot. In a pristine film, C-H σ^* / R^* features are very intense, while C-C σ^*

features above the edge are less intense than at grazing incidence. The decrease in the R^* and change in shape of the σ^* resonances above the edge with increasing beam exposure are indicative of a less-ordered monolayer. The appearance of the π^* feature indicates graphitization and possible cross-linking of molecules through the appearance of carbon-carbon double bonds. Moving to a new spot on the sample restores the spectra to one indistinguishable from the top, pristine spectra, and this was the method used throughout all experiments: every spectra were acquired on portions of the sample that had not been previously exposed to x-rays and care was taken to ensure radiation damage was a negligible effect. The beamline slits were also set to allow less flux than these test measurements throughout this work.

For NEXAFS experiments, high linear polarization is desirable, however, beamline 8.2 was designed to utilize elliptically polarized radiation for circular dichroism experiments. The emittance from “white” bend magnet beamlines approaches linear polarization in the plane of the storage ring, but the emittance above or below this plane leads to elliptical polarization. Prior to each experimental run, the beamline optics were optimized for maximum flux, which is near the maximum linear polarization. Then, the degree of linear polarization (Eq. (2.9)) was measured through the angular dependence of the π^* feature of highly ordered, pyrolytic graphite (HOPG) with transition dipole moment normal to the surface.

As a function of E_p and θ , the intensity for a vector like orbital (Eq. (2.15)) with $\alpha = 0$ (as in the case of the HOPG π^*) reduces to simply

$$I_v(E_p, \theta) \propto E_p^2 \cos^2(\theta). \quad (2.26)$$

One can then obtain spectra indicating the intensity as a function of angle about the axis and measure the major and minor axis amplitudes squared of electric field Fig. 2.7. The upper points and $\cos^2(\theta)$ trace are intensities of the π^* resonance when the sample is rotated from normal to grazing incidence, with the major electric field component E_p of the incoming synchrotron radiation in the plane of incidence, while E_s lies in the plane of the sample and does not contribute to the intensity of the π^* . The lower trace and two points are for normal incidence, and the spectra taken from HOPG mounted on a wedge at 30° grazing incidence such that the minor component E_s is now in the plane of incidence, and E_p is in the plane of the HOPG. Thus, the sinusoidal intensities of the

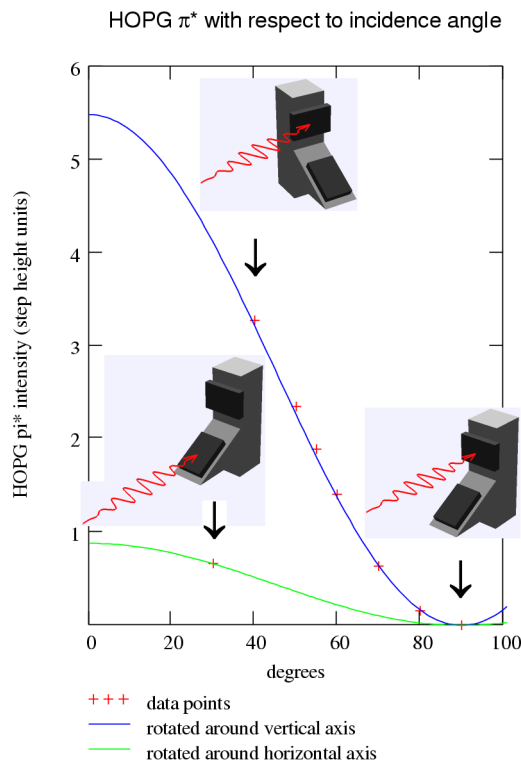


Fig. 2.7. HOPG π^* resonance intensity as a function of incidence angle. Top points and cos-squared fit are intensity as a function of manipulator angle, while lower point and fit are derived from HOPG mounted on a wedge, essentially rotating about the other axis. These two measurements determine the relative intensity of E_p and E_s respectively, and hence the degree of linear polarization.

top and bottom trace are the relative intensities of E_p^2 and E_s^2 . The degree of linear polarization is now known through Eq. (2.9). The maximum measured degree of linear polarization varied from about 87% to about 91.5% over the three-year period experiments were conducted at SSRL. Additionally, the energy scales of carbon XAS spectra were calibrated to the π^* resonance of HOPG which was taken to be at 285.38 eV[2.16].

Measuring X-ray absorption can be accomplished in a number of ways. In the most pristine and true case, the transmission of x-rays through the material is measured as a function of energy, with the absorption being the difference between the incident radiation and the transmission: $I_{incident} = I_{absorption} + I_{transmission}$. However, measuring NEXAFS of surface adsorbate species in the soft x-ray regime in transmission is impractical due to the extremely short mean free path ($\sim 1 \mu\text{m}$) of the photons in this energy regime. Thus, other indirect methods such as partial fluorescence yield, total fluorescence yield, total or partial electron yield, or auger electron yield are used to measure x-ray absorption. Auger electron yield (AEY) and total electron yield (TEY) are especially useful in NEXAFS spectroscopy because of their inherent surface sensitivity.

Auger electron yield, (Fig. 2.8) is one method to measure the absorption. Electrons taken from core-levels into unoccupied states create an unstable core hole.

For light elements, there are two decay channels: an electron from an outer-core or valence level drops into this core hole, and the atom emits fluorescent photon, or an outer-core or valence electron drops into the core and transfers energy to another electron in a nearby outer-core or valence state, yielding Auger electron emission. The probability for fluorescence yield in C, N, and O is only a few percent, so Auger decay dominates[2.17]. This Auger electron is emitted with kinetic energy related to the change in energy of the first electron dropping into the core-hole, the binding energy of the ejected second electron, and the work function of the material. The Auger electrons are detected using an electron energy analyzer set to the appropriate kinetic energy, and the intensity is proportional to x-ray absorption.

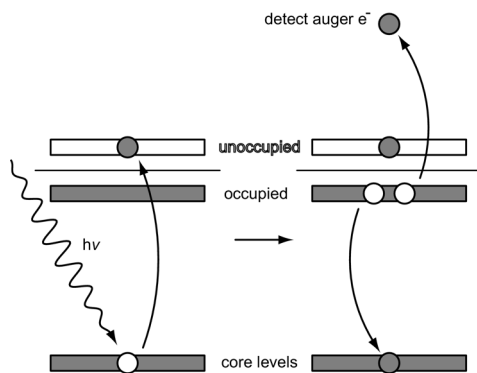


Fig. 2.8. Auger-yield energy level diagram. An x-ray excites an electron into an unoccupied orbital, and the absorption is deduced through the detection of auger electrons.

Total electron yield (Fig. 2.9) uses the relaxation of the core hole created by the absorption process. As an electron falls into the hole, it either emits an Auger electron or a photon. This electron or photon inelastically scatters creating a cascade of excited electrons leaving the sample. This current is large enough to be measured with a

picoammeter, and the electron current flowing back into the sample is proportional to absorption.

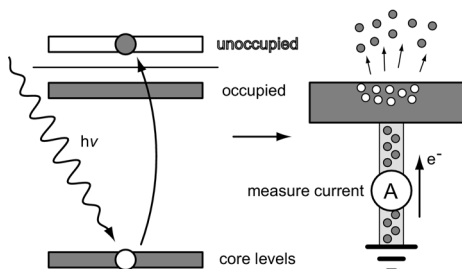


Fig. 2.9. Total electron yield diagram. The relaxation of the absorption event causes an electron cascade through inelastic scattering of auger electrons and re-absorption of fluorescence photons, detected as electron current into the sample.

Each of these techniques for measuring x-ray absorption in a surface sensitive way, Auger yield and total electron yield, has unique advantages. One of these distinctions is the difference in probing depth. The inelastic mean free path of electrons calculated for polystyrene, and experimental values for alkanethiol SAMs on gold are presented in Fig. 2.10 from references [2.18-20]. Auger electrons have kinetic energies of about 260 eV for carbon and 510 eV for oxygen, and mean free paths of 10 Å and 16 Å respectively. Thus, the Auger yield method has extremely high surface sensitivity. Alternatively, total electron yield measures electrons that have likely suffered energy losses or have been created through inelastic scattering. These lower-energy electrons statistically estimated mean free paths of escaping electrons of 35 Å [2.20] or higher, and thus total electron yield essentially uniformly probes molecular monolayers of 5 – 20 Å in thickness. Total electron yield also measures higher currents and leads to better signal to noise ratio.

Beamline optics must additionally be considered. The photon beam from the storage ring encounters various carbonaceous materials on slits, soft x-ray mirrors, and

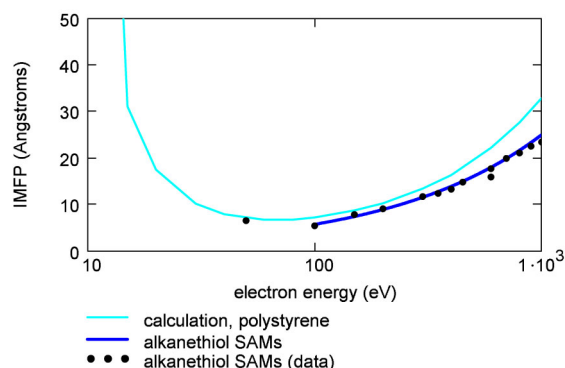


Figure 2.10. Inelastic mean free path of electrons: caculated for polystyrene, fit to data for alkanethiol SAMs on gold, and the actual data points for alkanethiols on gold, from references cited in text.

the grating, often exceeding the carbon and/or oxygen absorptivity in molecular monolayer samples. To correct for this, sample currents are divided by the total electron yield current from a clean transmissive grid with a freshly evaporated gold coating to normalize the absorption vs. flux. In this context, Auger yield offers high signal to background by primarily measuring electrons directly from Auger decay of the elements of interest. This minimizes even further the spurious carbon and oxygen structure from beamline optics. However, using Auger yield, one must be aware of photoelectrons that can enter the analyzer window.

X-ray photoelectron Spectroscopy

X-ray photoelectron spectroscopy (XPS) allows one to gain elemental and chemical information[2.21]. Photons, typically in the soft x-ray regime, are incident on

the sample at sufficient energy to excite electrons from bound states into the vacuum as depicted in Fig. 2.11. Analysis of the kinetic energy of the outgoing electrons gives rich information about the elemental composition and chemistry of the sample. When using lower photon energies that probe the valence bands and lower binding energy electrons (0-30 eV), this technique is often referred to as PES (photoelectron spectroscopy) or photoemission, and when using a lower energy excitation source, UPS (ultra-violet photoelectron spectroscopy.)

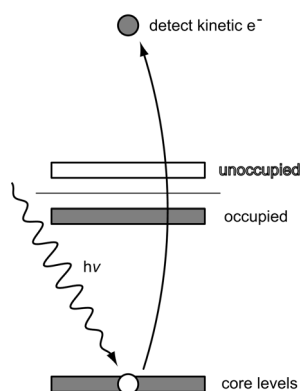


Fig. 2.11. Oversimplified energy level diagram of x-ray photoelectron spectroscopy or photoemission. Photons of constant energy excite electrons above the vacuum level. The resulting photoelectron spectrum contains peaks associated with core levels. Small "chemical shifts" occur in the binding energy of the core-levels depending on the chemical environment.

X-ray photoelectron spectra are acquired as the intensity of electrons as a function of electron kinetic energy. This binding energy of an electron is most simply related to the kinetic energy of the ejected photoelectron by $E_{\text{binding}} = h\nu - E_{\text{kinetic}}$ where E_{binding} is referenced to the vacuum level. However, for solid samples, grounding the sample to the analyzer matches the Fermi-levels and is a convenient experimental mode of operation. In this case, $E_{\text{binding}} = h\nu - E_{\text{kinetic}} - \phi_{\text{spectrometer}} + \phi_{\text{sample}}$ where the binding

energy is still referenced to the vacuum level, the electron kinetic energy is measured at the analyzer, $\phi_{spectrometer}$ is the workfunction of the spectrometer, and ϕ_{sample} is the workfunction of the sample[2.21]. Alternatively, binding energies can be referenced directly to the Fermi level, such that $E_{binding}^{Fermi} = h\nu - E_{kinetic} - \phi_{spectrometer}$. Photoelectron spectra are then plotted as a function of binding energy, and one can measure photoelectron peak binding energies independently of the x-ray source used (e.g. Al K α vs. Mg K α).

One of the most useful aspects of XPS for this work is chemical shifts for the determination of oxidation or chemical state of a given element. The measured binding energy of a given photoelectron is sensitive to both the relaxation of the core-hole as the electron is ejected (final state effects) and to the environment of the electron prior to the excitation event including the valence electron density at the atom (initial state effects.) An example of the utility of XPS in this work is measuring the purity of bonding between the sulfur headgroup and the gold substrate through chemical shifts of the S 2p photoelectrons[2.22]. In a simple example, the spin-orbit split doublet S 2p_{3/2} / S 2p_{1/2} is found to show different binding energies in different chemical environments: gold-bound thiolates at 162.0 / 163.2 eV; disulfides within alkyl chains at 163.1 / 164.3 eV; unbound thiol at 163.8 / 165.0 eV; and various oxidized sulfur species arising between 167 and 172 eV. These various photoelectron peak positions illustrate the higher binding energies of sulfur atoms in more electron-density withdrawing environments. XPS is also used in this work to investigate the chemical nature of various components within surface-attached molecules and self-assembled monolayers.

XPS can also estimate film thickness. Electrons with kinetic energies on the order of 100 eV have mean free paths of 10's of Ångströms, a similar length scale for thicknesses of SAMs and molecular monolayer adsorbates[2.19, 23-26]. Thickness is obtained by analyzing the attenuation of sulfur and gold photoelectron peaks through the layer and/or by directly comparing intensities of the carbon 1s peaks between a film of known thickness and the film in question. Angle resolved measurements also give an indication of film thickness.

X-ray photoelectron spectra were obtained both at a synchrotron source and using a laboratory source. Synchrotron-based experiments were acquired at SSRL using a PHI 15-255G CMA electron energy analyzer and its associated OEM electronics. The pass energy was set to 25 eV for XPS spectra. S 2p spectra were typically obtained at a photon energy of 280 eV, which lies just below the carbon edge. C 1s spectra were obtained at 400eV. The spectra were not normalized to the beam current. Spectra of the Au 4f peaks of the substrates were taken immediately after each sulfur and carbon spectrum to calibrate the binding energy scales. The samples were grounded to the analyzer, and the Au 4f_{7/2} photoelectron peak of substrates at 84.01 +/- 0.05 eV was used to convert the kinetic energy scales to binding energy scales. As with the absorption experiments, base pressure in the Stanford experiments were about 1.0×10^{-9} torr or less.

Other XPS measurements were acquired using a PHI Quantum 2000 laboratory-based system. One system was at The Environmental Sciences Laboratory at The Pacific Northwest National Laboratory in Richland, Washington. A second Quantum 2000 system was acquired by the Materials Science Division at Lawrence Livermore

National Laboratory during the course of these experiments. The system uses an Al $K\alpha$ monochromatic x-ray (1486.7 eV) source for excitation, which can be focused from $\sim 50\ \mu\text{m}$ to $\sim 200\ \mu\text{m}$, and in a final mode can be rastered over a 1 mm x 1 mm area. For these experiments, the source was set to either the $200\ \mu\text{m}$ or 1 mm x 1 mm spot size. The incident x-rays are nearly normal to the surface when in the default, horizontal mode, and the analyzer is about 45° from normal. The system uses a spherical section analyzer, with a 16-element multi-channel detection system. The pass energy was 23.5 eV, giving an overall energy resolution of about 0.3 eV. Energy scales for both systems are referenced to binding energies of Cu $2p_{3/2}$ at 932.72 ± 0.05 eV and Au $4f_{7/2}$ at 84.01 ± 0.05 eV. Spectra were recorded at base pressures less than 10^{-9} torr. Low energy electrons and argon ions are available for charge neutralization in insulating samples, but were not needed for molecular monolayers on gold. Instead, the highly conductive gold substrates were grounded to the analyzer so that the Fermi levels between the two were at the same potential.

Reflection-Absorption Fourier Transform Infrared Spectroscopy

Reflection-absorption Fourier-transform infrared (RA-FTIR) spectroscopy complements NEXAFS. Like many experimental techniques, IR spectroscopy is fundamentally very simple. A nearly “white” source of infrared radiation passes through a Michelson interferometer. The output beam is then directed toward the sample where the beam specularly reflects from the monolayer and substrate into the detector. The detector simply detects the intensity of the incoming infrared light as a function of the

movable mirror position in the interferometer. A Fourier transform converts the spectrum to the wavelength scale.

Any chemical bond between two different elements is slightly polarized, and all bonds at finite temperature vibrate. This vibrating charge can emit or absorb radiation in the infrared region. The sample selectively absorbs wavelengths of vibrational eigenmodes, allowing the identification of different chemical species and bonds. In reflection absorption mode, where Maxwell's equations show the electric field is perpendicular to the highly conductive surface, bonds oriented orthogonal to the surface are preferentially excited. Although this method is not directly used in this work to obtain orientational information of bonds on surfaces, one must consider this effect.

Fourier transform infrared (FTIR) spectra were obtained using a Nicolet 560 FTIR with an MCT detector and a reflecting grazing incidence accessory. The largest aperture was used (1.7cm x 2.7cm) for analysis, and either freshly H₂ flame annealed gold substrates or SAMs consisting of undecanethiol on gold were used as background references.

Summary

In summary, near-edge x-ray absorption fine structure spectroscopy (NEXAFS) directly probes the chemical nature of films through the element-specific mapping of unoccupied density of states. For second-row elements, NEXAFS polarization

dependencies powerfully determine directionality of molecular orbitals and hence the orientation of molecules on surfaces. X-ray photoelectron spectroscopy (XPS) gives chemical information through chemical shifts of photoelectron peaks, and is especially useful in determining extent of gold-thiolate bonding. As XPS is an extremely surface sensitive technique, film thickness may also be determined. Fourier Transform Infrared (FTIR) Spectroscopy through the vibrational excitation of atoms in electrically polarized bonds gives rich information about chemical species on the surface. These techniques quantitatively characterize molecular monolayers for coverage, substrate binding, chemical nature, and orientation on surfaces.

References

- 2.1. Hydrogen flame annealing follows the method described by Molecular Imaging, available online as of April 2004 at <http://www.molec.com>.
- 2.2. J. J. Rehr and R. C. Albers, *Theoretical approaches to x-ray absorption fine structure*. Reviews of Modern Physics, 2000. **72**(3): p. 621-654.
- 2.3. P. S. Bagus, K. Weiss, A. Schertel, et al., *Identification of transitions in Rydberg states in the X-ray absorption spectra of condensed long-chain alkanes*. Chemical Physics Letters, 1996. **248**: p. 129-135.
- 2.4. J. Stöhr, *NEXAFS Spectroscopy*. 1992, Berlin Heidelberg: Springer Verlag.
- 2.5. R. L. Liboff, *Introductory Quantum Mechanics 2nd Edition*. 1992: Addison-Wesley Publishing Company, Inc.
- 2.6. E. Merzbacher, *Quantum Mechanics*. third ed. 1998: John Wiley and Sons, Inc.
- 2.7. K. Gottfried, *Quantum Mechanics Volume 1: Fundamentals*. 1989: Addison-Wesley Publishing Co., Inc.
- 2.8. H. A. Bethe and E. E. Salpeter, *Quantum Mechanics of One- and Two- Electron Atoms*. 1957, Berlin - Goettingen - Heidelberg: Springer-Verlag.
- 2.9. G. Hahner, M. Kinzler, C. Wöll, and M. Grunze, *Near edge x-ray absorption fine-structure determination of alkyl chain orientation: breakdown of the 'building-block' scheme*. Physical Review Letters, 1991. **67**(7): p. 851-854.
- 2.10. S. Frey, A. Shaporenko, M. Zharnikov, et al., *Self-Assembled Monolayers of Nitrile-Functionalized Alkanethiols on Gold and Silver Substrates*. Journal of Physical Chemistry B, 2003. **107**(31): p. 7716-7725.
- 2.11. J. D. Jackson, *Classical Electrodynamics*. Third Edition ed. 1999: John Wiley and Sons, Inc.
- 2.12. G. Margaritondo, *Introduction to Synchrotron Radiation*. 1988, New York: Oxford University Press, Inc.
- 2.13. A. L. Robinson, *History of Synchrotron Radiation*, in *X-ray Data Booklet*, A. C. Thomson, et al., Editors. 2001, Lawrence Berkeley National Laboratory: Berkeley, CA.
- 2.14. G. K. Tirsell and V. P. Karpenko, *A General Purpose Sub-keV X-ray Facility at the Stanford Synchrotron Radiation Laboratory*. Nucl. Instrum. Methods, 1990. **A291**(1-2): p. 511-517.

- 2.15. M. Zharnikov and M. Grunze, *Modification of thiol-derived self-assembling monolayers by electron and x-ray irradiation: Scientific and lithographic aspects*. Journal of Vacuum Science & Technology B, 2002. **20**(5): p. 1793-1807.
- 2.16. P. E. Batson, *Carbon 1s near-edge-absorption fine structure in graphite*. Physical Review B, 1993. **48**(4): p. 2608-2610.
- 2.17. A. C. Thomson and A. Vaughan, eds. *X-ray Data Booklet*. 2001, Center for X-Ray Optics and the Advanced Light Source, Lawrence Berkeley National Laboratory: Berkeley, CA 94720.
- 2.18. J. C. Ashley, C. J. Trung, and R. H. Ritchie, *Inelastic Interactions of Electrons with Polystyrene: Calculations of Mean Free Paths, Stopping Powers, and CDSA Ranges*. IEEE Transactions on Nuclear Science, 1978. **NS-25**(6): p. 1566-1570.
- 2.19. C. L. A. Lamont and J. Wilkes, *Attenuation Length of Electrons in Self-Assembled Monolayers of n-Alkanethiols on Gold*. Langmuir, 1999. **15**: p. 2037-2042.
- 2.20. H. Ohara, Y. Yamamoto, K. Kajikawa, et al., *Effective escape depth of photoelectrons for hydrocarbon films in total electron yield measurement at the C K-edge*. Journal of Synchrotron Radiation, 1999. **6**: p. 803-804.
- 2.21. C. S. Fadley, *Basic Concepts of X-ray Photoelectron Spectroscopy*, in *Electron Spectroscopy, Theory, Techniques, and Applications*, C. R. Brundle, et al., Editors. 1978, Pergamon Press.
- 2.22. D. G. Castner, K. Hinds, and D. W. Grainger, *X-ray photoelectron spectroscopy sulfur 2p study of organic thioc and disulfide binding interactions with gold surfaces*. Langmuir, 1996. **12**(21): p. 5083-5086.
- 2.23. P. E. Laibinis, C. D. Bain, and G. M. Whitesides, *Attenuation of Photoelectrons in Monolayers of n-Alkanethiols Adsorbed on Copper, Silver, and Gold*. Journal of the American Chemical Society, 1991. **95**: p. 7017-7021.
- 2.24. C. J. Powell and A. Jablonski, *NIST Electron Effective-Attenuation-Length Database - Version 1.0*. 2001: National Institute of Standards and Technology, Gaithersburg, MD.
- 2.25. C. J. Powell and A. Jablonski, *NIST Electron Inelastic-Mean-Free-Path Database - Version 1.1*. 2001, National Institute of Standards and Technology, Gaithersburg, MD.

- 2.26. M. Zharnikov, S. Frey, K. Heister, and M. Grunze, *An extension of the mean free path approach to X-ray absorption spectroscopy*. Journal of Electron Spectroscopy and Related Phenomena, 2002. **124**(1): p. 15-24.

Chapter 3

Rapid Degradation of Alkanethiol-Based Self-Assembled Monolayers on Gold in Ambient Laboratory Conditions

Introduction

Solution exposure of alkanethiols to gold creates easily formed, relatively stable self-assembled monolayers that can be used for chemically or biologically functionalizing surfaces. The stability of such monolayers to ambient conditions is often taken for granted, however recent reports have cast the assertions into doubt by suggesting a limited shelf-life for alkanethiols on gold under e.g. biological conditions[3.1]. In this chapter, we first review some of the literature on degradation of SAMs under different types of exposure, and then present some of our own data on this important aspect of functionalized surfaces.

Early laser desorption experiments first saw oxidation features in hexadecanethiol on gold exposed to air[3.2] but did not quantitatively explore the stoichiometry and assumed (possibly incorrectly) that the oxidation was small. Other mass spectrometry desorption studies found oxidized fragments consisting of M-C-SO₂- (sulfinate) and M-C-SO₃- (sulfonate) species[3.3, 4].

Later, a method for SAM removal using ultraviolet light and the associated ozone (O₃) such light produces was presented[3.5], with the ozone allegedly oxidizing

the thiolates. Subsequently, photochemical removal methods using wavelengths insufficient to create O_3 from O_2 degraded and removed an oxygen-containing mercaptoundecanoic SAM, but were slow in removing an alkanethiol[3.6]. These studies concluded that UV light and the presence of oxygen could remove SAMs from gold surfaces.

Further exploration supports ozone is a primary culprit for SAM degradation. In one study, SAMs were exposed to N_2 , pure O_2 , H_2O , and O_2 , enclosed pressurized air, and O_3 . Only the O_3 exposed thiolates oxidized[3.7]. Another showed that the presence of light was not required to oxidize the SAMs, and that highly-crystalline, Au(111) substrates fare better than rougher surfaces with sulfur moieties oxidizing to both sulfinate and sulfonate[3.8]. Additional reports conclude that for alkanethiols, oxidation occurs extremely rapidly and efficiently through ozone exposure[3.7, 9-11].

Morphological changes have also been reported for degrading alkanethiols. Scanning tunneling microscopy measurements found thiolates oxidize first at domain boundaries. The oxidized molecules begin forming a striped phase[3.12][3.13] between pristine domains. A final “fluid” phase is both disordered and deforms the underlying gold surface[3.14].

Here, we investigate the degradation of alkanethiols on substrates used in this work under ambient, atmospheric, laboratory conditions using x-ray photoelectron spectroscopy (XPS) and x-ray absorption spectroscopy (XAS). Rapid degradation could be extremely important not only to SAMs, but to surface-attached loops and interlocking molecules on surfaces with a more exposed Au-S interface. Both the

changes in the sulfur, carbon, and oxygen chemistry and stoichiometry using XPS are quantitatively explored for five dodecanethiol-on-gold samples: (1) a freshly prepared sample, (2) a sample stored in capped vials in darkness, (3) a vial-stored sample under fluorescent lighting, (4) a sample simply exposed to air in the dark, and (5) a sample exposed to air in the light. XAS measurements were also carried out to investigate chemical and morphological changes on two samples: a fresh one, similar to sample (1) above, and a second exposed to ambient lighting and atmosphere overnight, in similar fashion to sample (5).

We find SAMs oxidize most readily when exposed to air, and that oxidation is minor if the SAMs are stored in closed, air-containing vials, compared to pristine films. As the film oxidizes, the SAMs lose their ordered, crystalline nature.

Experimental

Reagents and Materials

Reagents were purchased from commercial sources and used as received. Dodecanethiol(98%) was purchased from Aldrich. Ethanol was purchased from Aaper and used as received. Fischer vials of 15 ml in volume with polyethylene stoppers were used for sample storage/aging. Au(111) substrates were formed by evaporating 5 nm Ti and then 100nm Au on Si(100) under high vacuum. All gold substrates were hydrogen flame annealed immediately before use[3.15].

Sample Preparation

Samples were prepared by immersing freshly annealed gold substrates in 1 mmol dodecanethiol in ethanol for 24-36 hours. Samples were pulled from solution, rinsed with ethanol, and blown dry with nitrogen. Samples for XPS measurements were as follows. The first, fresh sample was immediately introduced into ultra-high vacuum and subsequently analyzed. Other samples were placed in clean 15 ml vials. The second was placed in an air-containing stoppered vial, wrapped thoroughly in aluminum foil, and labeled “vial/dark.” Sample 3 was placed in a capped vial and placed on the laboratory bench under common fluorescent lighting conditions and labeled “vial/light.” The fourth vial was left open, but wrapped in foil and placed under a foil tent to allow some ambient air flow/exchange and labeled “air/dark.” The final, fifth sample was placed in an open vial, and placed on the bench under light and labeled “air/light.” These samples were left overnight in the laboratory, and placed in UHV the next morning for analysis. For separate XAS measurements, two pristine SAMs were prepared in the same manner. The “fresh” sample was analyzed immediately, while the second was allowed to sit in the ambient laboratory conditions overnight.

Instrumentation

X-ray photoelectron spectra were recorded using a PHI Quantum 2000 XPS system with details explained in Chapter 2. The anode was set to high energy and the analyzer pass energy was set to 23.5eV while the x-ray source was set to 40 watts and a 200 micron focal spot, giving an overall resolution of about 0.3eV. Spectra were

acquired at $\sim 10^{-9}$ torr. Spectra were calibrated by setting the center of the strong Au $4f_{7/2}$ peak to 84.01 eV.

X-ray absorption spectra were recorded at VUV BL 8.2 of The Stanford Synchrotron Radiation Laboratory (SSRL, SPEAR II) at the Stanford Linear Accelerator Center under conditions for the C K-edge presented in Chapter 2. Additional XAS experiments were conducted with an energy resolution of about 0.25 eV at the Sulfur L-edge. Absorption spectra were recorded using total electron yield (TEY) and were normalized to the incident beam via the current from a clean transmissive grid with a freshly evaporated gold coating. Spectra were recorded at a base pressure of less than 1×10^{-9} torr.

Results

Sulfur 2p XPS spectra are presented in Fig. 3.1. Spectra are presented from top to bottom, for (1) the freshly prepared SAM, (2) the sample in a capped vial stored in the dark, (3) the capped vial in the light, (4) the uncapped air-exposed sample in darkness, and (5) uncapped in the light. Drastic changes occur in the sulfur spectrum. Presented are both data and best-fit line for clarity. The fit consists of S 2p spin orbit split components: S $2p_{3/2}$ (S $2p_{1/2}$) of approximate branching ratio 2:1 and energy difference of 1.2 eV. Peaks were fit with pure Gaussian functions with error function (integrated Gaussian) backgrounds centered at the peak positions. Four doublets were allowed in the fits. Full width half maxima were allowed to vary between 0.8eV and 1.3eV. The lower binding energy peaks (161.97 - 164.36eV) tended to have a smaller

width of about 0.85 eV compared to higher binding energy peaks (167.1 – 168.3 eV) at about 1.2 eV. The fresh sample contains primarily a spin orbit split doublet with S 2p_{3/2} at 161.97 eV, while the air-exposed samples contain primarily a doublet at 167.1 eV. Fit doublets and intensities are summarized in Table 3.1.

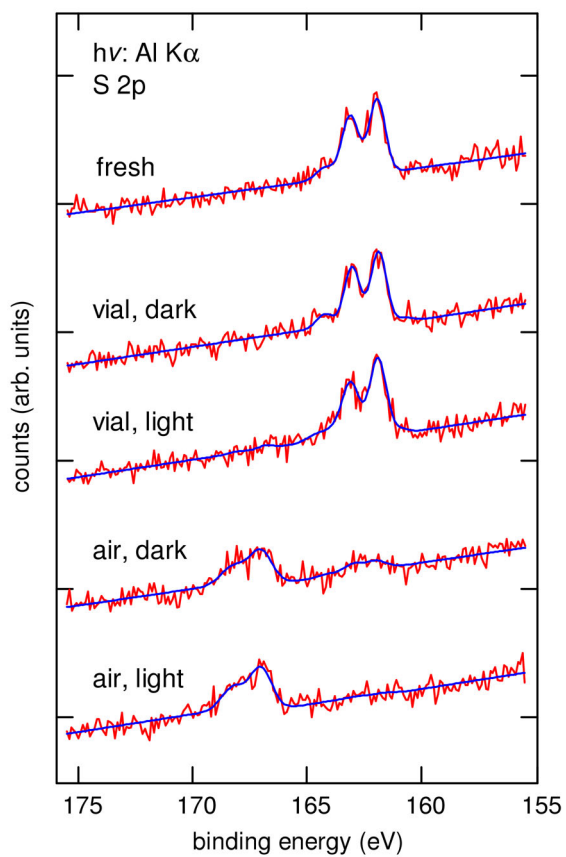


Fig. 3.1. Sulfur 2p XPS for dodecanethiol adsorbed on Au(111): see text for description.

Table 3.1: S 2p integrated intensities, pristine / air exposed SAMs
monochromatized Al K α source

S 2p _{3/2} (S 2p _{1/2}) in eV		fresh	vial, dark	vial, light	air, dark air, light
160.91(162.12)	0%	4%	4%	0%	0%
161.97(163.17)	74%	70%	73%	17%	3%
163.17(164.36)	26%	26%	20%	7%	0%
167.09(168.30)	0%	0%	3%	76%	97%

synchrotron based, $h\nu = 280\text{eV}$

S 2p_{3/2} in eV

161.9	82%	43%
163.5	10%	8%
166.8	7%	49%

error estimated at up to 10%.

Sulfur x-ray absorption spectra are presented in Fig. 3.2 for a fresh dodecanethiol sample and one exposed to ambient laboratory conditions. Changes also occur in these spectra, with two prominent peaks appearing above the absorption onset at about 175 eV and 184 eV. Pre-edge features in the fresh sample at about 167 eV are also reduced in the air-exposed sample.

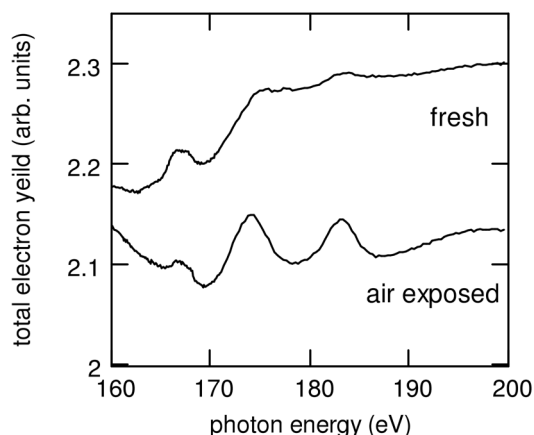


Fig. 3.2. Sulfur L-edge XAS for dodecanethiol adsorbed on Au(111) fresh sample (top) and another left on the bench overnight uncovered (bottom.)

Oxygen 1s XPS spectra are presented in Fig. 3.3 for the same series of five preparation conditions. Oxygen concentrations are below detection limits for the fresh and vial-stored samples, as expected. However, for the air-exposed samples, the appearance of oxygen strongly supports oxidation of the sulfur species in Fig. 3.1 and Fig. 3.2 in the air-exposed samples.

Carbon 1s spectra are presented in Fig. 3.4 for the series of samples. The integrated carbon signal is, as a percentage of the fresh SAM carbon intensity, 98% for the vial/dark, 97% for the vial/light, 68% for the air/dark, and 59% for the air/light. The peak position changes little for the vial stored samples, but the air exposed C1s peaks are shifted to lower binding energy by about .75eV. These air-exposed sample peaks are also slightly broader and more asymmetric.

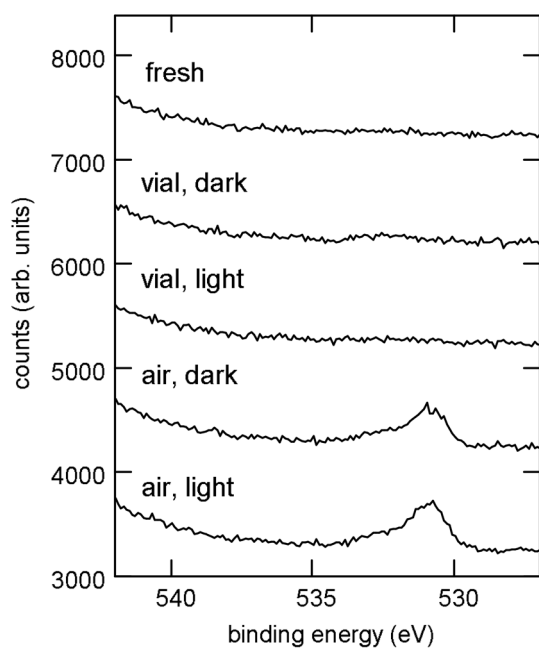


Fig. 3.3. Oxygen 1s XPS for dodecanethiol adsorbed on Au(111): see text for description.

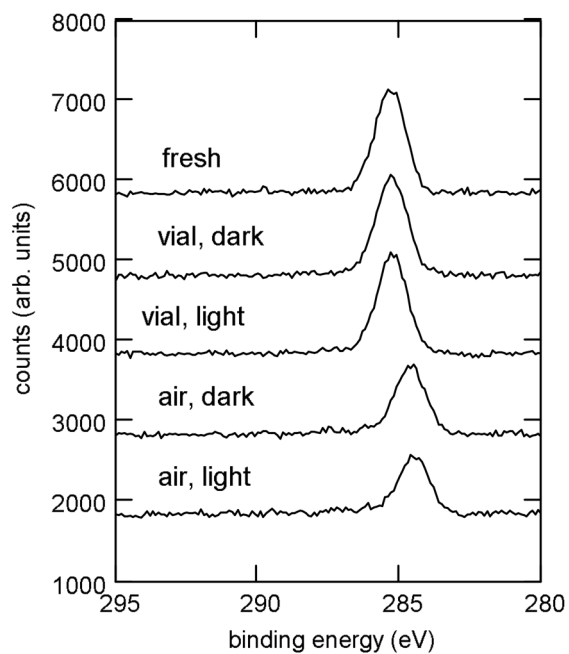


Fig. 3.4. Carbon 1s XPS for dodecantethiol adsorbed on Au(111): see text for description.

Carbon NEXAFS spectra for the freshly prepared dodecanethiol-based SAM are presented in Fig. 3.5. Features include the sharp C-H σ^* / R* features near the absorption edge at around 288 eV. Also visible are C-C σ^* and C-C' σ^* features at roughly 293 eV and 301 eV respectively. Spectra are as expected with a strong linear dichroism indicating a well-ordered, densely-packed, self-assembled monolayer with alkyl chains tilted about 35° from normal.

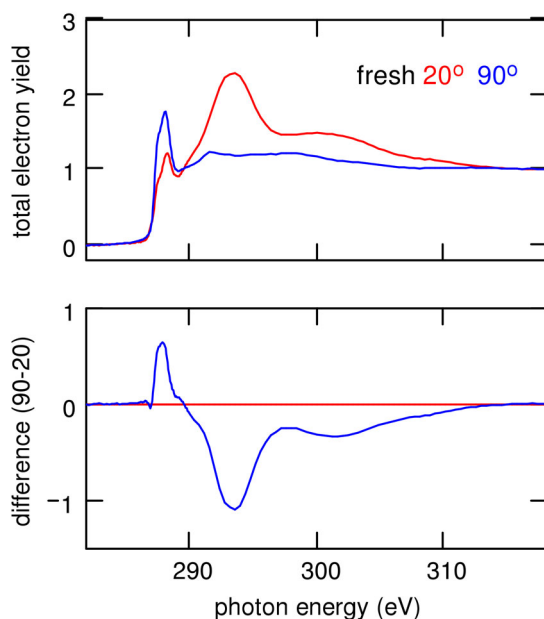


Fig. 3.5. Carbon NEXAFS for the freshly prepared and analyzed sample. Top: spectra acquired at normal (90 degrees) and grazing incidence (20 degrees.) Bottom: difference spectra.

Carbon NEXAFS spectra for the sample exposed to air, however, show different results in Fig. 3.6. The spectra continue to have a small amount of dichroism, but much less than the fresh sample. The first R* / C-H σ^* feature is attenuated, but other σ^* features look similar to the freshly prepared sample.

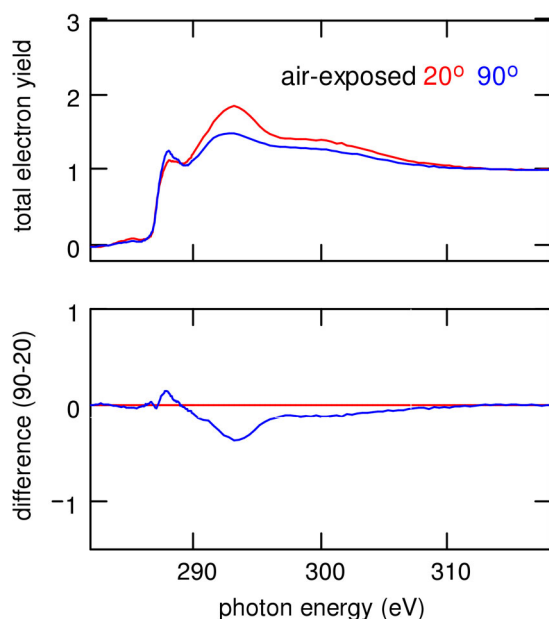


Fig. 3.6. Carbon NEXAFS for the sample exposed to air. Top: spectra acquired at normal (90 degrees) and grazing incidence (20 degrees.) Bottom: difference spectra.

Discussion

The freshly prepared samples look as expected in sulfur 2p, carbon 1s, and oxygen 1s XPS spectra. The main doublet S 2p_{3/2} peak at 161.9eV is gold-bound thiolate[3.16] indicating monolayers well-bound to the substrate. Fresh samples exhibit carbon NEXAFS dichroism consistent with well-formed SAMs.

The SAMs stored in capped vials showed small changes. Sulfur environments were similar within experimental detection limits. The carbon intensity is slightly less, indicating that a small percentage of the molecules have desorbed. This desorption may increase under exposure to light in the vial as the C1s intensity was slightly less in this case, but the difference was also within experimental error. Additionally, UV exposure and the associated ozone production may have been minimal due to the absorption of UV light by the glass vial.

For the air-exposed samples, the sulfur is oxidized, especially in the air and light exposed sample. The oxidation is seen in the S 2p XPS spectra with a decrease in the bound component and an appearance of a new doublet with S 2p_{3/2} component at 166.8 - 167.1 eV. This is sulfinate, which has been reported to have binding energy of about 166.5eV[3.8]. (Alternatively, this same reference reported also seeing sulfonate features at 168.4eV.) Stark changes in the S L-edge spectra and the appearance of O 1s peaks in air-exposed samples strongly support oxidation of the thiolate. Interestingly, the capped samples show only slight oxidation. This lends support to the idea that the process occurs through a dilute atmospheric constituent such as ozone, as reported previously[3.5, 7, 9-11]. When the ozone is depleted, the process is quenched, and the remaining gold-bound thiolates survive.

As the SAMs degrade, the sulfur and carbon photoemission features are reduced in intensity, while Au 4f peaks (not shown) increase in intensity, indicating desorption and a lower concentration of molecules left on the surface. Carbon NEXAFS spectra show similar features, indicating minimal carbonaceous contamination, but a reduction in dichroism, indicating a much less ordered film. R* / C-H σ^* features are attenuated likely due to the chemical and structural changes occurring in the molecules. Finally, shifts in energy and peak broadening in C 1s are consistent with both changes in carbon chemical environments and changes towards a less-ordered monolayer with some of the molecules possibly prostrate on the gold surface as observed with previous STM measurements[3.14].

Conclusions

We have measured S 2p, C 1s, and O 1s XPS spectra for dodecanethiol-based self-assembled monolayers (SAMs) on Au(111) both freshly prepared, and exposed to various levels of ambient laboratory conditions. Samples were removed from solutions, rinsed in ethanol, and placed in dark capped vials, capped vials under light, and under air exposure in uncapped vials in both darkness and light. Capped vial samples survive reasonably well, retaining sulfur-gold bonds and losing only a few percent of the molecules. Uncapped vials, where the SAMs are exposed to air, degrade rapidly. Sulfur features oxidize, as seen in chemical shifts of S 2p photoelectrons and the appearance of O 1s photoelectrons.

We have also measured sulfur L-edge x-ray absorption spectra, and carbon K-edge NEXAFS. Sulfur absorption spectra change upon exposure to air, consistent with XPS results indicating oxidation. Freshly prepared samples have the expected high polarization dependence from well-packed, ordered films. SAMs which have been exposed to air have some polarization dependence, but much less than fresh SAMs indicating the layer is becoming significantly less ordered.

These results have important implications for applications that depend upon the durability of SAMs under atmospheric conditions. Alkanethiols, or other organics adsorbed on gold through gold-thiolate bonding degrade rapidly exposed to air. Care must be taken to avoid SAM degradation by using freshly prepared samples, carefully storing samples in benign environments, and ensuring alkanethiolates on gold have sufficient durability for each intended application.

References

- 3.1. N. T. Flynn, T. N. T. Tran, M. J. Cima, and R. Langer, *Long-term stability of self-assembled monolayers in biological media*. *Langmuir*, 2003. **19**(26): p. 10909-10915.
- 3.2. Y. Z. Li, J. Y. Huang, R. T. Mciver, and J. C. Hemminger, *Characterization of Thiol Self-Assembled Films by Laser Desorption Fourier-Transform Mass-Spectrometry*. *Journal of the American Chemical Society*, 1992. **114**(7): p. 2428-2432.
- 3.3. J. R. Scott, L. S. Baker, W. R. Everett, et al., *Laser desorption Fourier transform mass spectrometry exchange studies of air-oxidized alkanethiol self-assembled monolayers on gold*. *Analytical Chemistry*, 1997. **69**(14): p. 2636-2639.
- 3.4. M. J. Tarlov and J. G. Newman, *Static Secondary Ion Mass-Spectrometry of Self-Assembled Alkanethiol Monolayers on Gold*. *Langmuir*, 1992. **8**(5): p. 1398-1405.
- 3.5. C. G. Worley and R. W. Linton, *Removing Sulfur from Gold Using Ultraviolet Ozone Cleaning*. *Journal of Vacuum Science & Technology A - Vacuum Surfaces and Films*, 1995. **13**(4): p. 2281-2284.
- 3.6. N. J. Brewer, R. E. Rawsterne, S. Kothari, and G. J. Leggett, *Oxidation of self-assembled monolayers by UV light with a wavelength of 254 nm*. *Journal of the American Chemical Society*, 2001. **123**(17): p. 4089-4090.
- 3.7. M. H. Schoenfisch and J. E. Pemberton, *Air stability of alkanethiol self-assembled monolayers on silver and gold surfaces*. *Journal of the American Chemical Society*, 1998. **120**(18): p. 4502-4513.
- 3.8. M. T. Lee, C. C. Hsueh, M. S. Freund, and G. S. Ferguson, *Air oxidation of self-assembled monolayers on polycrystalline gold: The role of the gold substrate*. *Langmuir*, 1998. **14**(22): p. 6419-6423.
- 3.9. K. L. Norrod and K. L. Rowlen, *Ozone-induced oxidation of self-assembled decanethiol: Contributing mechanism for "photooxidation"?* *Journal of the American Chemical Society*, 1998. **120**(11): p. 2656-2657.
- 3.10. Y. M. Zhang, R. H. Terrill, T. A. Tanzer, and P. W. Bohn, *Ozonolysis is the primary cause of UV photooxidation of alkanethiolate monolayers at low irradiance*. *Journal of the American Chemical Society*, 1998. **120**(11): p. 2654-2655.

- 3.11. Y. Zhang, R. H. Terrill, and P. W. Bohn, *Ultraviolet photochemistry and ex situ ozonolysis of alkanethiol self-assembled monolayers on gold*. Chemistry of Materials, 1999. **11**(8): p. 2191-2198.
- 3.12. Striped phases often appear during the formation (or in this case degradation) of self-assembled monolayers. They consist of molecules prostrate on the surface self-organized into parallel rows. They appear as "stripes" in STM measurements as seen in the two other references listed in this paragraph.
- 3.13. G. E. Poirier and E. D. Pylant, *The Self-Assembly Mechanism of Alkanethiols on Au(111)*. Science, 1996. **272**: p. 1145.
- 3.14. G. E. Poirier, T. M. Herne, C. C. Miller, and M. J. Tarlov, *Molecular-scale characterization of the reaction of ozone with decanethiol monolayers on Au(111)*. Journal of the American Chemical Society, 1999. **121**(41): p. 9703-9711.
- 3.15. Hydrogen flame annealing follows the method described by Molecular Imaging, available online as of April 2004 at <http://www.molec.com>
- 3.16. D. G. Castner, K. Hinds, and D. W. Grainger, *X-ray photoelectron spectroscopy surfur 2p study of organic thioc and disulfide binding interactions with gold surfaces*. Langmuir, 1996. **12**(21): p. 5083-5086.

Chapter 4

Chemically Transformable Configurations of Mercaptohexadecanoic Acid Self-Assembled Monolayers Adsorbed on Au(111)*

Abstract

Carboxyl-terminated self-assembled monolayers (SAMs) are commonly used in a variety of applications, with the assumption that the molecules form well-ordered monolayers. In this work, NEXAFS verifies well ordered monolayers can be formed using acetic acid in the solvent. Disordered monolayers with unbound molecules present in the film result using only ethanol. A stark reorientation occurs upon deprotonation of the endgroup by rinsing in a KOH solution. This reorientation of the endgroup is reversible with tilted over, hydrogen bound carboxyl groups while carboxylate ion endgroups are upright. C1s photoemission shows that SAMs formed and rinsed with acetic acid in ethanol have protonated end groups, while SAMs formed without acetic acid have a large fraction of carboxylate-terminated molecules.

* Reproduced in part, with permission, from reference [4.1]: Langmuir, 2004, 20, 2746-2752. Copyright 2004, American Chemical Society.

Introduction

Surface modification by using ω -functionalized alkanethiols is the most simple way to create chemically or biologically functionalized surfaces. Often, well ordered monolayers of molecules beyond alkanethiols with such functionalizations are non-trivial to achieve[4.2, 3].

Carboxyl terminated self-assembled monolayers (SAMs) are one basis for chemically and biologically functionalized surfaces. Often this type of SAM is used as a starting point for fabricating biologically active surfaces in order to immobilize proteins or other biological agents for further analysis[4.4, 5]. Carboxylate terminated SAMs have also recently been mechanically and conformationally switched on a surface[4.6]. The molecules were deposited in dilute fashion on a surface and the carboxylate end-group was electrochemically pushed toward or away from the electrode with the associated conformational and hydrophilic-to-hydrophobic surface property changes. Understanding of biological molecules attached to SAMs and molecular mechanically switching devices requires a fundamental understanding of how these monolayers form, and their conformations upon formation.

Results have varied on the structure of carboxyl-terminated SAMs. One of the first comprehensive studies of the structure and formation of mercaptohexadecanoic acid adsorbed on Au(111) observed well-packed self-assembled monolayers through the sharpness of Fourier-transform infrared (FTIR) CH_2 stretching peaks and determined the chains had a tilt-angle similar to that of alkanethiols through their relative intensities[4.7]. This study also found the polar angle of the carbonyl bond to be about 66° from the normal with the OH group exposed to the surface. Subsequent, near-edge

x-ray absorption fine structure (NEXAFS) measurements showed a high degree of disorder in these carboxyl-terminated alkyl-thiols[4.8, 9]. However, recent FTIR studies, with a strict protocol for SAM preparation, confirm the ordering in these SAMs that is highly dependent on the state of the carboxyl group[4.10].

In this paper, ordering in carboxyl terminated SAMs under the proper preparation conditions of a solution containing acetic acid is verified with NEXAFS and the orientation of the carboxyl plane is determined. These monolayers are compared to those prepared with the standard protocol of dissolving the SAM precursors in ethanol only. This work reports the first observation of stark conformational changes occurring in the end-group upon deprotonation to carboxylate.

Experimental

Reagents and Materials

Reagents were purchased from commercial sources and used as received. 16-mercaptohexadecanoic acid (90%), hexadecanethiol (95%) and ethanol (99.9%) were purchased from Aldrich. Acetic acid (HPLC grade, 99.7%) was purchased from VWR. Au(111) substrates were formed by evaporating 5 nm Ti and then 100nm Au on Si(100) under high vacuum. All gold substrates were hydrogen flame annealed immediately before use[4.11].

Sample Preparation

Solutions were prepared as per Arnold et al.[4.10] by dissolving mercaptohexadecanoic acid into 5% (by volume) acetic acid/ethanol to reach the

desired concentrations between 1 μ mol and 1 mmol. The ethanol-only sample and corresponding methyl-terminated SAM were prepared by diluting the mercaptohexadecanoic acid into ethanol. Gold substrates were placed in these solutions for 24-36 hours. Each sample was then removed and rinsed with its pure solvent: 5% acetic in ethanol for samples formed in 5% acetic/ethanol, or pure ethanol for samples made without acetic acid in solution. Samples were immediately introduced into ultra-high vacuum. The samples presented here for acetic/ethanol prepared SAMs were formed concurrently under the same ambient conditions.

Instrumentation

X-ray absorption spectra were taken at VUV BL 8.2 of The Stanford Synchrotron Radiation Laboratory (SSRL, SPEAR II) at the Stanford Linear Accelerator Center with conditions as described in Chapter 2[4.12]. Absorption spectra were recorded simultaneously using both total electron yield (TEY) and Auger electron yield (AEY). The degree of linear polarization was measured with highly-oriented pyrolytic graphite (HOPG) to be about 88% in the plane of the storage ring during these experiments. The energy scales of carbon XAS spectra were calibrated to the π^* resonance of HOPG set to 285.38 eV[4.13].

X-ray photoelectron spectra were obtained using a PHI 15-255G CMA electron energy analyzer with pass energy was set to 25 eV. Spectra of the Au 4f_{7/2} (84.01 \pm 0.05 eV) were acquired immediately after each sulfur and carbon spectra to calibrate and convert the kinetic energy scales to binding energy scales. Fourier-transform infrared (FTIR) spectra were obtained using specifications outlined in Chapter 2.

Results and Discussion

Changes in the ordering of carboxyl-terminated SAMs were investigated using films prepared in various environments. SAMs were prepared in concentrations of 1 μ mol to 1 mmol with 5% acetic acid in ethanol and rinsed in clean solvent. For comparison, SAMs were prepared with only ethanol as the solvent and rinse. Samples were also prepared by using the acetic acid/ethanol solvents and then rinsed in a basic solution (results presented here are a KOH solution, pH 12-13) to investigate how deprotonation affects the SAM.

Carbon K-edge absorption spectra are displayed in Fig. 4.1. Total electron yield measurements are in the left panes and Auger yield are in the right panes. The topmost panels are the average of 4 samples (0.001, 0.01, 0.1, and 1 mmol) formed and rinsed in 5% acetic acid in ethanol. Middle panels contain spectra from a sample formed from a solution of 1 mmol mercaptohexadecanoic acid in only ethanol. The lower panels contain spectra from a sample formed in acetic acid / ethanol, but later rinsed in a KOH solution. Two features at 297 and 300 eV in the KOH rinsed spectra are due to the potassium L-edge rather than the carbon in the monolayer. All other features are common to all the spectra. The first two resonances near the ionization potential at 287.65 and 288.10 eV are Rydberg states associated with alkyl (CH_2) chains[4.14]. The next feature at 288.7eV is a transition into a π^* state of the carboxyl functionalization of the SAM. The two broad features above the edge are primarily C-C σ^* transitions.

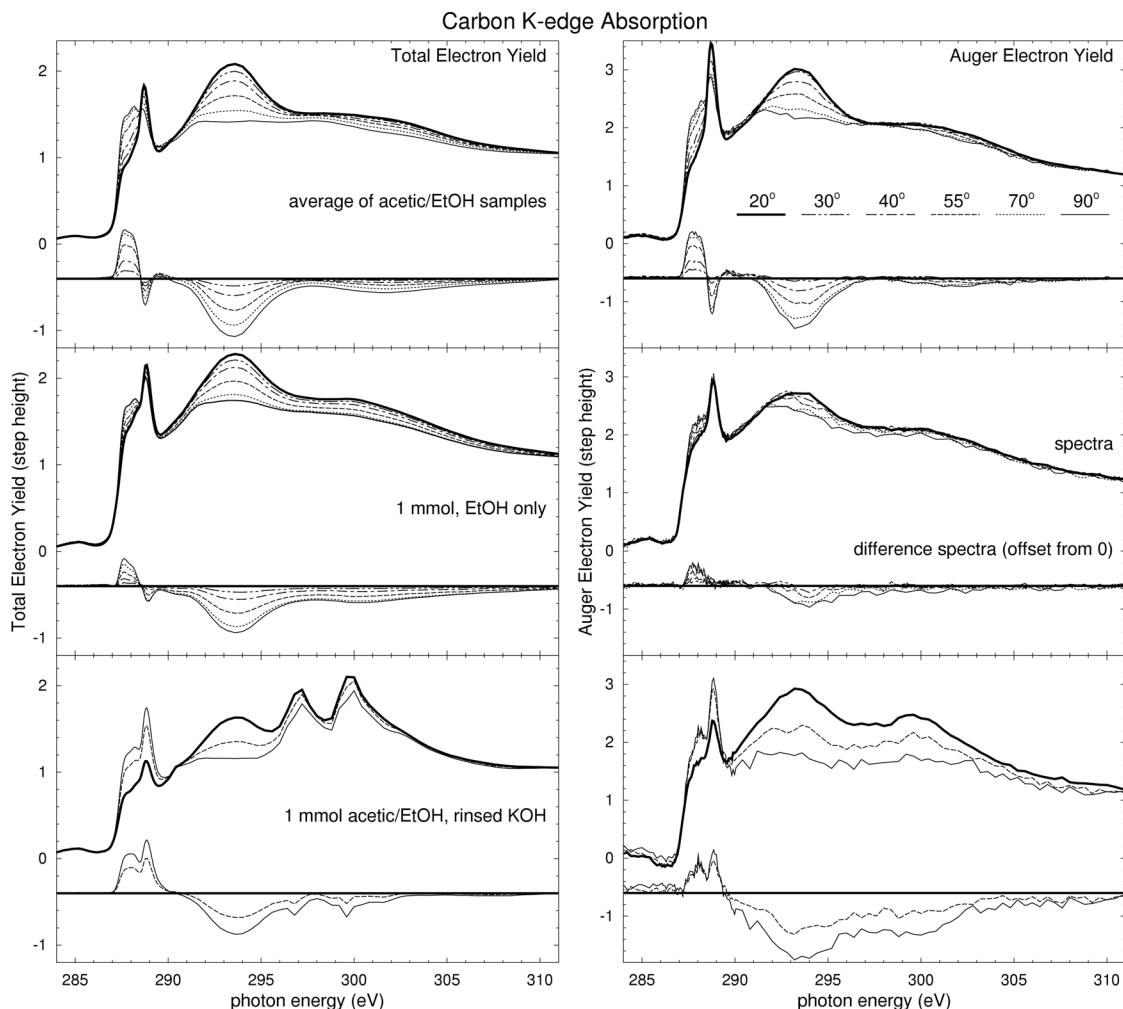


Fig. 4.1. Carbon K-edge total-electron and Auger-electron yield spectra and difference spectra. Top panes: average of 0.001, 0.01, 0.1 and 1mmol samples formed and rinsed in acetic acid / ethanol. Middle panes: 1mmol sample formed in ethanol only. Lower panes: Sample formed in acetic/ethanol, but then subsequently rinsed in KOH; peaks due to K 2p photoelectrons are visible in TEY spectra, and AEY measurements have a higher S/N due to shorter acquisition time.

Carbon polarization dependencies can be computed using these five resonances that have large intensity changes: the Rydberg like states, which have transition dipole moments along the C-H bonds, the carboxyl π^* feature that has a transition dipole moment perpendicular to the O-C=O plane, and the C-C and C-C' σ^* which have a transition dipole moment along the alkyl chain molecular axis[4.14, 15]. The CH₂

Rydberg and carboxyl π^* resonances overlap and, in many cases have opposite polarization dependencies. This excludes directly using the commonly used difference method to analyze these resonances as the magnitude of the overlapping peaks in difference spectra partially cancel each other. However, deconvolution of these resonances via simultaneous raw and difference spectra peak fitting allows accurate determination of the orientation of the molecule as described in Chapter 2.

Table 4.1 lists angles found through analysis of the polarization dependencies. Alkyl R^* , σ^* , and carboxyl π^* were found using the slopes and offsets of regressions from Equations (2.22) and (2.23), while angles found through Equations (2.24) and (2.25) are listed diff. R^* , diff σ^* , and diff. π^* . Few differences occur between the SAMs formed in acetic acid solutions, with a possible slight decrease in polar angle of the alkyl chains with increasing concentration. The carboxyl group is tilted over such that the polar angle of the vector perpendicular to the O-C=O plane is roughly 45° from the surface normal.

Table 4.1: Carbon tilt angles between alkyl chain (or O-C=O plane normal) and sample normal for all samples.

	0.001	0.01	0.1	1		
	mmol	mmol	mmol	mmol	EtOH	KOH ^b
alkyl R^*	39.9	39.7	40.0	38.4	48.4	39.1
diff. R^*	39.9 ^a	40.2	41.2	39.8	46.8	
alkyl σ^*	41.6	41.1	39.1	38.0	46.9	
diff. σ^*	41.6 ^a	41.8	38.2	34.7 ^c	36.0 ^c	
carboxyl π^*	44.6	45.5	44.2	44.5	52.1	71.6
diff. π^*	44.6 ^a	45.0	43.8	44.9	48.6	

^a Used as a reference for difference spectra.

^b High uncertainty or unavailable due to potassium features in the C K-edge spectra.

^c Diff. σ^* underestimates tilt due to thicker layers in 1 mmol and EtOH samples.

In the case without acetic acid, the angle derived for the O-C=O plane (52°) is approaching the magic angle, indicating randomly oriented carboxyl groups. In this case, the alkyl-chain is also significantly less ordered with a tilt angle of on average $47-8^\circ$. In additional samples prepared without acetic acid, alkyl-chain results were irreproducible but generally less ordered than samples prepared with acetic acid. In the KOH-rinsed sample, the potassium $L_{2,3}$ edge appears above the carbon edge and make normalization of the spectra difficult. However, these spectra in Fig. 4.1 indicate a polarization dependence for the carboxyl group that is opposite that of the acetic acid rinsed SAMs, with roughly 70° between the carboxyl plane normal and sample normal. This indicates a reorientation of the end group. Analysis of oxygen K-edge absorption spectra determine this angle as well as confirm tilt angles found with carbon spectra.

Oxygen K-edge AEY absorption spectra are displayed in Fig. 4.2, and calculated orientational angles presented in Table 4.2. For these samples, Auger yield was advantageous and chosen over TEY because of the much better signal to background ratio and enhanced surface sensitivity. However, Auger-yield also has disadvantages in a lower signal to noise ratio, and the possibility that low binding-energy photoelectrons could sweep through the kinetic energy window of the analyzer and hence, exist in the spectra. The analyzer was set on the oxygen Auger peak and such that Au 4f photoelectron peaks appear well above the absorption edge, while Au valence photoelectron peaks are well below the absorption onset. Unfortunately and unavoidably, the much weaker Au 5p electrons contribute slightly to the intensity of the O K-edge absorption spectra at about 566eV. Also, K photoelectrons appear in the spectra rinsed in KOH.

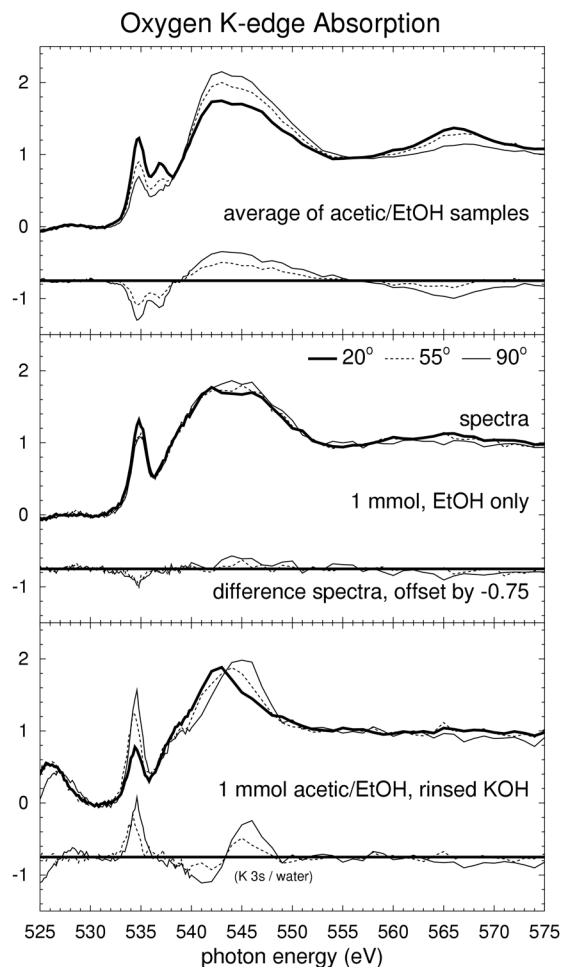


Fig. 4.2. Oxygen K-edge Auger-electron yield spectra and difference spectra. The top pane is average obtained from the acetic/EtOH prepared samples, the middle pane spectra are from a 1mmol sample prepared and rinsed in EtOH only, and the bottom panel spectra are from the KOH rinsed sample.

All Oxygen spectra have 1 or 2 pre-edge features at 535eV - 537eV. The first is assigned to transitions from the O1s into π^* orbitals of the carboxyl group. The second feature at 537eV is attributed to a small amount of extra acetic acid left on the surface as it appears only in samples that have been exposed to acetic acid. The broad feature just above the edge from 540-553eV is assigned to a σ^* resonance between the C and O atoms. The third feature centered about 566eV from 561eV - 574eV has intensity

contributed from both another σ^* feature and the Au 5p photoelectrons that have entered the kinetic energy window of the analyzer.

The top pane of Fig. 4.2 depicts O K-edge polarization dependencies of samples prepared with 1 mmol to 1 μ mol of mercaptohexadecanoic acid in 5% acetic acid / ethanol. All have polarization dependence with the π^* feature largest at grazing incidence and the σ^* feature largest at normal incidence, indicating the normal to the carboxyl group is tilted about 45° from the substrate normal.

The middle pane of Fig. 4.2 shows the polarization dependence of a sample that did not have acetic acid present during the formation or rinsing of the SAM; it lacks the polarization dependence of the previous samples. The angles calculated and listed in Table 4.2 (50.8° - 51.9°) approach the magic angle of $\arcsin\left(\sqrt{\frac{2}{3}}\right)$, indicating a large distribution of orientations for the carboxyl groups and a lack of ordering. In samples prepared in this manner, Ca and Na and other ions were observed in the samples in absorption and photoemission spectra indicating carboxylate-terminated molecules exist on the surface.

The bottom pane of Fig. 4.2 shows the polarization dependence of a sample that was prepared in acetic acid, but then was rinsed in a KOH solution. Spurious features appear that are not due to the carboxyl oxygen atoms at 526 and 544 eV. These features are presumably from the K 3p (17 eV) and K 3s (33 eV) photoelectrons as well as a small amount of water that now is on the surface seen in subsequent FTIR spectra. The polarization dependence, with π^* feature most intense at normal incidence, is opposite that of the samples formed with acetic in solution. This π^* feature indicates the normal to the O=C-O plane is on average 64° from normal meaning the carboxyl groups are

"upright." K photoelectrons hinder determining an angle using the σ^* resonance of the C-O bonds. This effect is reversible as subsequent protonation returns the endgroup to its previous tilted over state and deprotonation to its upright state, however, data may indicate gradual degradation of the film through multiple rinsings.

Table 4.2: Oxygen tilt angles (between the O-C=O plane normal and sample normal) for all samples.

	0.001	0.01	0.1	1		
	mmol	mmol	mmol	mmol	EtOH	KOH
π^*	45.2	44.6	44.5	46.7	51.9	63.6
diff. π^*	45.2 ^b	44.8	45.4	44.7	51.0	65.5
σ^*	41.6	43.3	40.0	41.6	50.8	^a
diff. σ^*	41.6 ^b	43.5	39.3	45.6	51.4	^a

^a σ^* not available on KOH rinsed sample due to K photoelectron peaks.

^b Used as difference spectra reference sample.

The possibility that this effect could be due to odd-even effects was also investigated by comparing the mercaptohexadecanoic acid based SAMs with those formed from mercaptoundecanoic acid.[4.7] For the mercaptoundecanoic acid based SAM, the tilt of the alkyl chain (42.0°) and carboxyl angle (45.5°) are similar to the angles of the mercaptohexadecanoic acid. This indicates that the orientation of the carboxyl group is not due to odd-even effects and that dimerization of the endgroups is the primary reason for the orientation of the carboxyl group.

In order to further investigate these films and confirm their composition, C 1s photoelectron spectroscopy was used. Carbon photoelectron spectra appear in Fig. 4.3.

The most intense feature in all spectra is due to the alkyl-chain of the molecules. The feature completely resolved from this peak at higher energy is due to the endmost carbon atom of the carboxyl group, and this feature is shifted to higher energy due to the electron-withdrawing effect of its binding to two oxygen atoms. The asymmetry of the alkyl peak with intensity to higher binding energy may be due to the carbon atoms near the carboxyl group and/or attributed to recently observed differences in alkyl-chain orbital overlap.[4.16]

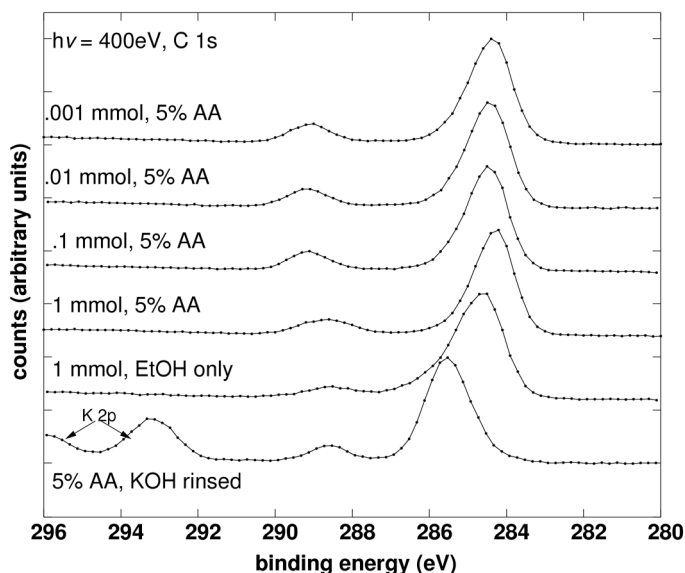


Fig. 4.3. Carbon 1s photoelectron spectra of the series of samples prepared in 5% acetic acid in EtOH, the sample prepared in only EtOH, and the sample rinsed in KOH.

The peak associated with the carbon within the carboxyl group indicates the chemical state of this functionalized surface. This peak is similar for concentrations between 0.001 mmol and 1 mmol formed and rinsed in 5% acetic acid in ethanol, with a peak at 289.09-289.15 eV, full width at half-maximum (fwhm) 1.17-1.25 eV. For the 1 mmol sample, the peak is broadened (fwhm 1.60 eV) and shifted to lower binding

energy at 288.66 eV. The ethanol-only sample peak is broadened and shifted even more, with fwhm 1.65eV at 288.48eV, while the KOH rinsed sample exhibits a sharp peak with fwhm 1.12eV at 288.56eV. This shift to lower binding energy is due to deprotonation of the carboxyl group to carboxylate with the accompanying charge transfer from the cation and screening of the endgroup. The alkyl peak is asymmetric in the acetic acid/ethanol samples with sharper onset at lower binding energy. In the ethanol only sample, the alkyl peak is broadened, likely due to the non-uniform environments the alkyl-units experience in this disordered film. In the sample rinsed in KOH, the alkyl peak is shifted to a higher binding energy relative to the gold substrate, presumably due to the substrate and alkyl-chain screening the K cations at the surface.

This result is also shown in FTIR spectra as seen in Fig.4.4.4. The SAM formed with acetic acid shows clear carbonyl stretches from 1740-1700 cm^{-1} . These have been previously shown to be from single, non-hydrogen bound carboxyl groups at $\sim 1740 \text{ cm}^{-1}$, carboxyl groups hydrogen bound with one hydrogen bond or hydrogen bonds to two different neighboring molecules at $\sim 1720 \text{ cm}^{-1}$, and completely dimerized carboxyl groups with two hydrogen bonds to one neighboring molecule at $\sim 1700 \text{ cm}^{-1}$. [4.7, 10, 17, 18] The acetic-formed SAMs show a mixture of dimerizations. For the case where the SAM is formed with only ethanol as the solvent, these peaks are reduced, especially those associated with single non-hydrogen bound groups or those with one hydrogen bond. The carboxylate band (1450 cm^{-1}) is much larger, while one associated with water (1600 cm^{-1}) also appears. This indicates that the ethanol-only sample carboxyl groups exist as highly dimerized pairs and carboxylates.

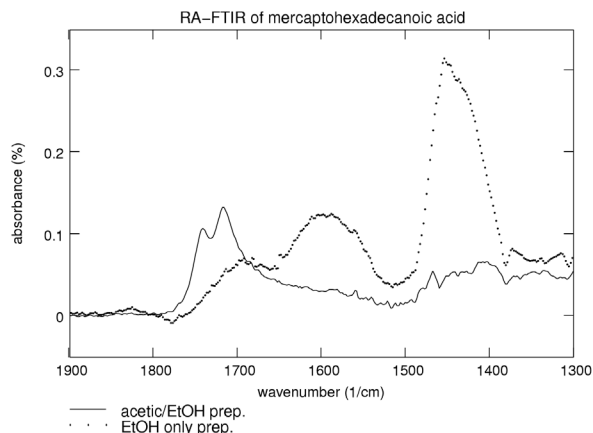


Fig.4.4. Reflection-absorption Fourier-transform infrared (FTIR) spectra of mercaptohexadecanoic acid films on Au(111) formed with 5% acetic acid in ethanol (solid line) and layers formed with only ethanol.

Sulfur photoelectron spectra were used to determine attachment of the molecules to the substrate. Monolayers formed with carboxyl-terminated alkanethiols were never completely free of unbound thiol. There is a dependence of the relative intensities vs. concentration as shown in Fig. 4.5. The percentage of unbound thiol is estimated using a mean free path of electrons of 5.5\AA for this kinetic energy range and material[4.19-22]. There is a slight decrease in unbound sulfur with decreasing concentration. This occurs for two reasons: There is a higher relative concentration of acetic acid to mercaptohexadecanoic acid in the solution, and there is hydrogen bonding in the molecules, and a molecule hydrogen bound to acetic acid rather than another long alkyl-chain molecule will be more accessible to the surface, especially at lower concentration (kinetic effects). The improved film at lower concentration also indicates that this film is most likely closest to a true monolayer of molecules. In the ethanol only sample, a large unbound intensity concentration indicates that there are many unbound molecules

in this sample and that using only ethanol for the formation and rinsing of the SAM is not sufficient to form a true monolayer.

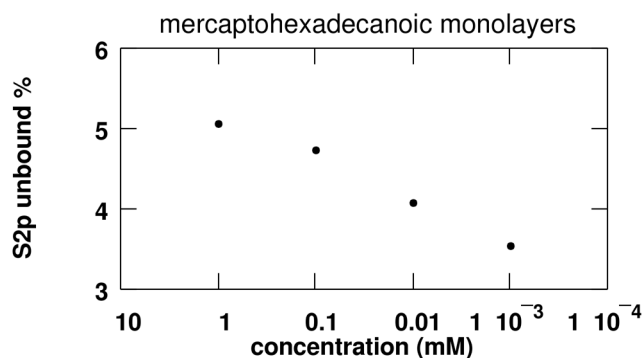


Fig. 4.5. The percentage of unbound thiol intensity in the S 2p spectra measured with photon energy of 280 eV. Unbound thiol increases with increasing molecule concentration.

Conclusions

The various conformations of carboxyl-terminated alkylthiols are summarized in Fig. 4.6. Well-ordered, carboxyl terminated self-assembled monolayers of mercaptohexadecanoic acid on Au(111) can be formed by adding acetic acid to the ethanol solution. This paper conclusively shows well ordered films measured using NEXAFS, complementing recent FTIR results[4.10]. Carbon K-edge absorption features reveal an alkyl chain ordered upright to the surface and tilted about 39° from normal. In addition, the carboxyl group normal is tilted about 45° from the surface normal, and this is confirmed with analysis of the Oxygen K-edge π^* and σ^* features. Molecules not bound to the surface (3-5%) exist in the layers, and are not expected to significantly effect NEXAFS results. This ratio of unbound sulfur to bound sulfur decreases with decreasing concentration. The decrease is due to the higher relative

concentration of acetic acid to the molecules in solution ensuring protonated carboxyl endgroups, and due to higher accessibility of the single molecules to the surface compared to large long-chain molecules dimerized to each other.

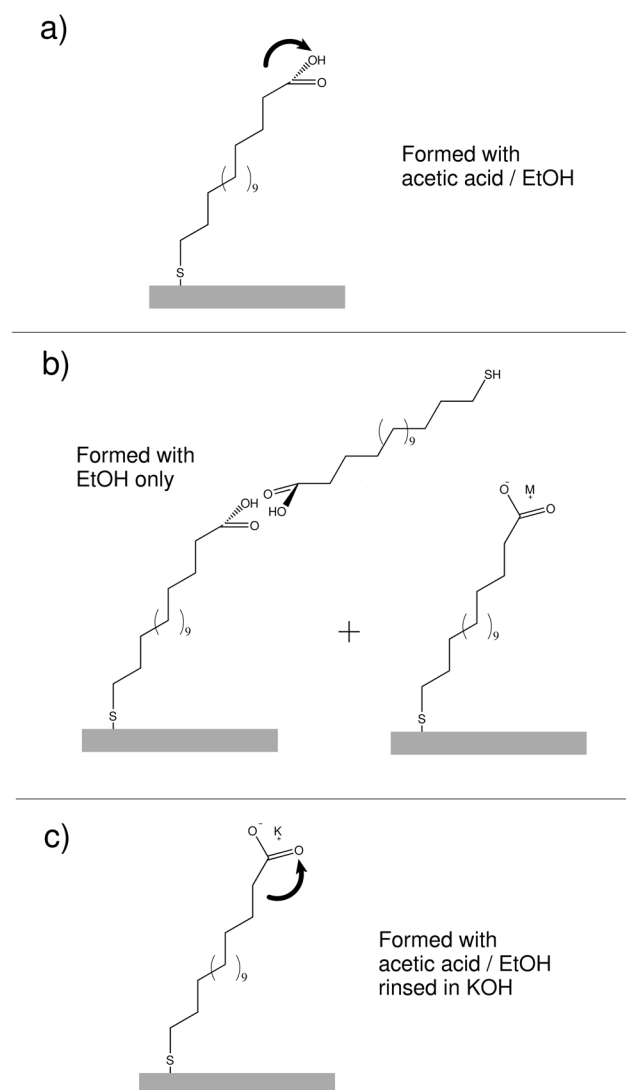


Fig. 4.6. Schematic representation of orientation of terminating endgroup of mercaptohexadecanoic acid on gold. a) Formed with acetic acid. b) Formed in ethanol only. c) Monolayer formed with acetic acid, but then rinsed in KOH solution.

When carboxyl-terminated alkyl-thiols are adsorbed on gold from the commonly used method of dissolving the molecules in ethanol, Carbon K-edge absorption spectra reveal a monolayer that shows less order within the alkyl chains. C K-edge NEXAFS also has little polarization dependence in the carboxyl σ^* peak, which indicates nearly randomly oriented carboxyl groups. FTIR spectra and C1s photoemission indicate that much of the endgroups are actually carboxylate, while S 2p photoemission spectra show a large fraction of unbound molecules on the surface. Electrostatically charged endgroups and dimerized pairs of molecules hinder SAM formation in this case.

A stark conformational change occurs in the carboxyl group of well-formed monolayers upon exposure to nonvolatile basic solutions. Here, exposure to KOH causes the carboxyl group to be oriented much more upright, indicating carboxyl group orientation chemical switchability within these films. Carbon and Oxygen K-edge spectra indicate the normal to the carboxyl group plane changes from an average of 45 degrees to about 64-72°[4.23].

References

- 4.1. T. M. Willey, A. L. Vance, T. van Buuren, et al., *Chemically transformable configurations of mercaptohexadecanoic acid self-assembled monolayers adsorbed on Au(111)*. Langmuir, 2004. **20**(7): p. 2746-2752.
- 4.2. A. L. Vance, T. M. Willey, T. van Buuren, et al., *XAS and XPS characterization of a surface-attached rotaxane*. Nano Letters, 2003. **3**(1): p. 81-84.
- 4.3. A. L. Vance, T. M. Willey, A. J. Nelson, et al., *XAS and XPS Characterization of Monolayers Derived from a Dithiol and Structurally Related Disulfide-Containing Polyamides*. Langmuir, 2002. **18**(21): p. 8123-8128.
- 4.4. N. Patel, M. C. Davies, M. Hartshorne, et al., *Immobilization of protein molecules onto homogeneous and mixed carboxylate-terminated self-assembled monolayers*. Langmuir, 1997. **13**(24): p. 6485-6490.
- 4.5. N. Patel, M. C. Davies, R. J. Heaton, et al., *A scanning probe microscopy study of the physisorption and chemisorption of protein molecules onto carboxylate terminated self-assembled monolayers*. Applied Physics A - Materials Science & Processing, 1998. **66**: p. S569-S574.
- 4.6. J. Lahann, S. Mitragotri, T.-N. Tran, et al., *A reversibly Switching Surface*. Science, 2003. **299**: p. 371-374.
- 4.7. R. G. Nuzzo, L. H. Dubois, and D. L. Allara, *Fundamental-Studies of Microscopic Wetting on Organic-Surfaces .I. Formation and Structural Characterization of a Self-Consistent Series of Polyfunctional Organic Monolayers*. Journal of the American Chemical Society, 1990. **112**(2): p. 558-569.
- 4.8. O. Dannenberger, K. Weiss, H. J. Himmel, et al., *An orientation analysis of differently endgroup-functionalized alkanethiols adsorbed on Au substrates*. Thin Solid Films, 1997. **307**: p. 183-191.
- 4.9. H. J. Himmel, K. Weiss, B. Jäger, et al., *Ultrahigh Vacuum Study on the Reactivity of Organic Surfaces Terminated by OH and COOH Groups Prepared by Self-Assembly of Functionalized Alkanethiols on Au Substrates*. Langmuir, 1997. **13**: p. 4943-4947.
- 4.10. R. Arnold, W. Azzam, A. Terfort, and C. Wöll, *Preparation, Modification, and Crystallinity of Aliphatic and Aromatic Carboxylic Acid Terminated Self-Assembled Monolayers*. Langmuir, 2002. **18**(10): p. 3980-3992.
- 4.11. Hydrogen flame annealing follows the method described by Molecular Imaging, available online as of April 2004 at <http://www.molec.com>.

- 4.12. G. K. Tirsell and V. P. Karpenko, *A General Purpose Sub-keV X-ray Facility at the Stanford Synchrotron Radiation Laboratory*. Nucl. Instrum. Methods, 1990. **A291**(1-2): p. 511-517.
- 4.13. P. E. Batson, *Carbon 1s near-edge-absorption fine structure in graphite*. Physical Review B, 1993. **48**(4): p. 2608-2610.
- 4.14. P. S. Bagus, K. Weiss, A. Schertel, et al., *Identification of transitions into Rydberg states in the X-ray absorption spectra of condensed long-chain alkanes*. Chemical Physics Letters, 1996. **248**(3-4): p. 129-135.
- 4.15. G. Hähner, M. Kinzler, C. Wöll, et al., *Near Edge X-Ray-Absorption Fine-Structure Determination of Alkyl-Chain Orientation - Breakdown of the Building-Block Scheme*. Physical Review Letters, 1991. **67**(7): p. 851-854.
- 4.16. K. Heister, L. S. O. Johansson, M. Grunze, and M. Zharnikov, *A detailed analysis of the C 1s photoemission of n-alkanethiolate films on noble metal substrates*. Surface Science, 2003. **529**(1-2): p. 36-46.
- 4.17. E. L. Smith, C. A. Alves, J. W. Anderegg, and M. D. Porter, *Deposition of Metal Overlayers at End-Group-Functionalized Thiolate Monolayers Adsorbed at Au. I. Surfaced and Interfacial Chemical Characterization of Deposited Cu Overlayers at Carboxylic Acid-Terminated Structures*. Langmuir, 1992. **8**: p. 2707-2714.
- 4.18. Y. T. Tao, G. D. Hietpas, and D. L. Allara, *HCl vapor-induced structural rearrangements of n-alkanoate self-assembled monolayers on ambient silver, copper, and aluminum surfaces*. Journal of the American Chemical Society, 1996. **118**(28): p. 6724-6735.
- 4.19. C. J. Powell and A. Jablonski, *NIST Electron Effective-Attenuation-Length Database - Version 1.0*. 2001: National Institute of Standards and Technology, Gaithersburg, MD.
- 4.20. C. J. Powell and A. Jablonski, *NIST Electron Inelastic-Mean-Free-Path Database - Version 1.1*. 2001, National Institute of Standards and Technology, Gaithersburg, MD.
- 4.21. P. E. Laibinis, C. D. Bain, and G. M. Whitesides, *Attenuation of Photoelectrons in Monolayers of n-Alkanethiols Adsorbed on Copper, Silver, and Gold*. Journal of the American Chemical Society, 1991. **95**: p. 7017-7021.
- 4.22. C. L. A. Lamont and J. Wilkes, *Attenuation Length of Electrons in Self-Assembled Monolayers of n-Alkanethiols on Gold*. Langmuir, 1999. **15**: p. 2037-2042.

- 4.23. Supporting information for this chapter is available with reference [4.1]. C K-edge total electron and auger yield absorption, O K-edge auger yield absorption, C1s and S2p X-ray photoelectron spectra are available for all samples. Also, example regression plots and all derived NEXAFS angles and errors are presented in the supporting information. This material is available free of charge via the Internet at <http://pubs.acs.org>.

Chapter 5

Surface Structure and Chemical Switching of Thioctic Acid

Adsorbed on Au(111) as Observed Using NEXAFS*

Abstract

Thioctic acid (alpha-lipoic acid) is a molecule with a large disulfide-containing base, a short alkyl-chain with four CH₂ units, and a carboxyl termination. Self-assembled monolayer (SAM) films of thioctic acid adsorbed on Au(111) have been investigated with near-edge x-ray absorption fine structure (NEXAFS) spectroscopy and x-ray photoelectron spectroscopy (XPS) to determine film quality, bonding and morphology. Using standard preparation protocols for SAMs, that is, dissolving thioctic acid in ethanol and exposing gold to the solution, results in poor films. These films are highly disordered, contain a mixture of carboxyl and carboxylate terminations, have more than monolayer coverage, and exhibit unbound disulfide. Conversely, forming films by dissolving 1 mmol thioctic acid into 5% acetic acid in ethanol (as previously reported with carboxyl-terminated alkyl-thiols) forms ordered monolayers with small amounts of unbound sulfur. NEXAFS indicates tilted over endgroups with

*Reproduced in part, with permission, from reference [5.1]: Langmuir, in press as of April, 2004. Copyright 2004, American Chemical Society.

the carboxyl group normal on average 38° from the surface normal. Slight dichroism in other features indicates alkyl chains statistically more upright than prostrate on the surface. Reflection-absorption Fourier transform infrared (RA-FTIR) spectra indicate hydrogen bonding between neighboring molecules. In such well-formed monolayers, a stark reorientation occurs upon deprotonation of the endgroup by rinsing in a KOH solution. The carboxylate plane normal is now about 66° from sample normal, a much more upright orientation. Data indicate this reorientation may also cause a more upright orientation to the alkyl portion of the molecules.

Introduction

Surface modification by using ω -functionalized self-assembled monolayers (SAMs) on gold or other noble metals is the simplest way to create flat, chemically or biologically functionalized surfaces. Although alkyl-thiols are often used for carboxyl-terminated SAMs, thioctic acid has distinct advantages for surface modification. The disulfide-containing base gives added stability, and yields two gold-sulfur bonds per molecule in surface-attached species.

Potential uses for thioctic acid monolayers include bio- and immuno-sensors[5.2-6], components in molecular electronic applications[5.7], and molecular anchors for surface-attachment of catenanes and rotaxanes[5.8-10]. Our group is currently pursuing thioctic acid for superior gold surface attachment for functionalized and molecular electronic interlocking molecules[5.11, 12]. A thorough understanding of the binding and orientation is necessary for further use of thioctic acid to ensure claims that conformational and chemical changes lead to observed phenomena in molecular electronic and interlocking molecule applications[5.13]. Although previous studies have characterized thioctic acid layers electrochemically for layer stability and an indication of packing[5.14-18], to our knowledge, no direct morphological characterizations of this molecule exist to date.

The surface structure of thioctic acid is intriguing compared to thiol based, long alkyl-chain carboxyl-terminated SAMs. For example, SAM ordering, substrate binding and surface attachment has been extensively studied for mercaptohexadecanoic acid[5.19-22]. This molecule has 15 CH_2 units encouraging order through

intermolecular interactions, a small-footprint thiol for attachment, and a carboxyl termination. Conversely, thioctic acid (Fig. 5.1) has a very short alkyl-chain with weak van der Waals interactions between neighboring molecules. The disulfide base has a larger footprint than a thiol, which intuitively should further hinder self-assembly. These differences in thioctic acid allow a more focused study on the carboxyl endgroup and the role it plays in organic monolayer film structure.

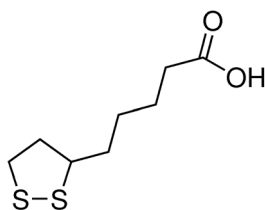


Fig. 5.1. Thioctic acid, the adsorbed molecule studied in this chapter.

In this chapter, we quantitatively investigate substrate binding, monolayer formation, and chemical switching of film morphology for thioctic acid on Au(111) using NEXAFS and XPS for the first time. This work explores films derived from three preparation conditions. The first consists of dissolving 1mmol thioctic acid in ethanol only, exposing gold to this solution, and then rinsing with ethanol only, which is found to result in disordered films of more than one monolayer in thickness. The second method, using 1 mmol thioctic acid dissolved in 5% acetic acid in ethanol for both SAM formation and rinsing is analogous to a successful method for producing reproducibly well-ordered monolayers of carboxyl-terminated alkyl-thiols[5.20]. Using this method yields thioctic acid monolayers with tilted-over, hydrogen-bound endgroups and alkyl

chains statistically more upright than prostrate on the surface. In the third case, where well-prepared thioctic acid molayers via the second method are exposed to KOH for deprotonation, the carboxylate endgroups exhibit a strong reorientation to an upright position, similar to changes observed in alkyl-thiols[5.19]. The more thorough understanding of the switchable morphology and substrate binding thus provided will aid the emerging applications requiring surfaces modified with thioctic acid.

Experimental Details

Reagents and Materials

Reagents were purchased from commercial sources and used as received. Thioctic acid (98%) was purchased from Aldrich. Ethanol (200 proof, USP) was purchased from Aaper. Acetic acid (HPLC grade, 99.7%) was purchased from VWR. Au(111) substrates were formed by evaporating 5 nm Ti and then 100nm Au on Si(100) under high vacuum. All gold substrates were hydrogen-flame annealed immediately before use[5.23].

Sample Preparation

Thioctic acid solutions were prepared similarly to previously reported carboxyl-terminated alkyl-thiols[5.20] by dissolving thioctic acid into either pure ethanol or 5% (by volume) acetic acid in ethanol at concentrations of approximately 1 mmol. Gold substrates were placed in these solutions for 24-36 hours. Under these conditions, disulfide-containing thioctic acid molecules adsorb to the gold surface through gold-

sulfur bonds as in thiol containing molecules [5.24]. Each sample was then removed, rinsed with its corresponding pure solvent – pure ethanol or 5% acetic acid in ethanol.

Instrumentation

X-ray absorption spectroscopy (XAS) measurements were acquired at VUV BL 8.2 of The Stanford Synchrotron Radiation Laboratory (SSRL, SPEAR II) with conditions described in Chapter 2. Spectra were recorded simultaneously using both total electron yield (TEY) and auger electron yield (AEY). The degree of linear polarization was measured with highly-oriented pyrolytic graphite (HOPG) in conjunction with these measurements to be about 88% in the plane of the storage ring.

X-ray photoelectron spectra were obtained at SSRL using a PHI 15-255G Cylindrical Mirror Analyzer (CMA) and associated PHI electronics. The pass energy was set to 25 eV for XPS spectra, while for Auger electron yield absorption, the pass energy was set to 200 eV. XPS measurements have an overall estimated resolution of about 0.5 eV. S 2p spectra were obtained at a photon energy of 280 eV or 400 eV; C1s spectra were obtained at a photon energy of 400 eV. Au 4f spectra of the substrates were taken immediately after each sulfur and carbon spectrum to calibrate the binding energy scales. The Au 4f_{7/2} photoelectron at 84.01 +/- 0.05 eV was used to convert the kinetic energy scales to binding energy scales. FTIR spectra were obtained using methods described in Chapter 2.

Results and Discussion

Carbon NEXAFS can be used to derive both the chemical nature and orbital orientation within the thioctic acid films. The spectra from our study are shown in Fig. 5.2, Fig. 5.3, and Fig. 5.4 for thioctic acid deposited from solution on Au(111) using the three methods described above, respectively. The spectra in upper panes are all normalized to the absorption step edge with the pre-edge set to 0 and the absorption step height set to 1 at about 320eV. Spectra were acquired at various angles from normal incidence (90°) to grazing at 20° . The lower panes consist of the difference between each spectra and the scan acquired at 20° degrees to emphasize polarization dependent peaks. Visible spectral features include a shoulder at 287.8eV from resonances into (C-H σ^* - like) R^* resonances from alkyl portions of the molecule[5.25]. The pronounced, sharp feature at 288.7eV is from C 1s transitions into the π^* orbital of the carboxyl group. Above the edge, two broad resonances appear at around 293.5eV and 298.5eV primarily due to C-C σ^* resonances. The variation in intensity of these features determines order and orientation on the surface.

Thioctic acid layers prepared using only ethanol (Fig. 5.2) show very little polarization dependence. This is interpreted as a film with a high degree of disorder. The nature of this film is further investigated with other techniques.

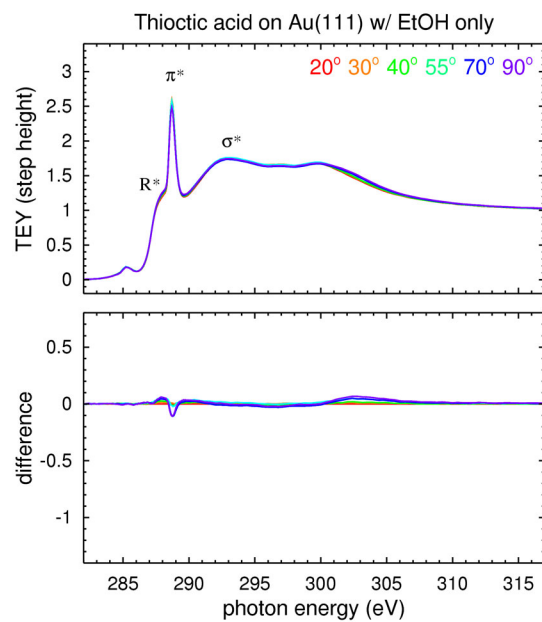


Fig. 5.2. Carbon NEXAFS of thioctic acid on Au prepared with EtOH only

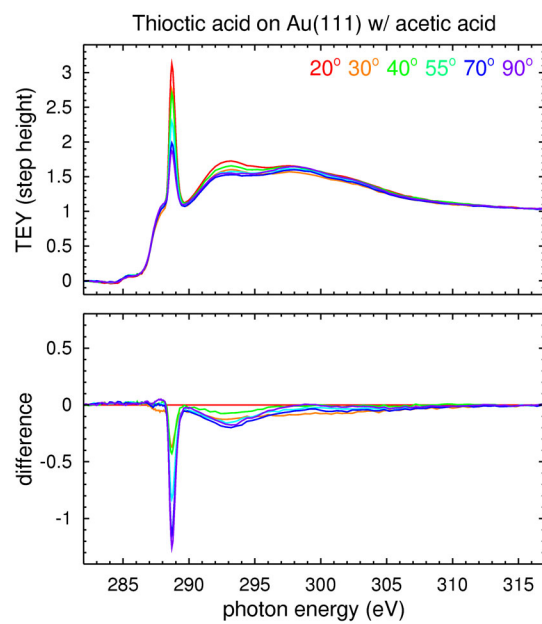


Fig. 5.3. Carbon NEXAFS of thioctic acid prepared with 5% acetic acid in EtOH.

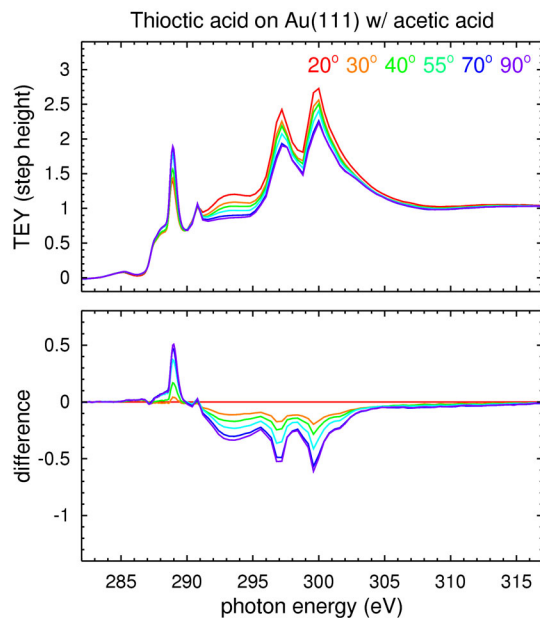


Fig. 5.4. Thioctic acid on Au, subsequent rinsing in KOH.

Conversely, and surprisingly, the film prepared with acetic acid (Fig. 5.3) have a π^* feature with a strong polarization dependence. Using the intensities of this resonance at each angle through Equations (2.22) and (2.23) the carboxyl plane normal is about 38° from the surface normal. Polarization dependence in σ^* features above the absorption edge yield 53.5° , a degree less than the magic angle. The R^* features, considering high convolution with the carboxyl π^* feature, return 51.5° . Although indicative of a disordered film, both resonances show an upright tendency of the alkyl portion of the molecules.

As noted previously, films prepared in acetic acid were also later rinsed in a KOH solution in order to deprotonate the carboxyl groups. NEXAFS spectra of such SAMs (Fig. 5.4) reveal additional features that are not due to carbon. The first, at 291

eV, is presumably due to contaminant Na in our KOH solution. This K-edge, which arises from synchrotron light of higher order, is strong in samples rinsed in NaOH, and is absent in Auger-yield spectra that are more sensitive to only the carbon in the sample. (See supplemental information, [5.1]) Features at 297eV and 300eV are due to the potassium L-edge from the counterions that now decorate the surface. Endgroup NEXAFS features have opposite polarization dependence compared to protonated carboxyl groups, indicating a strong orientational change. With consideration of difficulties in normalization due to Na and K features in the spectra obscuring the step edge normalization, the carboxyl plane normal on average is roughly estimated to be about 66° from the surface normal. Along with the change in endgroup orientation, which is confirmed with oxygen NEXAFS, σ^* features due to alkyl-units return angles about 5° less than in the acetic rinsed case, while little change occurs in the highly convoluted R^* features. All derived angles from C K-edge NEXAFS are summarized in Table 5.1.

Oxygen K-edge spectra (Fig. 5.5) were acquired using AEY for better signal to background and enhanced surface sensitivity. However, Auger-yield has disadvantages in a lower signal to noise ratio, and the possibility that low binding-energy photoelectrons could sweep through the kinetic energy window of the analyzer and hence, exist in the spectra. All spectra show pre-edge features due to excitations from the Oxygen 1s into the carboxyl π^* , and broad σ^* features due to C-O bonds.

Table 5.1: Thioctic acid angles derived from C K-edge NEXAFS spectra

Sample	carboxyl π^*	R* (C-H σ^*)	C-C σ^*
acetic acid / ethanol prep.			
slopes	37.9 +/- 0.8	51.2 +/- 0.1	53.5 +/- 0.1
offsets	38.2 +/- 0.8	51.8 +/- 2.9	53.6 +/- 1.6
KOH rinsed			
slopes (a)	66.0 +/- 0.3	51.1 +/- 0.1	48.5 +/- 0.3
offsets (a)	65.4 +/- 1.1	51.7 +/- 0.9	48.7 +/- 0.8

(a) K photoelectron peaks may introduce systematic errors

Errors presented in this table are standard deviations from results obtained using slopes and offsets from equations (2.22) and (2.23) at each incidence angle.

The left panes present O K-edge NEXAFS of thioctic acid monolayers prepared with acetic acid in ethanol. The top spectra are normalized to the foot and step acquired at 90°, 55°, and 20°. The lower panes contain differences between spectra. Polarization dependencies, with the π^* resonance most intense grazing incidence and O-C σ^* most intense at normal incidence, confirm carbon results – the carboxyl group plane is tilted toward the surface plane.

For the KOH rinsed sample, in the right panes, polarization dependence indicates that the endgroup is much more upright on the surface. The π^* resonance is now most intense at normal incidence. The O-C σ^* is now somewhat obscured due to an extra feature not due to endgroup oxygen at about 545 eV. This feature is likely due

to K 3s photoelectrons (33 eV) entering the analyzer window, and/or water present on the surface.

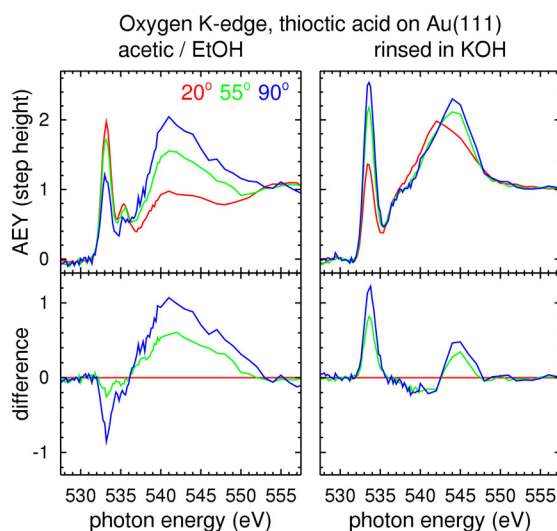


Fig. 5.5. Oxygen K-edge spectra (top) and difference spectra (bottom) for SAMs prepared and rinsed with 5% acetic acid in EtOH (left) and SAMs prepared and then rinsed in KOH (right).

RA-FTIR spectra (Fig. 5.6) show differences in the endgroup chemical nature. The layers show clear carbonyl stretches from 1740-1700 cm^{-1} . These have been previously shown to be from single, non-hydrogen bound carboxyl groups at 1740 cm^{-1} , carboxyl groups hydrogen bound with one hydrogen bond or hydrogen bonds to two different neighboring molecules at 1720 cm^{-1} , and completely dimerized carboxyl groups with two hydrogen bonds to one neighboring molecule at 1700 cm^{-1} [5.20, 22, 26, 27]. The acetic-formed thioctic layers show a mixture of dimerizations. In the case where the film is formed with only ethanol as the solvent, the peak associated with single carboxyl groups is greatly reduced, the middle peak is reduced, and intensity at

1740 for fully dimerized pairs increases. The carboxylate band (1450cm^{-1}) is much larger, while one associated with water (1600cm^{-1}) also appears. This indicates that the ethanol-only sample carboxyl groups exist as highly dimerized pairs and carboxylates. To further investigate endgroup nature, carbon x-ray photoelectron spectroscopy was employed.

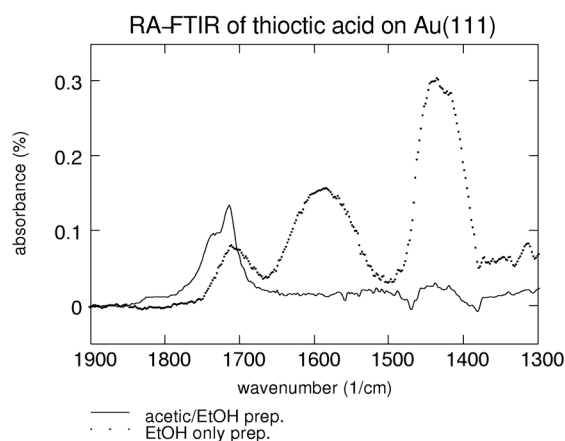


Fig. 5.6. FTIR spectra of thioctic acid films produced with and without acetic acid

Carbon 1s spectra (Fig. 5.7) show chemical differences between thioctic acid layers adsorbed on Au. For those formed with acetic acid, (bottom trace) a sharp carboxyl feature at 289 eV and a larger feature due to the remaining aliphatic carbon in the molecule at 284.4eV[5.28]. For adsorbates solution deposited without acetic acid, the carboxyl/carboxylate peak is broadened (1.4eV compared to 1.15eV) and shifted to slightly lower binding energy relative to the gold substrate. This indicates that without acetic acid, some of the end-groups are deprotonated in the final film. The alkyl peak is

also slightly broadened, shifted to higher binding energy, and has a slightly different shape. This is due to different chemical environments of the deprotonated carboxylate groups. The relative carboxyl to alkyl peak intensity is also weaker in this case, which could be due to a combination of a short mean-free-path of the photoelectrons and more than a monolayer on the surface, and a small amount of acetic acid still on the surface in the acetic acid / ethanol case. This possibility and substrate bonding are resolved with sulfur photoemission.

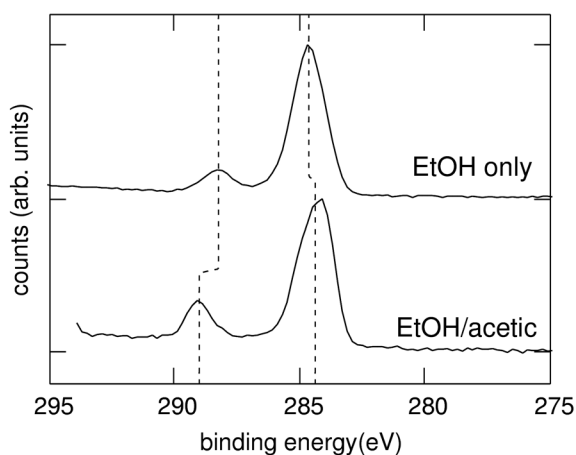


Fig. 5.7. Carbon 1s photoelectron spectra for thioctic acid layers on Au prepared with and without acetic acid in solution when layer was formed

Sulfur 2p spectra indicate the degree of bonding to the substrate (Fig. 5.8). The spectra can be deconvoluted using the S2p doublet with branching ratio about 2:1 and energy difference about 1.2eV. Two species are predominant on the surface: gold bound thiolate, with S 2p_{3/2} (S 2p_{1/2}) at 161.9 eV (163.1 eV) and unbound disulfide, with S 2p_{3/2} (S 2p_{1/2}) at 163.3 eV (164.5 eV)[5.29]. As with carboxyl terminated SAMs,

no sample is completely free from unbound molecules. This is due to prevailing carboxyl dimers even with acetic acid, and does not eliminate the possibility that some molecules may be attached to the substrate through the carboxyl end. However, additional XPS spectra indicate unbound sulfur atoms are not near the gold interface with samples prepared in this manner. (See supplemental information, [5.1].) In any case, with the ultra-high surface sensitivity of photoelectron spectroscopy with electron kinetic energies just over 100eV, the top spectrum shows the majority of the molecules using acetic acid in solution are bound to the substrate through gold-thiolate bonds.

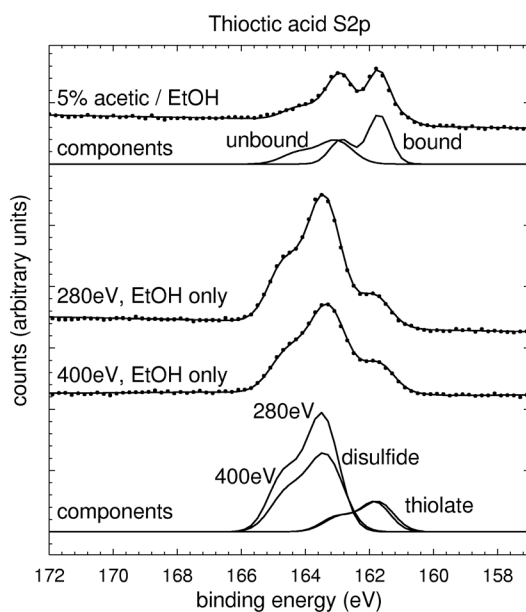


Fig. 5.8. Sulfur 2p photoemission of the thioctic acid films formed with and without acetic acid in solution.

For the ethanol only case, a very large disulfide component exists. To estimate the position within the layer of this extra disulfide, spectra at photon energies of 280 eV

and 400 eV were acquired. Based on differences in mean-free paths of S 2p photoelectrons from two photon energies and the exponential decrease of photoelectron intensity with overlayer thickness[5.30-33], we estimate the unbound disulfide is on average 9 ± 4 Ångströms above the Au-S interface. This indicates carboxyl group dimerization, in some instances with one molecule anchored to the surface, and a second molecule attached through carboxyl groups with disulfide near the layer-vacuum interface. Additional results show that this monolayer is 3-5 Ångströms thicker than the sample prepared with acetic acid. (See supplemental information, [5.1].)

Combining NEXAFS, XPS and FTIR results, a model of thioctic acid under three different preparation conditions is roughly depicted in Fig. 5.9. Using only ethanol to prepare and rinse films leads to disordered, more than monolayer films as seen in Fig. 5.9 a). Unbound disulfide exists about 9 Å above the gold-sulfur interface, and the endgroups are a mixture of highly dimerized carboxyl groups and carboxylate. Preparing and rinsing thioctic acid SAMs using 5% acetic in ethanol gives well (although not completely) bound monolayers with a high degree of interaction and hydrogen bonding between carboxyl groups as depicted in Fig. 5.9 b). NEXAFS results indicate carboxyl group planes are statistically 38° from the surface plane. Similar tilting in the endgroups of SAMs have been seen in other types of polar molecules, due to the energy minimization of the electric dipoles[5.34]. Although this effect may contribute to the tilting of the headgroups, especially in partially dimerized films, we believe the primary cause to be hydrogen bonding between endgroups as seen in FTIR spectra. The remainder of the molecular film has a slight upright tendency with

polarization dependence in σ^* and R^* features yielding angles from 51.5° - 53.5° , a few degrees less than the magic angle. This underestimates the upright nature of these films considering the variation in orientation of aliphatic carbon at the ring-like base of the molecules driving derived angles toward the magic angle. Rinsing these well-formed monolayers in KOH for deprotonation causes a reorientation of the endgroups to a much more upright orientation as seen in Fig. 5.9 c). The carboxylate plane normal is now 66° from the surface normal. Angles derived from the highly convoluted R^* features do not change significantly. However, alkyl portions of these films may also have a more upright nature as σ^* features indicate a 5° degree change in the average orientation of the alkyl units.

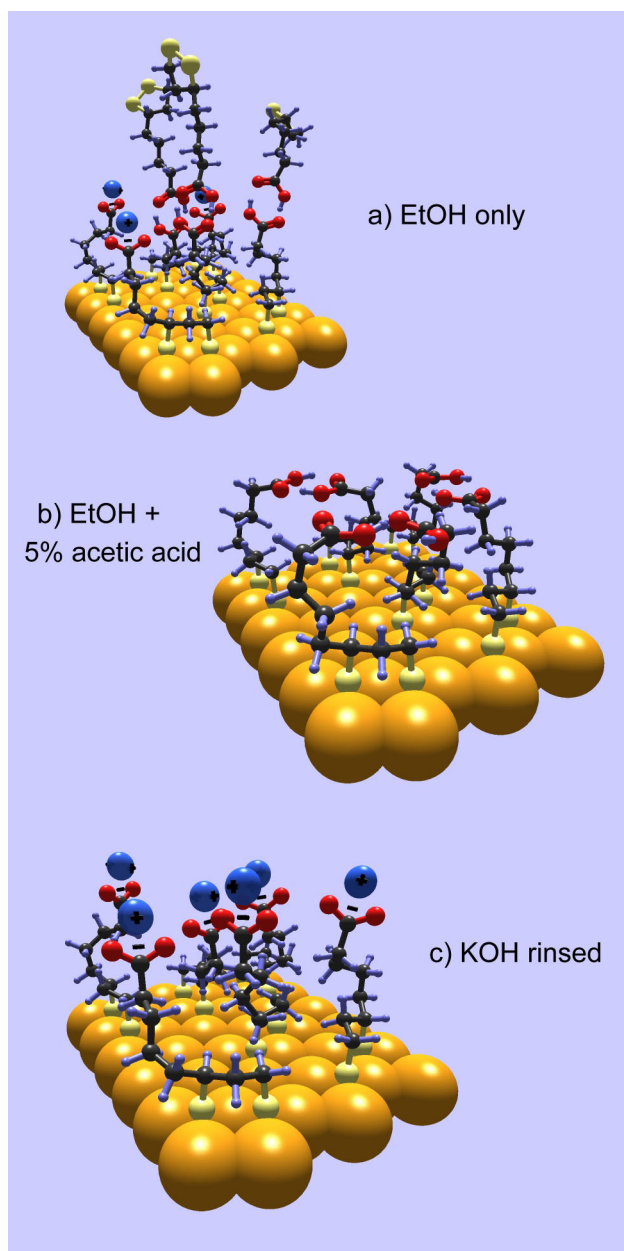


Fig. 5.9. Three dimensional rough model of thiocetic acid on $\text{Au}(111)$. a) prepared with 1mmol thiocetic acid in EtOH and rinsed in EtOH. b) prepared with 1mmol thiocetic acid in 5% acetic acid in EtOH, rinsed in 5% acetic acid in EtOH. c) sample prepared as in b, but then rinsed in KOH solution

Conclusions

The extent of substrate binding, endgroup chemical nature, and orientational structure of thioctic acid films adsorbed on gold were investigated with NEXAFS, XPS and RA-FTIR. Depending upon the solvent and rinsing step, various configurations exist.

Using ethanol only, thioctic acid forms a completely disordered, more-than-monolayer film of molecules. Many of the endgroups are deprotonated to carboxylate.

Using 5% acetic acid in ethanol for the formation solution, thioctic acid surprisingly forms ordered films. Carboxyl-carboxyl interaction plays heavily on film structure as carboxyl group planes are tilted towards the surface as the NEXAFS angle between the group normal and surface normal is 38° . The bases of the molecules are also statistically more upright than prostrate with a tilt angle a few degrees less than the magic angle.

Upon deprotonation to carboxylate by rinsing in KOH, the carboxylate groups change orientation indicating a chemically driven conformational switching. They are upright with respect to the surface, with carboxylate plane normal 66° from the surface normal. This may also induce alkyl chains to exhibit a more upright orientation, with the tilt angle decreasing by 5° in C-C σ^* NEXAFS features.

These results allow for better understanding of self-assembly process in carboxyl terminated films. In this case, when alkyl-chain interactions are minimized, carboxyl group interactions tend to form tilted-over dimers. To date, the best films are formed using a process similar to that used in carboxyl terminated alkyl-thiols by

adding acetic acid to ethanol solutions to form and rinse films. In addition, this quantitative characterization of thioctic acid monolayers adsorbed on Au builds a foundation for the use of these films in biological and chemical sensor applications and for surface-attached macromolecules[5.35].

References

- 5.1. T. M. Willey, A. L. Vance, C. Bostedt, et al., *Surface Structure and Chemical Switching of Thioctic Acid Adsorbed on Au(111) as Observed Using NEXAFS*. Langmuir, 2004. **in press**.
- 5.2. D. M. Disley, D. C. Cullen, H. X. You, and C. R. Lowe, *Covalent coupling of immunoglobulin G to self-assembled monolayers as a method for immobilizing the interfacial-recognition layer of a surface plasmon resonance immunosensor*. Biosensors & Bioelectronics, 1998. **13**(11): p. 1213-1225.
- 5.3. V. P. Y. Gadzekpo, K. P. Xiao, H. Aoki, et al., *Voltammetric detection of the polycation protamine by the use of electrodes modified with self-assembled monolayers of thioctic acid*. Analytical Chemistry, 1999. **71**(22): p. 5109-5115.
- 5.4. Y. Z. Dong and C. Shannon, *Heterogeneous immunosensing using antigen and antibody monolayers on gold surfaces with electrochemical and scanning probe detection*. Analytical Chemistry, 2000. **72**(11): p. 2371-2376.
- 5.5. K. Wang, D. C. Jiang, J. L. Kong, et al., *Sensitively detecting recombinant hirudin variant-2 with capacitive immunoassay based on self-assembled monolayers*. Analytical Letters, 2003. **36**(12): p. 2571-2583.
- 5.6. Y. Wang and A. E. Kaifer, *Interfacial molecular recognition. Binding of ferrocenecarboxylate to beta-aminocyclodextrin hosts electrostatically immobilized on a thioctic acid monolayer*. Journal of Physical Chemistry B, 1998. **102**(49): p. 9922-9927.
- 5.7. S. Berchmans, C. Ramalechume, V. Lakshmi, and V. Yegnaraman, *Diode like electron transfer in mixed monolayer assembly*. Journal of Materials Chemistry, 2002. **12**(8): p. 2538-2542.
- 5.8. K. Kim, W. S. Jeon, J. K. Kang, et al., *A pseudorotaxane on gold: Formation of self-assembled monolayers, reversible dethreading and rethreading of the ring, and ion-gating behavior*. Angewandte Chemie-International Edition, 2003. **42**(20): p. 2293-2296.
- 5.9. H. Azebara, W. Mizutani, Y. Suzuki, et al., *Fixation and Systematic Dilution of Rotaxane Molecules on Self-Assembled Monolayers*. Langmuir, 2003. **19**: p. 2115-2123.
- 5.10. E. Coronado, A. Forment-Aliaga, P. Gavina, and F. M. Romero, *Copper(I) Pseudorotaxane Monolayers Assembled on Gold Electrodes*. Inorganic Chemistry, 2003. **42**(22): p. 6959-6961.

- 5.11. A. L. Vance, T. M. Willey, T. van Buuren, et al., *XAS and XPS characterization of a surface-attached rotaxane*. Nano Letters, 2003. **3**(1): p. 81-84.
- 5.12. A. L. Vance, T. M. Willey, A. J. Nelson, et al., *XAS and XPS Characterization of Monolayers Derived from a Dithiol and Structurally Related Disulfide-Containing Polyamides*. Langmuir, 2002. **18**(21): p. 8123-8128.
- 5.13. R. F. Service, *Next-Generation Technology Hits an Early Midlife Crisis*, in *Science*. 2003. p. 556-558.
- 5.14. Q. Cheng and A. Brajter-Toth, *Permselectivity, Sensitivity, and Amperometric pH Sensing at Thioctic Acid Monolayer Microelectrodes*. Analytical Chemistry, 1996. **68**(23): p. 4180-4185.
- 5.15. Q. Cheng and A. Brajter-Toth, *Selectivity and Sensitivity of Self-Assembled Thioctic Acid Electrodes*. Analytical Chemistry, 1992. **64**(17): p. 1998-2000.
- 5.16. M. Dijkema, B. A. Boukamp, B. Kamp, and W. P. van Bennekom, *Effect of hexacyanoferrate(II/III) on self-assembled monolayers of thioctic acid and 11-mercaptoundecanoic acid on gold*. Langmuir, 2002. **18**(8): p. 3105-3112.
- 5.17. M. Dijkema, B. Kamp, J. C. Hoogvliet, and W. P. van Bennekom, *Formation and electrochemical characterization of self-assembled monolayers of thioctic acid on polycrystalline gold electrodes in phosphate buffer pH 7.4*. Langmuir, 2000. **16**(8): p. 3852-3857.
- 5.18. Y. Z. Dong, S. Abaci, C. Shannon, and M. J. Bozack, *Self-assembly and electrochemical desorption of thioctic acid monolayers on gold surfaces*. Langmuir, 2003. **19**(21): p. 8922-8926.
- 5.19. T. M. Willey, A. L. Vance, T. van Buuren, et al., *Chemically Transformable Configurations of Mercaptohexadecanoic Acid Adsorbed on Au(111)*. Langmuir, 2004. **in press**.
- 5.20. R. Arnold, W. Azzam, A. Terfort, and C. Wöll, *Preparation, Modification, and Crystallinity of Aliphatic and Aromatic Carboxylic Acid Terminated Self-Assembled Monolayers*. Langmuir, 2002. **18**(10): p. 3980-3992.
- 5.21. O. Dannenberger, K. Weiss, H. J. Himmel, et al., *An orientation analysis of differently endgroup-functionalized alkanethiols adsorbed on Au substrates*. Thin Solid Films, 1997. **307**: p. 183-191.
- 5.22. R. G. Nuzzo, L. H. Dubois, and D. L. Allara, *Fundamental Studies of Microscopic Wetting on Organic Surfaces. 1. Formation and Structural Characterization of a Self-Consistent Series of Polyfunctional Organic*

- Monolayers*. Journal of the American Chemical Society, 1990. **112**(2): p. 558-569.
- 5.23. Hydrogen flame annealing follows the method described by Molecular Imaging, available online as of April 2004 at <http://www.molec.com>.
 - 5.24. H. A. Biebuyck, C. D. Bain, and G. M. Whitesides, *Comparison of Organic Monolayers on Polycrystalline Gold Spontaneously Assembled from Solutions Containing Dialkyl Disulfides or Alkanethiols*. Langmuir, 1994. **10**(6): p. 1825-1831.
 - 5.25. P. S. Bagus, K. Weiss, A. Schertel, et al., *Identification of transitions in Rydberg states in the X-ray absorption spectra of condensed long-chain alkanes*. Chemical Physics Letters, 1996. **248**: p. 129-135.
 - 5.26. E. L. Smith, C. A. Alves, J. W. Anderegg, and M. D. Porter, *Deposition of Metal Overlayers at End-Group-Functionalized Thiolate Monolayers Adsorbed at Au. I. Surfaced and Interfacial Chemical Characterization of Deposited Cu Overlayers at Carboxylic Acid-Terminated Structures*. Langmuir, 1992. **8**: p. 2707-2714.
 - 5.27. Y. T. Tao, G. D. Hietpas, and D. L. Allara, *HCl vapor-induced structural rearrangements of n-alkanoate self-assembled monolayers on ambient silver, copper, and aluminum surfaces*. Journal of the American Chemical Society, 1996. **118**(28): p. 6724-6735.
 - 5.28. C. D. Bain, E. B. Troughton, Y.-T. Tao, et al., *Formation of Monolayer Films by the Spontaneous Assembly of Organic Thiols from Solution onto Gold*. Journal of the American Chemical Society, 1989. **111**: p. 321-335.
 - 5.29. D. G. Castner, K. Hinds, and D. W. Grainger, *X-ray photoelectron spectroscopy surfur 2p study of organic thioc and disulfide binding interactions with gold surfaces*. Langmuir, 1996. **12**(21): p. 5083-5086.
 - 5.30. C. L. A. Lamont and J. Wilkes, *Attenuation Length of Electrons in Self-Assembled Monolayers of n-Alkanethiols on Gold*. Langmuir, 1999. **15**: p. 2037-2042.
 - 5.31. P. E. Laibinis, C. D. Bain, and G. M. Whitesides, *Attenuation of Photoelectrons in Monolayers of n-Alkanethiols Adsorbed on Copper, Silver, and Gold*. Journal of the American Chemical Society, 1991. **95**: p. 7017-7021.
 - 5.32. C. J. Powell and A. Jablonski, *NIST Electron Effective-Attenuation-Length Database - Version 1.0*. 2001: National Institute of Standards and Technology, Gaithersburg, MD.

- 5.33. C. J. Powell and A. Jablonski, *NIST Electron Inelastic-Mean-Free-Path Database - Version 1.1*. 2001, National Institute of Standards and Technology, Gaithersburg, MD.
- 5.34. S. Frey, A. Shaporenko, M. Zharnikov, et al., *Self-Assembled Monolayers of Nitrile-Functionalized Alkanethiols on Gold and Silver Substrates*. Journal of Physical Chemistry B, 2003. **107**(31): p. 7716-7725.
- 5.35. Supporting information for this chapter is available in conjunction with reference [5.1]. Derived NEXAFS angles and errors, and additional spectra are presented in the supporting information. This material is available free of charge via the Internet at <http://pubs.acs.org>.

Chapter 6

XAS and XPS Characterization of Monolayers Derived from a Dithiol and Structurally Related Disulfide-containing Polyamides*

Abstract

X-ray absorption spectroscopy and x-ray photoemission spectroscopy have been used to examine sulfur-gold bond formation in monolayers derived from a dithiol monomer and related disulfide-containing polyamides. These compounds were designed to allow the molecules to adsorb to gold through two terminal sulfurs, forming surface-attached loops. Element and site-specific density of unoccupied electronic states were probed by x-ray absorption spectroscopy at the C, N, and O K-edges. Photoemission measurements of the C 1s, N 1s, O 1s [6.1] and S 2p core lines were also used to estimate relative coverage, confirm layer formation, and evaluate chemical bonding of the monomer and polyamide to the gold-coated substrates. In the case of the dithiol monomer, the spectroscopic evidence clearly shows that most of the molecules adsorb through a single thiol end. The disulfide-containing precursors, in contrast to the monomer, attach to the surface through both sulfurs to form the anticipated surface-attached loop.

* Reproduced in part, with permission, from reference [6.1]: Langmuir, 2002, 18, 8123-8126. Copyright 2002, American Chemical Society.

Introduction

With the goal of building a technical foundation for the construction of surface-attached molecular devices, we are investigating the formation of surface-attached loops from a variety of dithiol and disulfide precursors. While there is much interest in self-assembled monolayers (SAMs) formed by the adsorption of thiols or disulfides onto gold surfaces[6.2-5], less attention has been focused on systems derived from α, ω - dithiols. In most cases, dithiols have been found to attach to gold through only one sulfur[6.6-15]. The free thiol of these “standing” dithiol SAMs is then available for further reactions to form bilayers or to attach additional ions, molecules, or particles to surfaces[6.16-21]. Other dithiols and disulfides have been designed to attach to gold through both sulfurs, forming chelating monolayers[6.22-24]. Bis-disulfides derived from thiocetic acid have also been shown to form monolayers in which both disulfide ends attach to gold, forming especially stable surface-attached species[6.25, 26]. Since the sulfur-gold bond is relatively weak (ca. 40 kcal/mol vs. 87 kcal/mol for a thiol S-H bond[6.2], monolayers of the spiroalkanedithiols and the thiocetic acid derivatives are stabilized by the chelate effect of multiple sulfur-gold bonds. When α, ω - dithiols or bis-disulfides are utilized to form monolayers in which both ends are attached to gold, these could be referred to as surface-attached loops.

Another approach that could generate surface-attached loops is to expose a disulfide-containing polymer to a gold surface. Cleavage of the disulfide bonds upon attachment to gold would result in loop formation. Monolayers formed from disulfide-containing polymers have been reported, although the details of their adsorption on gold were not the focus of that work[6.27-30]. By utilizing disulfide-containing polymers,

the polymer is broken down to surface-attached monomeric units. This differs from other work in which polymers were bound intact to the gold surface via pendant sulfide or disulfide moieties[6.31-33].

We are investigating the formation of surface-attached loops from a variety of dithiol and disulfide precursors. This report concerns the results of our experiments with two of these compounds, an α, ω - dithiol and its related disulfide-containing polyamides. The compounds were prepared by Andrew Vance (LLNL) from readily available starting materials to give the dithiol monomer and the disulfide-containing polyamide (Fig. 6.1). The interfacial condensation of the polyamide during synthesis yielded a polymer with a wide polydispersity as well as a small, but significant, percentage of low molecular weight units such as the [2+2] macrocycle. In principle, any of these compounds could lead to the same surface-attached species in which both sulfurs attach to gold to form a loop. Alternatively, the monomer could adsorb through a single sulfur end (Fig. 6.1).

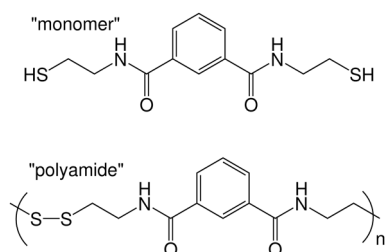


Fig. 6.1. The monomer dithiol molecule, and the disulfide-containing polyamide investigated in this chapter.

Using synchrotron-based x-ray absorption spectroscopy (XAS) and x-ray photoemission spectroscopy (XPS), we have probed molecular orientation and the

nature of the sulfur-gold bonds formed in our monomer and polyamide derived monolayers.

X-ray absorption probes unfilled states. Features near edges (often referred to as near-edge x-ray absorption spectroscopy or NEXAFS) reveal chemical information near the atoms being probed. Cross-sections of transitions from core-levels into such unfilled states often depend on the polarization of the exciting radiation. Utilizing the high degree of linear polarization of synchrotron radiation, the order and orientation of chemical bonds can be determined by rotating the samples with respect to the x-ray beam. Such polarization dependencies in the carbon K-edge (and nitrogen K-edge) are used to determine order and orientation in this work.

XPS has been used to determine bonding of the thiols and disulfides to the gold surface. Core level shifts in the XPS spectra are indicative of the chemical state of the emitting atom, and intensities of components of emitted photoelectrons can be used to quantitatively determine chemical composition. Relative intensities of various photoelectrons (e.g. N1s) between monolayers formed from the monomer and polymer precursors can be used to determine the relative coverage of the surface by the adsorbed species.

Experimental Methods

Reagents and Materials.

All reagents were purchased from commercial sources and used as received. The molecules in Fig. 6.1 were synthesized by Andrew Vance of LLNL as described in

[6.1]. Au(111) on mica substrates were purchased from Molecular Imaging and hydrogen flame annealed immediately prior to use.

Instrumentation

X-ray photoelectron spectra were obtained using a Physical Electronics Quantum 2000 scanning XPS system located at the Environmental Sciences Laboratory, Pacific Northwest National Laboratory. X-ray absorption spectra were taken at VUV BL 8.2 of The Stanford Synchrotron Radiation Laboratory (SSRL) at the Stanford Linear Accelerator Center as described in Chapter 2. Measurements obtained throughout data acquisition at the beamline gave 90.1% (± 0.8) polarization in the plane of the storage ring.

Results and Discussion

X-ray absorption spectra reveal the local bonding environment around specific atoms, and hence the chemical state of these atoms. When the sample is rotated in the x-ray beam, polarization effects are observed as intensity modulations of the peaks in the spectra. Differences in spectra taken at various angles of incidence allow determination of average orientation of the molecules[6.34-39]. Through the dipole approximation, the intensity of a resonance is proportional to the square of the scalar product of the electric field of the x-rays and the direction of the final state orbital when exciting from s-like core levels. Hence, when the electric field of the radiation is parallel to the direction of the final state orbital, the resonance into this orbital is strong and the absorption signal at the resonance is strong. Conversely, when the electric field

of the radiation is orthogonal to the direction of the final state orbital, the resonance is greatly attenuated. These linear dichroism effects disappear when the molecules are oriented totally randomly or when the final state orbitals are oriented with respect to the surface near $\arcsin\left(\sqrt{\frac{2}{3}}\right)$ (54.7°), often referred to as the magic angle[6.34]. For this reason, angles chosen and presented here are 55° , as well as 90° (normal) and 20° (grazing), which are both 35° from the magic angle.

Fig. 6.2 shows carbon K-edge spectra for the monomer and polyamide monolayers at various angles of incidence as well as the differences of these spectra. Features typical to carbon-containing organic molecules are present in all carbon absorption spectra and are related to the distinct environments of carbon atoms in the molecule[6.40-42]. The peak at 285.1 eV arises from C=C π bonds and is assigned to a transition from the C 1s level into a π^* orbital of the central phenyl ring in each molecule. The next resonance at 288.0 eV arises primarily from the C 1s to π^* transition in carbonyl groups. At this energy, additional π^* states in the phenyl ring and Rydberg resonances in the alkyl chain carbon atoms near the ends of the molecules contribute to the intensity[6.41]. Features at 288.8 eV in the polyamide as well as features from 290-300 eV that are not present in monomer spectra are due to a small amount of trifluoroacetic acid still present in the polyamide sample, confirmed by XPS via a small F1s photoelectron peak which was not present in the monomer. Other transitions from C 1s into σ^* states make up the broad features from ~ 290 eV to ~ 310 eV.

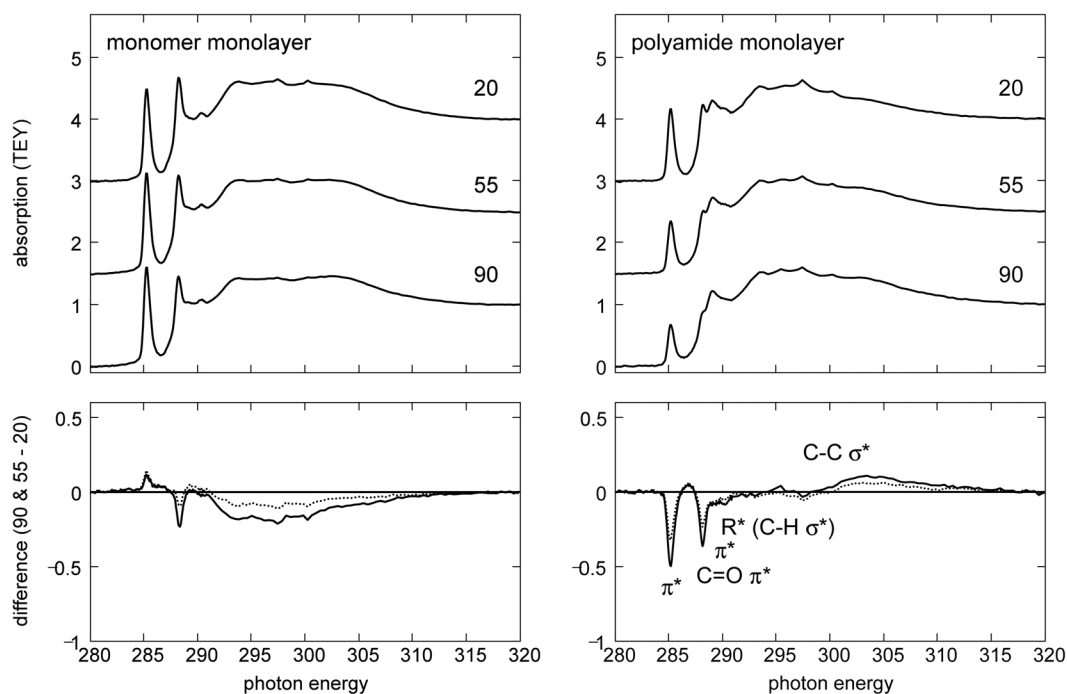


Fig. 6.2. C K-edge absorption spectra for the monomer and polyamide samples on Au/mica substrates.

Continuing with Fig. 6.2, spectra taken at three angles of incidence are shown: grazing at 20°, 55°, and normal at 90°. Carbon spectra are normalized to the step edge at ~320 eV. The bottom panes show the differences in spectra by subtracting the spectra taken at 20° from the spectra taken at 90° and 55°. To determine orientation of these monolayers, the phenyl ring π^* resonance at 285.1 eV is used. Additionally, the C=O π^* and C-C σ^* resonances prove useful.

In the monomer spectra, the aromatic π^* feature is slightly more intense at normal incidence than grazing. The C=O π^* feature at 288 eV is somewhat more intense at grazing than normal incidence. C-C σ^* features are faintly more intense at grazing incidence. This indicates disordered monolayers which, according to the aromatic and

C-C σ^* resonances, have molecules on average tilted slightly more than 54.7° , from the surface, or are more “standing up” than “lying down.”

The polyamide spectra, however, have linear dichroism that is larger and different than that of the monomer. The C 1s (C=C) to π^* C=C transition is relatively much stronger at grazing incidence, where the electric field of the synchrotron radiation is nearly perpendicular to the surface. At normal incidence, where the electric field of the radiation is in the plane of the surface, this π^* resonance is weak. This indicates that the plane of the phenyl ring is nearly parallel to the surface. The C=O π^* resonance shows a polarization dependence with strongest features at grazing incidence, and C-C σ^* features have slightly more intensity at normal incidence. Nitrogen NEXAFS (not shown) support the carbon spectra with a strong pre-edge excitation from the N1s into the C=O π^* at grazing incidence. These polarization dependencies indicate the polymer molecules on average, lie nearly flat on the surface.

Thus, carbon NEXAFS reveals that the monomer precursor forms a less ordered, more upright monolayer, where the molecules are tilted on average more than 54.7° from the surface. Polyamide-derived monolayers, on the other hand, have order with the molecules oriented nearly parallel to the surface.

High-resolution C 1s, N 1s, O 1s and S 2p_{3/2,1/2} core-level XPS spectra were obtained for the powders and the monolayers of the monomer and polyamide samples, with full results presented in reference [6.1]. Shifts indicative of sulfur-gold adsorption were observed in the S 2p_{3/2,1/2} spectra (Fig. 6.3) while the carbon, nitrogen and oxygen spectra showed little chemical variation upon monolayer formation, but showed a higher coverage for the monomer-based monolayers.

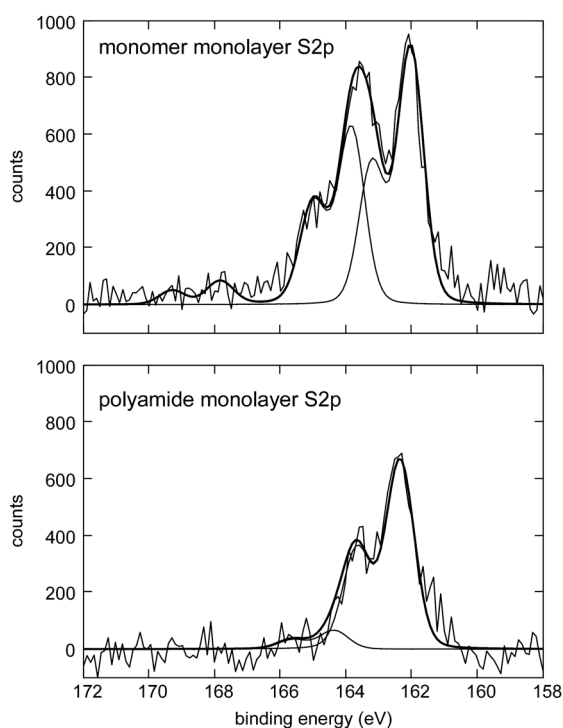


Fig. 6.3. Deconvolved high-resolution S 2p_{3/2}, 1/2 core-level spectra.

Deconvolution of the S 2p_{3/2,1/2} spectra reveals the spin-orbit pairs for both bound and unbound sulfurs (Fig. 6.3)[6.9, 43]. In the monomer-derived monolayer, about half (57.6%) of the sulfurs are bound to gold, while the other half are either unbound (36%) or present as sulfates (6.4%). In contrast to the monomer, over 90% of the sulfurs in the polyamide-derived monolayer are bound to the gold surface.

Conclusions

X-ray absorption spectroscopy (XAS) and x-ray photoemission spectroscopy (XPS) have been used to characterize the chemical interaction between gold surfaces and monolayers derived from either a dithiol monomer or disulfide-containing

polyamides. These experiments differentiate between surface-attached loops on gold and simple monolayers in which one sulfur in each molecule binds to the surface (i.e. non-loops). In the case of the dithiol monomer monolayer, the spectroscopic evidence clearly shows the molecules adsorb predominantly through only one sulfur. The disulfide-containing polyamides, in contrast to the monomer, attach to the surface through both sulfurs to form the anticipated surface-attached loop (Fig. 6.4).

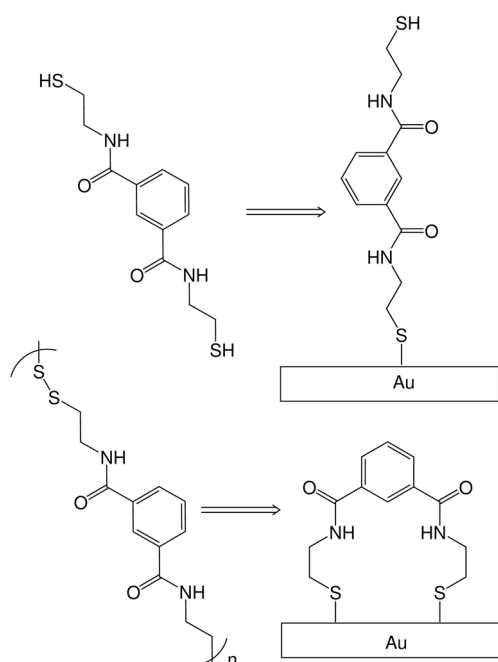


Fig. 6.4. The monomer leads to films primarily consisting of molecules attached at one end (top) while the polyamide molecules lead to surface attached loops (bottom).

In the NEXAFS spectra, spectral features vary with the angle of incidence of the polarized exciting radiation. XAS polarization dependence measurements indicate a higher degree of ordering in the polyamide-derived monolayer with the phenyl rings oriented nearly parallel to the gold surface. The monomer-derived monolayer shows only very slight polarization dependence, indicative of more upright, disordered

aromatic moieties. XPS studies showed the only significant changes in the chemical structure of the compounds occurred in the sulfurs upon attachment to the gold surface.

The surface coverage of the monolayer formed from the polyamide is less than that of the dithiol monomer monolayer, as might be expected due to the increased surface area of the loop versus the standing monomer. That the polyamides preferentially form loops while the monomer attaches primarily through only one sulfur may be attributed to the fact that the sulfurs of the disulfide adsorb to the gold simultaneously while the sulfurs of the monomer are at separate ends of the molecule. At the concentrations used to form these systems, the monomer is present in large excess over what is required to form a monolayer. There may simply be too little space for both sulfurs to access the surface for adsorption. In contrast, as the polyamides, with either the polymers or low molecular weight macrocycles, approach the gold surface, their adjacent disulfide sulfurs are positioned to effectively “unzip” the polyamide as it is exposed to the gold, leaving surface-attached loops. The fact that the monomer had a small percentage of molecules bound through both sulfurs means it may yet be possible to manipulate reaction conditions (e.g. concentration) to favor loop formation. We are pursuing further studies of these and similar compounds and are especially interested in determining the role of disulfide-containing macrocycles in the formation of surface-attached loops.

The results obtained from the experiments presented here demonstrate the importance of designing monolayer precursors that will bind to surfaces in a predictable manner. In the case of surface-attached loops, simply preparing compounds with terminal binding moieties does not guarantee loop formation. Other factors such as anticipated surface coverage, solution concentration and steric interactions must be taken into account in

order to produce a desired surface-attached system. We are currently working to design and characterize monolayers derived from monomers incorporating features that will significantly enhance loop formation[6.44].

References

- 6.1. A. L. Vance, T. M. Willey, A. J. Nelson, et al., *XAS and XPS characterization of monolayers derived from a dithiol and structurally related disulfide-containing polyamides*. *Langmuir*, 2002. **18**(21): p. 8123-8128.
- 6.2. A. Ulman, *Formation and structure of self-assembled monolayers*. *Chemical Reviews*, 1996. **96**(4): p. 1533-1554.
- 6.3. R. G. Nuzzo and D. L. Allara, *Adsorption of Bifunctional Organic Disulfides on Gold Surfaces*. *Journal of the American Chemical Society*, 1983. **105**(13): p. 4481-4483.
- 6.4. C. D. Bain, E. B. Troughton, Y. T. Tao, et al., *Formation of Monolayer Films by the Spontaneous Assembly of Organic Thiols from Solution onto Gold*. *Journal of the American Chemical Society*, 1989. **111**(1): p. 321-335.
- 6.5. H. Gronbeck, A. Curioni, and W. Andreoni, *Thiols and disulfides on the Au(111) surface: The headgroup-gold interaction*. *Journal of the American Chemical Society*, 2000. **122**(16): p. 3839-3842.
- 6.6. J. M. Tour, L. Jones, D. L. Pearson, et al., *Self-Assembled Monolayers and Multilayers of Conjugated Thiols, Alpha,Omega-Dithiols, and Thioacetyl-Containing Adsorbates - Understanding Attachments between Potential Molecular Wires and Gold Surfaces*. *Journal of the American Chemical Society*, 1995. **117**(37): p. 9529-9534.
- 6.7. T. Nakamura, H. Kondoh, M. Matsumoto, and H. Nozoye, *Scanning tunneling microscopy observations of alpha,omega-bis(mercaptomethylthienyl)alkane derivatives self-assembled on Au(111)*. *Langmuir*, 1996. **12**(25): p. 5977-5979.
- 6.8. T. Nakanishi, B. Ohtani, K. Shimazu, and K. Uosaki, *Layer-by-layer self-assembly of composite films of CdS nanoparticle and alkanedithiol on gold: an X-ray photoelectron spectroscopic characterization*. *Chemical Physics Letters*, 1997. **278**(4-6): p. 233-237.
- 6.9. H. Rieley, G. K. Kendall, F. W. Zemicael, et al., *X-ray studies of self-assembled monolayers on coinage metals. 1. Alignment and photooxidation in 1,8-octanedithiol and 1-octanethiol on Au*. *Langmuir*, 1998. **14**(18): p. 5147-5153.
- 6.10. A. S. Duwez, L. M. Yu, J. Riga, et al., *Molecular structure and surface order in monolayers of alkanethiols evidenced by HREELS*. *Thin Solid Films*, 1998. **329**: p. 156-160.
- 6.11. P. Kohli, K. K. Taylor, J. J. Harris, and G. J. Blanchard, *Assembly of covalently-coupled disulfide multilayers on gold*. *Journal of the American Chemical Society*, 1998. **120**(46): p. 11962-11968.

- 6.12. S. W. Joo, S. W. Han, and K. Kim, *Multilayer formation of 1,2-ethanedithiol on gold: Surface-enhanced Raman scattering and ellipsometry study*. Langmuir, 2000. **16**(12): p. 5391-5396.
- 6.13. S. W. Joo, S. W. Han, and K. Kim, *Adsorption characteristics of 1,3-propanedithiol on gold: Surface-enhanced Raman scattering and ellipsometry study*. Journal of Physical Chemistry B, 2000. **104**(26): p. 6218-6224.
- 6.14. A. S. Duwez, L. M. Yu, J. Riga, et al., *Vibrational structure and organization of various self-assembled alkanethiol monolayers: A HREELS study*. Langmuir, 2000. **16**(16): p. 6569-6576.
- 6.15. T. Y. B. Leung, M. C. Gerstenberg, D. J. Lavrich, et al., *1,6-hexanedithiol monolayers on Au(111): A multitechnique structural study*. Langmuir, 2000. **16**(2): p. 549-561.
- 6.16. D. Bethell, M. Brust, D. J. Schiffrin, and C. Kiely, *From monolayers to nanostructured materials: An organic chemist's view of self-assembly*. Journal of Electroanalytical Chemistry, 1996. **409**(1-2): p. 137-143.
- 6.17. T. Nakanishi, B. Ohtani, and K. Uosaki, *Fabrication and characterization of CdS-nanoparticle mono- and multilayers on a self-assembled monolayer of alkanedithiols on gold*. Journal of Physical Chemistry B, 1998. **102**(9): p. 1571-1577.
- 6.18. M. Brust, D. Bethell, C. J. Kiely, and D. J. Schiffrin, *Self-assembled gold nanoparticle thin films with nonmetallic optical and electronic properties*. Langmuir, 1998. **14**(19): p. 5425-5429.
- 6.19. H. X. He, H. Zhang, Q. G. Li, et al., *Fabrication of designed architectures of Au nanoparticles on solid substrate with printed self-assembled monolayers as templates*. Langmuir, 2000. **16**(8): p. 3846-3851.
- 6.20. W. Deng, L. Yang, D. Fujita, et al., *Silver ions adsorbed to self-assembled monolayers of alkanedithiols on gold surfaces form Ag-dithiol-Au multilayer structures*. Applied Physics a-Materials Science & Processing, 2000. **71**(6): p. 639-642.
- 6.21. W. L. Deng, D. Fujita, L. J. Yang, et al., *Multilayer formation of copper ions (Cu²⁺) deposited onto self-assembled monolayers of alkanedithiols on Au (111) surfaces*. Japanese Journal of Applied Physics Part 2-Letters, 2000. **39**(7B): p. L751-L754.
- 6.22. Y. S. Shon, S. Lee, S. S. Perry, and T. R. Lee, *The adsorption of unsymmetrical spiroalkanedithiols onto gold affords multi-component interfaces that are homogeneously mixed at the molecular level*. Journal of the American Chemical Society, 2000. **122**(7): p. 1278-1281.

- 6.23. Y. S. Shon and T. R. Lee, *Chelating self-assembled monolayers on gold generated from spiroalkanedithiols*. Langmuir, 1999. **15**(4): p. 1136-1140.
- 6.24. H. Fujihara, H. Nakai, M. Yoshihara, and T. Maeshima, *Alkane-tetrathiol induced formation of remarkably stable self-assembled monolayer and polymer films containing electroactive tetrathiafulvalene moieties on metal electrodes*. Chemical Communications, 1999(8): p. 737-738.
- 6.25. H. Y. Liu, S. G. Liu, and L. Echegoyen, *Remarkably stable self-assembled monolayers of new crown-ether annelated tetrathiafulvalene derivatives and their cation recognition properties*. Chemical Communications, 1999(16): p. 1493-1494.
- 6.26. S. G. Liu, H. Y. Liu, K. Bandyopadhyay, et al., *Dithia-crown-annelated tetrathiafulvalene disulfides: Synthesis, electrochemistry, self-assembled films, and metal ion recognition*. Journal of Organic Chemistry, 2000. **65**(11): p. 3292-3298.
- 6.27. H. Tsutsumi and K. Fujita, *New-Type Polyamides Containing Disulfide Bonds for Positive Active Material of Energy-Storage Batteries*. Electrochimica Acta, 1995. **40**(7): p. 879-882.
- 6.28. H. Tsutsumi, K. Okada, and T. Oishi, *Electrochemical behavior of new polyamides containing disulfide bonds and pyridine rings in organic electrolyte solution*. Electrochimica Acta, 1996. **41**(16): p. 2657-2659.
- 6.29. H. Tsutsumi, S. Okada, and T. Oishi, *A potentially biodegradable polyamide containing disulfide bonds as a positive material for secondary batteries*. Electrochimica Acta, 1998. **43**(3-4): p. 427-429.
- 6.30. H. Tsutsumi, K. Takeoka, and T. Oishi, *Preparation and characterization of new self-assembled polyamide film containing disulfide bonds on gold electrode*. Journal of Colloid and Interface Science, 1997. **185**(2): p. 432-435.
- 6.31. F. Sun and D. W. Grainger, *Ultrathin Self-Assembled Polymeric Films on Solid-Surfaces .I. Synthesis and Characterization of Acrylate Copolymers Containing Alkyl Disulfide Side-Chains*. Journal of Polymer Science Part a-Polymer Chemistry, 1993. **31**(7): p. 1729-1740.
- 6.32. T. J. Lenk, V. M. Hallmark, J. F. Rabolt, et al., *Formation and Characterization of Self-Assembled Films of Sulfur-Derivatized Poly(Methyl Methacrylates) on Gold*. Macromolecules, 1993. **26**(6): p. 1230-1237.
- 6.33. M. Niwa, T. Mori, and N. Higashi, *Control of Adsorption State Based on Conformational Change of Poly(Methacrylic Acid)-Functionalized, Double-Chain Monolayers on Gold Substrates*. Macromolecules, 1993. **26**(8): p. 1936-1940.

- 6.34. J. Stöhr, *NEXAFS Spectroscopy*. 1992, Berlin Heidelberg: Springer Verlag.
- 6.35. J. Stöhr and D. A. Outka, *Determination of Molecular Orientations on Surfaces from the Angular-Dependence of near-Edge X-Ray-Absorption Fine-Structure Spectra*. Physical Review B, 1987. **36**(15): p. 7891-7905.
- 6.36. A. Imanishi, K. Isawa, F. Matsui, et al., *Structural studies of adsorbed alkanethiols on Cu(111) by use of S and C K-edge X-ray absorption fine structures*. Surface Science, 1998. **407**(1-3): p. 282-292.
- 6.37. P. Harder, K. Bierbaum, C. Woell, et al., *Induced orientational order in long alkyl chain aminosilane molecules by preadsorbed octadecyltrichlorosilane on hydroxylated Si(100)*. Langmuir, 1997. **13**(3): p. 445-454.
- 6.38. M. Himmelhaus, I. Gauss, M. Buck, et al., *Adsorption of docosanethiol from solution on polycrystalline silver surfaces: an XPS and NEXAFS study*. Journal of Electron Spectroscopy and Related Phenomena, 1998. **92**(1-3): p. 139-149.
- 6.39. S. Frey, V. Stadler, K. Heister, et al., *Structure of thioaromatic self-assembled monolayers on gold and silver*. Langmuir, 2001. **17**(8): p. 2408-2415.
- 6.40. R. Giebler, B. Schulz, J. Reiche, et al., *Near-edge X-ray absorption fine structure spectroscopy on ordered films of an amphiphilic derivate of 2,5-diphenyl-1,3,4-oxadiazole*. Langmuir, 1999. **15**(4): p. 1291-1298.
- 6.41. P. S. Bagus, K. Weiss, A. Schertel, et al., *Identification of transitions into Rydberg states in the X-ray absorption spectra of condensed long-chain alkanes*. Chemical Physics Letters, 1996. **248**(3-4): p. 129-135.
- 6.42. J. Stohr, M. G. Samant, J. Luning, et al., *Liquid crystal alignment on carbonaceous surfaces with orientational order*. Science, 2001. **292**(5525): p. 2299-2302.
- 6.43. D. G. Castner, K. Hinds, and D. W. Grainger, *X-ray photoelectron spectroscopy surfur 2p study of organic thioc and disulfide binding interactions with gold surfaces*. Langmuir, 1996. **12**(21): p. 5083-5086.
- 6.44. Supporting information is available in conjunction with reference [6.1]: Sulfur L2,3-edge absorption spectra for monomer and polymer precursor powders and monolayers on Au(111) (including spectrum of oxidized sulfur for comparison), C 1s, N 1s, and O 1s XPS spectra, a table summarizing the XPS compositional analysis and elemental ratios for the powder samples and monolayers, as well as probable structures of the low MW materials present in the polyamide. This material is available free of charge via the Internet at <http://pubs.acs.org>.

Chapter 7

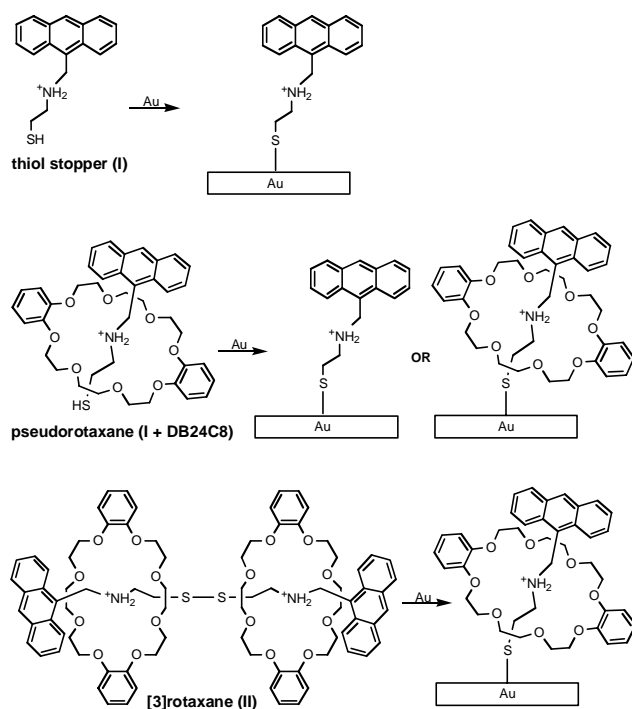
Characterization of a Simple Surface-Attached Rotaxane*

Introduction

Mechanically interlocking molecules such as rotaxanes are both aesthetically fascinating and of interest for their potential in molecular-scale devices[7.1-5]. While the solution chemistry of both catenanes (interlocking rings) and rotaxanes (rod threaded through ring) has been explored extensively, the study of the surface chemistry of these species has been limited to a few examples[7.6-14]. In order to build a technical foundation for the preparation of molecular-scale devices, we are pursuing the characterization of surface-attached molecules with unique structures and topologies[7.15]. Toward that end, synchrotron radiation based X-ray absorption spectroscopy (XAS) and X-ray photoemission spectroscopy (XPS) were utilized to quantitatively determine coverages, binding, and orientation of both a rotaxane and its thiol precursor attached to a gold surface. The thiol stopper, 9-anthrylmethyl(2-mercaptoethyl)ammonium bromide (I), the pseudorotaxane (a labile rotaxane in which the ring is not locked into position by a stopper unit) formed by addition of dibenzo-24-crown-8 (I + DB24C8), and finally, the hexafluorophosphate salt of the disulfide [3]-rotaxane(II)[7.16] were used to prepare monolayers on atomically flat gold-coated

* Reproduced in part, with permission, from reference [7.1]: Nano Letters, 2003, 3, 81-84. Copyright 2003, American Chemical Society.

substrates as shown in Scheme 1. This set of molecules was chosen because the system I does not contain any oxygen atoms. We presumed that oxygen specific spectroscopy would be useful in distinguishing between the surface-bound thiol stopper (I) and the surface-bound rotaxane (II), with its oxygen-rich crown ether. In fact, element specific XAS and XPS showed several clear distinctions between the monolayers, allowing us to identify spectral contributions from the separate components of the surface-attached rotaxane system. In addition, angle dependent x-ray absorption studies highlighted differences in the surface orientations of gold-bound I and II, and XPS was used to determine the extent of Au-S bond formation.



Scheme 1. Starting materials and anticipated surface-attached molecules. (Figure courtesy A. Vance)

Experimental Results and Discussion

Before examining the monolayer-covered gold-coated substrates, powder samples of the thiol stopper (I), DB24C8, and the [3]rotaxane (II) were characterized. The carbon K-edge XAS spectra show the signature peaks of each molecule (Fig. 7.1). The spectrum of thiol stopper (I) is dominated by anthracene, with fourteen carbon atoms comprising the anthracene moiety vs only three carbon atoms in the tether. Features in this spectrum include multiple π^* transitions of the anthracene[7.17] due to chemically inequivalent carbon sites and multiple unoccupied π molecular orbitals[7.18]. These excitations primarily form a doublet with peaks at 284.6 eV and 286.0 eV. Weaker, sharp features near the edge between 287.6 eV and 289.8 eV are attributed to higher π^* states and alkyl carbon Rydberg states while broad features at about 293.5 and 301 eV are excitations into σ^* resonances. In the spectrum of the crown ether (DB24C8) powder, a prominent aromatic π^* resonance appears in the middle of the anthracene doublet at 285.5 eV, and a chemically shifted π^* transition due to the four oxygen-bound, phenyl ring carbon atoms in each crown ether appears at 287.2 eV. The feature at 289.4 eV is related to C-O bonds, and the molecule also has broad σ^* transitions at about 294.2 and 303.5 eV. The peaks in the spectrum of II, the [3]-rotaxane powder, are a linear combination of the spectra of thiol stopper (I) and DB24C8.

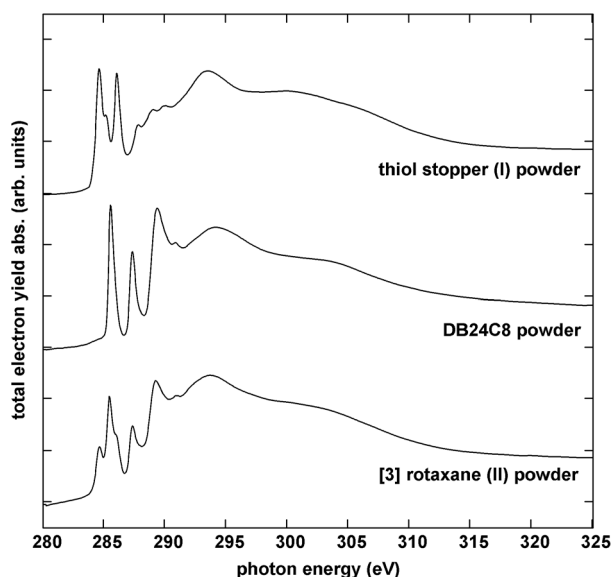


Fig. 7.1. Carbon K-edge XAS of powder samples. Top: thiol stopper only. Middle: Crown ether only. Bottom: [3]-rotaxane powder.

Monolayers were prepared by exposing gold-coated substrates (~ 100 nm Au evaporated onto atomically flat mica and/or 5 nm Ti/Si(100) substrates, H_2 flame annealed prior to use) to a solution of the corresponding molecule. The first monolayer system derived from the thiol stopper (I) was used to identify spectral characteristics of this gold-bound anthracene-containing stopper unit. To determine whether a surface-attached rotaxane could form from a solution containing a pseudorotaxane, thiol stopper (I) was mixed with an excess of DB24C8 prior to exposure of the gold-coated substrate to the solution. Kolchinski, et al. estimated a solution pseudorotaxane equilibrium concentration in excess of 90%[7.16]. Finally, the [3]-rotaxane, II, was exposed to a gold surface with the expectation that cleavage of the disulfide upon adsorption to gold would yield the desired surface-attached rotaxane.

The carbon K-edge absorption spectra reveal notable differences between the monolayers (Fig. 7.2). The carbon spectrum of thiol stopper (I) on gold contains the same features as the molecule prior to attachment. Intensity dependence of π^* and σ^* NEXAFS features upon the incidence angle of the incoming linearly polarized synchrotron radiation leads to determination of the orientation of the molecule with respect to the surface. Polarization studies showed significant angle dependence in the monolayer of I (Fig. 7.3), indicating order and an upright orientation of the anthracene planes with respect to the surface. In the second monolayer system derived from the pseudorotaxane solution (I + DB24C8), the spectroscopic evidence shows that only the surface-attached thiol stopper is formed. The pseudorotaxane monolayer carbon XAS spectrum of I + DB24C8 duplicates nearly identically the spectrum of thiol stopper (I) including the polarization dependence. The monolayer derived from the [3]-rotaxane (II) gave a distinctly different carbon K-edge absorption spectrum. As in the spectrum of the [3]-rotaxane powder sample, the anthracene features are clearly visible along with the peaks associated with the crown ether ring. Not all of the adsorbed species are surface-attached rotaxanes, but a comparison of the intensities of the anthracene to crown-ether π^* features shows that more than half of the crown ether rings are retained upon surface adsorption. Unlike the monolayer derived from thiol stopper I, the surface-attached rotaxane derived from compound II did not show a strong angular dependence, indicating a disordered surface (Fig. 7.4). Given the added bulk of the crown-ether ring, it is not surprising that the surface-attached rotaxane would not order as well as the relatively unencumbered thiol stopper.

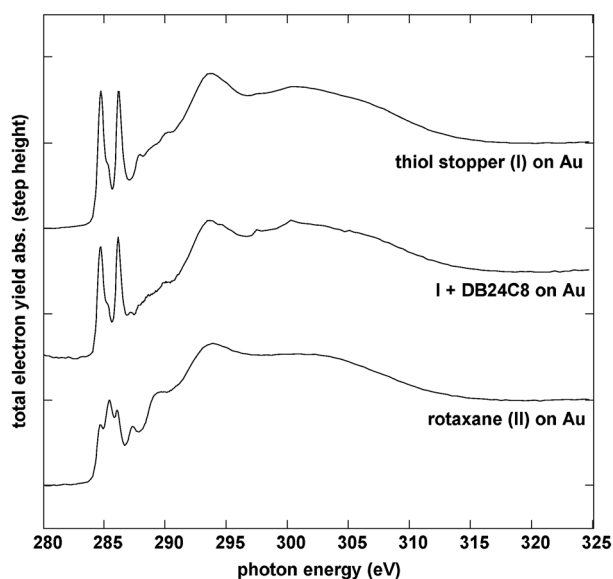


Fig. 7.2. Carbon K-edge XAS of monolayers on gold. Top spectra: anthracene-based stopper molecules. Middle: layer formed in a pseudorotaxane solution mixture of the stopper and an excess of crown ether. Bottom: layer formed using the [3]-rotaxane.

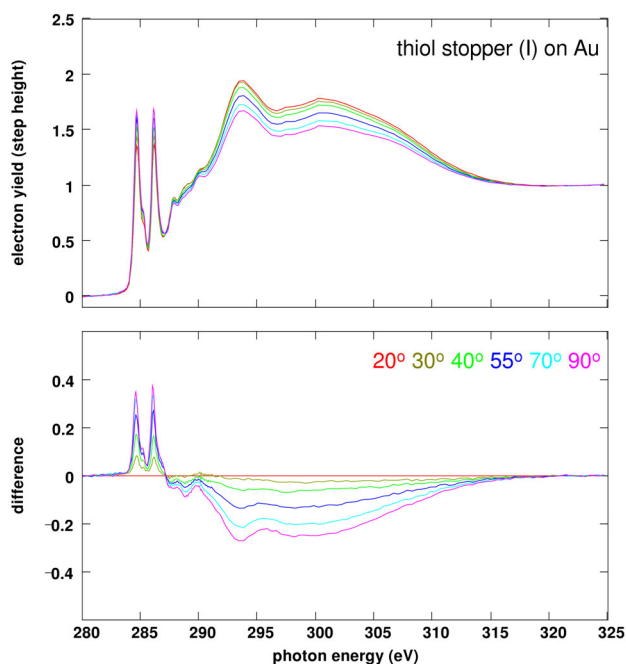


Fig. 7.3. Carbon K-edge polarization dependencies for the film of stopper only molecules. Top pane: Spectra acquired at angles from 90 to 20 degrees. Bottom pane: difference spectra using 20 degrees.

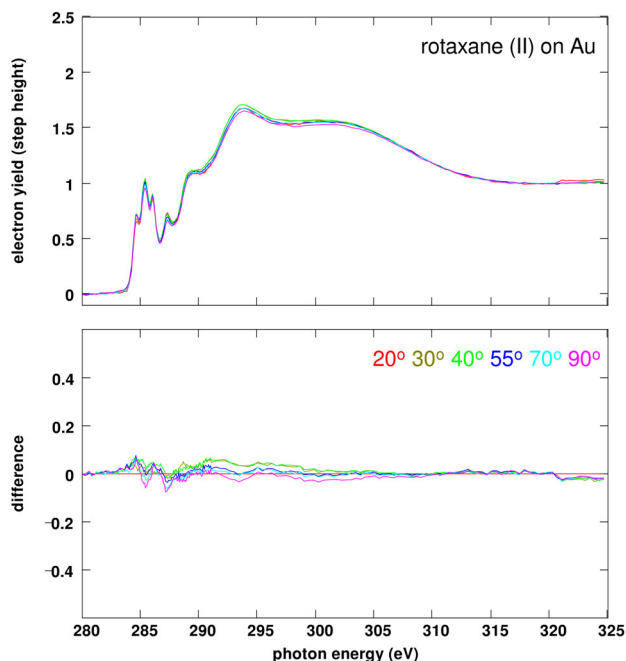


Fig. 7.4. C K-edge polarization dependence of the layer formed from the [3]-rotaxane.

Distinctions between the systems derived from the thiol stopper (I), pseudorotaxane (I + DB24C8), and rotaxane (II) in the C1s XPS spectrum (Fig. 7.5) support the conclusions drawn from the carbon K-edge absorption. In both the monolayers from the thiol stopper (I) and pseudorotaxane (I + DB24C8), the spectra contain primarily one peak at 284.4 eV (sp^2 -hybridized carbons) and a much weaker component at 285.6 eV (C-N bonding). In the monolayer of II, the surface-attached rotaxane, an additional feature was observed at 286.2 eV that is indicative of the C-O bonds of the crown ether. The 1s electrons of the oxygen-bound carbons are shifted to higher binding energy due to the electron withdrawing effect of the oxygen atoms. This C-O feature is absent in the pseudorotaxane-derived I + DB24C8 system, indicating an absence of the ring in this monolayer. An estimate of surface-attached rotaxane

formation in the monolayer derived from the [3]-rotaxane (II) precursor can be made by comparing the relative intensities of the C-O and C-C features in the C1s spectra of the monolayer derived from II with the number of constituent carbon atoms in a thiol stopper (I), DB24C8, and the surface-attached rotaxane molecule. In agreement with the carbon XAS data, at least 45% of the thiol stopper molecules retain their crown ether rings upon surface adsorption.

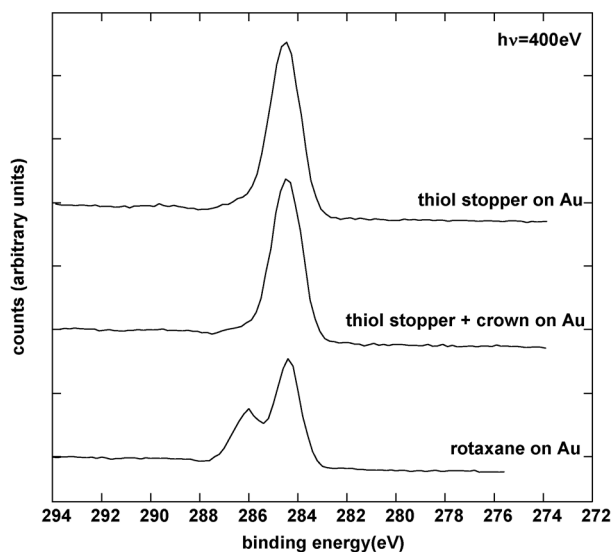


Fig. 7.5. C1s XPS spectra of monolayers on gold. Top spectra: monolayer formed with anthracene stopper molecules only. Middle: monolayer formed with the pseudorotaxane mixture. Bottom: Monolayer formed with the [3] rotaxane solution.

XPS provided valuable information on the extent of Au-S bond formation (Fig. 7.6)(Fig. 7.7) (Fig. 7.8). For each sample, sulfur XPS spectra were carefully referenced to concurrently acquired Au 4f spectra. Spectra consist primarily of three spin orbit split S 2p components. Using a splitting between S 2p_{3/2} and S 2p_{1/2} of 1.18 eV and a branching (intensity) ratio of ~2:1, the S 2p_{3/2} (S 2p_{1/2}) components lie at 163.8 eV

(165.0 eV), 161.9 eV (163.1 eV) and 160.9 eV (162.1 eV). Features with S 2p_{3/2} at 163.8 eV can be assigned to unbound sulfur while those at 161.9 eV can be assigned to gold-bound thiolate[7.19]. Intensity between 167 and 170 eV points to various oxidized sulfur species. The feature at 160.9 eV is highly reduced sulfur that we infer to be elemental sulfur from decomposition products or starting material impurities[7.11]. While this feature indicates the monolayers derived from I are not as pure as desired, the presence of elemental sulfur does not interfere with C 1s XPS or carbon K-edge XAS measurements. Based on these assignments, the system derived from thiol stopper (I) (Fig. 7.6) has large unbound sulfur intensity along with the bound thiols. At an excitation energy of 280 eV, the kinetic energy of the photoelectrons is ~100 eV and at this energy, the mean free path of electrons in solids is ~ 5 Å. Thus, the sulfur XPS is extremely sensitive to the first few atomic layers. While this observation requires further study, the unbound sulfurs may be due to a number of unbound thiol stopper molecules attached in an upside-down fashion through π -stacking interactions of the anthracene units. These anthracene units interestingly retain polarization dependencies as seen in Fig. 7.3. The surface sensitive C1s intensity of the film derived from only thiol stopper I is 12 +/- 2% stronger than in the system formed from the pseudorotaxane (I + DB24C8); this underestimates the relative coverages as the anthracene molecule is ~9 Å tall. Studies using a more stable flux of Al K- α X-rays on similar samples, with a much larger mean free path of the photoelectrons (~25 Å) also support this hypothesis. (See supporting information, [7.1].) Less unbound sulfur was observed in the case of the monolayer derived from the pseudorotaxane solution, I + DB24C8 (Fig. 7.7). It is probable that unbound thiol stopper molecules are removed from the surface by the

excess crown ether that was present in the solution. The most intense component in the monolayer derived from the [3]-rotaxane (II) (Fig. 7.8) is bound thiolate, confirming surface attachment of this molecule. For this film, sulfur XPS showed less unbound sulfur as well as almost no elemental sulfur. The weak signal is due to a much more diffuse concentration of sulfur on the surface due to the much bulkier molecule it anchors.

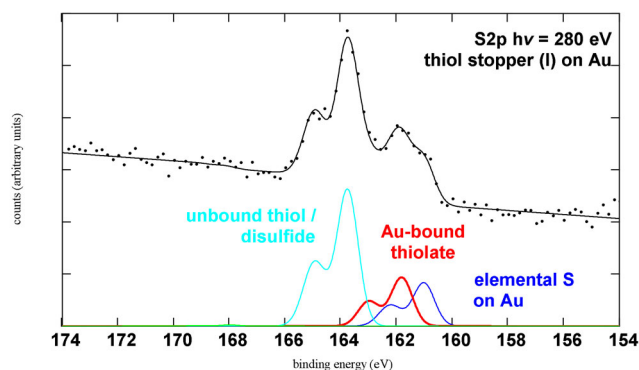


Fig. 7.6. S2p spectra of the anthracene stopper based monolayer. Data (dots) fit (line) and components (at the bottom of the pane) are presented.

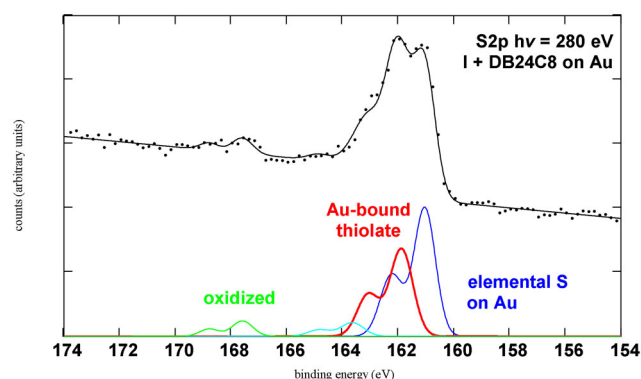


Fig. 7.7. S2p spectra of the monolayer formed in the pseudorotaxane solution. Data (dots) fit (line) and components (at the bottom of the pane) are presented.

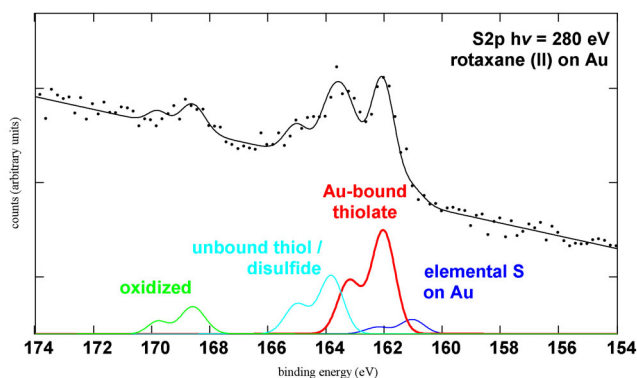


Fig. 7.8. S2p of the monolayer formed in the [3] rotaxane solution. Data, fits, and components are presented.

Conclusions

By utilizing both XAS and XPS concurrently for the first time to characterize surface-attached interlocking molecules, we have presented clear evidence for the formation of a surface-attached rotaxane from a disulfide-containing [3]-rotaxane. These techniques provide both qualitative data for the identification of separate components of surface-bound interlocking molecules, as well as quantitative information that can be used to determine the extent of retention of the mechanically anchored unit (crown ether ring) upon surface adsorption of the rotaxane. Our experiments showed that the form of the monolayer precursor (rotaxane vs. pseudorotaxane) dictated the outcome of surface adsorption. In this system, the [3]-rotaxane, with its crown ether rings locked in place prior to surface attachment, is required to form a surface-attached rotaxane. In the case of the mixture of thiol stopper with dibenzo-24-crown-8, while the pseudorotaxane dominates the solution equilibrium, these experiments show that for this thiol stopper + ring combination, sufficient

unthreaded thiol is present to favor exclusively adsorption of the thiol over the rotaxane. The role of the thiol/pseudorotaxane equilibrium is an area of interest, and future experiments will be pursued to examine whether modified reaction conditions (e.g. temperature) or pseudorotaxanes derived from threads with different alkyl chain lengths would yield surface-attached rotaxanes. Work is ongoing in our laboratory to study these and other surface-attached interlocking molecules[7.20].

References

- 7.1. A. L. Vance, T. M. Willey, T. van Buuren, et al., *XAS and XPS characterization of a surface-attached rotaxane*. Nano Letters, 2003. **3**(1): p. 81-84.
- 7.2. V. Balzani, A. Credi, F. M. Raymo, and J. F. Stoddart, *Artificial molecular machines*. Angewandte Chemie-International Edition, 2000. **39**(19): p. 3349-3391.
- 7.3. J. P. Sauvage, *Transition metal-containing rotaxanes and catenanes in motion: Toward molecular machines and motors*. Accounts of Chemical Research, 1998. **31**(19): p. 611-619.
- 7.4. D. B. Amabilino, F. M. Raymo, and J. F. Stoddart, eds. Comprehensive Supramolecular Chemistry, ed. J. P. Sauvage and M. W. Hosseini. Vol. 9. 1996, Pergamon: Oxford. 85-130.
- 7.5. M. C. T. Fyfe and J. F. Stoddart, in *Advances in Supramolecular Chemistry*, G. W. Gokel, Editor. 1999, JAI Press: London. p. 1-53.
- 7.6. T. Lu, L. Zhang, G. W. Gokel, and A. E. Kaifer, *The First Surface-Attached Canenane - Self-Assembly of a 2-Component Monolayer*. Journal of the American Chemical Society, 1993. **115**(6): p. 2542-2543.
- 7.7. J. M. Kern, L. Raehm, and J. P. Sauvage, *Formation of a copper(I) catenate on an electrode surface via S-Au interactions*. Comptes Rendus De L Academie Des Sciences Serie Ii Fascicule C-Chimie, 1999. **2**(1): p. 41-47.
- 7.8. I. Willner and B. Willner, *Layered molecular optoelectronic assemblies*. Journal of Materials Chemistry, 1998. **8**(12): p. 2543-2556.
- 7.9. L. Raehm, C. Hamann, J. M. Kern, and J. P. Sauvage, *Synthesis of copper(I) catenanes incorporating a disulfide bridge and their deposition on a gold surface*. Organic Letters, 2000. **2**(14): p. 1991-1994.
- 7.10. J. Liu, J. Alvarez, and A. E. Kaifer, *Metal nanoparticles with a knack for molecular recognition*. Advanced Materials, 2000. **12**(18): p. 1381-1383.
- 7.11. C. De Nadai, C. M. Whelan, C. Perollier, et al., *Self-assembly of mechanically interlocked and threaded rings: an HREELS and XPS study of thiol-functionalized canenane and rotaxane molecules on Au(111)*. Surface Science, 2000. **454**: p. 112-117.
- 7.12. D. Fitzmaurice, S. Nagaraja Rao, J. A. Preece, et al., *Heterosupramolecular chemistry: Programmed pseudorotaxane assembly at the surface of a nanocrystal*. Angewandte Chemie-International Edition, 1999. **38**(8): p. 1147-1150.

- 7.13. D. Ryan, S. Nagaraja Rao, H. Rensmo, et al., *Heterosupramolecular chemistry: Recognition initiated and inhibited silver nanocrystal aggregation by pseudorotaxane assembly*. Journal of the American Chemical Society, 2000. **122**(26): p. 6252-6257.
- 7.14. S. Y. Chia, J. G. Cao, J. F. Stoddart, and J. I. Zink, *Working supramolecular machines trapped in glass and mounted on a film surface*. Angewandte Chemie-International Edition, 2001. **40**(13): p. 2447.
- 7.15. A. L. Vance, T. M. Willey, T. van Buuren, et al., *XAS and XPS Characterization of Monolayers Derived from a Dithiol and Structurally Related Disulfide-Containing Polyamides*. Langmuir, 2002. **18**: p. 8123.
- 7.16. A. G. Kolchinski, N. W. Alcock, R. A. Roesner, and D. H. Busch, *Molecular riveting: High yield preparation of a [3]-rotaxane*. Chemical Communications, 1998. **17**(14): p. 1437-1438.
- 7.17. S. Frey, V. Stadler, K. Heister, et al., *Structure of thioaromatic self-assembled monolayers on gold and silver*. Langmuir, 2001. **17**(8): p. 2408-2415.
- 7.18. H. Ågren, O. Vahtras, and V. Carravetta, *Near-Edge Core Photoabsorption in Polyacenes - Model Molecules for Graphite*. Chemical Physics, 1995. **196**(1-2): p. 47-58.
- 7.19. D. G. Castner, K. Hinds, and D. W. Grainger, *X-ray photoelectron spectroscopy surface 2p study of organic thioc and disulfide binding interactions with gold surfaces*. Langmuir, 1996. **12**(21): p. 5083-5086.
- 7.20. Complete results are available in reference [6.1] and the supporting information associated with this reference, including detailed synthesis information, NMR results for synthesized molecules, and additional XPS and XAS spectra. This material is available at <http://pubs.acs.org>.

Chapter 8

A Functionalized, Surface-Attached Rotaxane

Introduction

The previous chapter showed methods for and provided evidence of a simple surface-attached rotaxane[8.1]. However, there is no chemically active site on this molecule. In this chapter, methods for chemically functionalizing this rotaxane in order to ultimately provide for conformational switching behavior are explored, and preliminary results are presented.

Previous chapters have presented ways in which chemical functionalities within molecules strongly affect structure, such as the dimerization in carboxyl groups, or the π -stacking in anthracene stopper molecules in the previous chapter. Going further, we now ask whether such simple interactions, as e.g. dimerization of carboxyl groups on neighboring molecule crown-ether rings could cause conformational changes within surface-attached rotaxanes. However, the synthesis of this particular type of rotaxane in the required amounts and purity has been difficult. Therefore, a similar option for rotaxane synthesis and switching is explored in this chapter.

In particular, the crown ether was synthesized [8.2] with an aldehyde attached to one of its aromatic groups (Fig. 8.1).

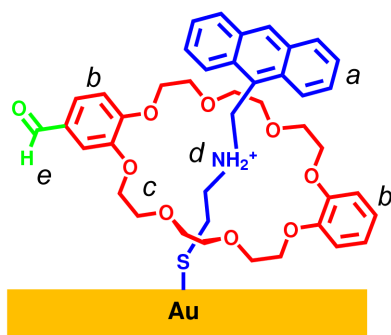


Fig. 8.1. The aldehyde functionalized crown ether within the surface-attached rotaxane investigated in this chapter.

The exposed carbonyl group (position *e*) will react with an amine via a Schiff base condensation reaction to yield an imine ($\text{C}=\text{N}$). To chemically change this rotaxane, exposure to aniline after surface attachment results in the extra aromatic ring as seen in Fig. 8.2, *f*.

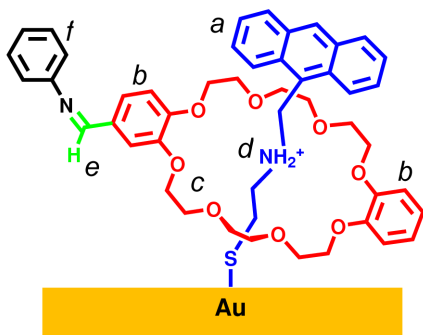


Fig. 8.2. The aldehyde functionalized rotaxane which has been exposed to and reacted with aniline.

Through the addition of this group, π interactions between molecules may induce chemically controllable conformational changes within the molecule, and this is what is now explored experimentally.

Experimental

Instrumentation

Spectra were acquired at the Advanced Light Source, at the Lawrence Berkeley National Laboratory, Beamline 8.0. This is a high-resolution, undulator beamline, with a small spot compared to beamline 8.2 at SSRL used in experiments in previous Chapters. Thus, organic monolayers degrade rapidly, and great care was taken to minimize damage to samples. Slits were closed to their mechanical limit, which is estimated to be a few microns. The beam was baffled w/ horizontal doors until higher harmonic parabolas were no longer visible on a phosphor coated screen, currently located just upstream from the exit slit of the monochromator. The beam was also vertically baffled to 50% intensity. The undulator was carefully calibrated for smooth operation to match its harmonic with the monochromator during scans to minimize noise in both the incident photon flux measured on a gold transmissive grid, and the sample current. Samples were cooled to liquid nitrogen temperatures (77 K), and moved to nearly the mechanical limit of the manipulator in the back of the chamber to take the sample out of focus for lower beam power per unit area. Although these precautions result in minimal radiation damage, care was taken to translate the sample to an unexposed position for all absorption scans presented. Scans repeated on the same spots were also compared to fresh areas to ensure minimal damage. Although some changes were occurring, they were not significant enough to indicate that damage was an issue with scans on pristine portions of the sample.

Sample synthesis and preparation

Samples were synthesized by B. Hart and A. Vance at the Lawrence Livermore National Laboratory by first preparing the aldehyde functionalized crown ether ring, and then preparing [3]-rotaxanes[8.3]. The molecules were dissolved in acetonitrile to $10\ \mu\text{mol}$. Initial indications from NEXAFS and XPS on the first few samples were that the anthracene stopper portion was preferentially adsorbing on the surface, due to a very small concentration of remaining fragments in the formation solution and its higher rate of adsorption. This was rectified by exposing about $2\ \text{cm}^2$ gold to 20 ml of the solution for 5 minutes, removing and discarding this primarily anthracene stopper coated substrate, and then exposing an additional gold-coated wafer into the same, “purified” solution. This produced films which exhibited slightly higher surface concentrations of rotaxanes than films from the previous chapter. Solution exposure time was at room temperature for 18-24 hours. Longer exposure time (48 hours and above) seemed to deposit greater than monolayer coverages of molecules on the surface, and is an issue that needs to be investigated further and may be a function of temperature, concentration, or other parameters.

After deposition of the rotaxanes, which occurred in the same solution under the same conditions (e.g. temperature) one aldehyde functionalized rotaxane was rinsed in acetonitrile while the second was removed from the formation solution, rinsed in clean acetonitrile, and placed in 10 mmol aniline in EtOH for approximately 4 hours. This aniline-exposed, aldehyde-functionalized sample was then rinsed in pure EtOH. After subsequent film formation and/or functionalization, both rotaxanes were only

exposed to air long enough to mount them on the same sample block for transfer into the analysis chamber at UHV.

Experimental Results

Carbon absorption scans for these rotaxanes were similar in overall shape to those of the rotaxane in the previous chapter. This is not unexpected as the aldehyde adds one carbon atom to the 41 existing carbon atoms in the rotaxane of the previous chapter, while the aldehyde-aniline functionalization adds 7. So, *at most* these new will contribute 2-14% of the overall intensity in the carbon spectra.

For the aldehyde-functionalized rotaxane (Fig. 8.1), a close up of the near-edge region is presented in Fig. 8.3. Three distinct peaks appear in the pre-edge region: the outer two (284.6 and 286.0 eV) are due to the anthracene unit (Fig. 8.1, *a*) at the end of the stopper molecule, while the central peak(s) (285.1 – 285.4 eV) and another chemically shifted one (287.3 eV) are due to the aromatics on either end of the crown-ether (Fig. 8.1, *b*). For this ALS data, which can be obtained at higher-resolution than our previous SSRL work, one also sees a splitting in the central peak. The outer anthracene peaks show polarization dependence, being slightly more intense at normal incidence than grazing. This indicates that the normal to the anthracene plane is statistically more than 54 degrees from normal, suggesting anthracene units that are statistically upright. Little or no polarization dependence appears in the central peak, while the chemically shifted crown-ether peak shows a very slight polarization dependence. The crown-ether aromatics have higher intensity at grazing incidence indicating a slightly more prostrate than upright orientation with respect to the surface.

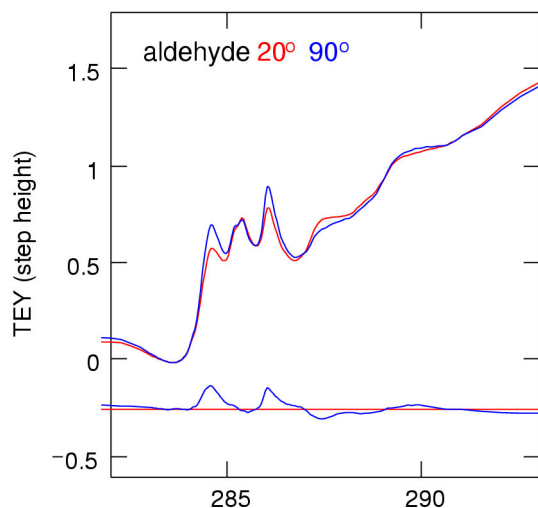


Fig. 8.3. Carbon K-edge close-up from the aldehyde functionalized rotaxane. Anthracene peaks show polarization dependence.

For the aniline-exposed, aldehyde functionalized rotaxane (Fig. 8.2) the carbon near-edge region is presented in Fig. 8.4. The central pre-edge feature is 25% more intense than the unexposed samples, indicating a significant portion of the aldehyde has reacted with the aniline. Additional intensity appears in a polarization dependent peak at 286.9eV, attributed to aniline as it appears in essentially the same position as a peak in samples with excess aniline (Fig. 8.2, *f*). Polarization dependencies are different than the previous sample. Anthracene peaks have slightly less polarization dependence, while a dichroism appears in the central peak. These two peaks are strongest at normal incidence, indicating a slightly more upright orientation of the aromatics within the ring.

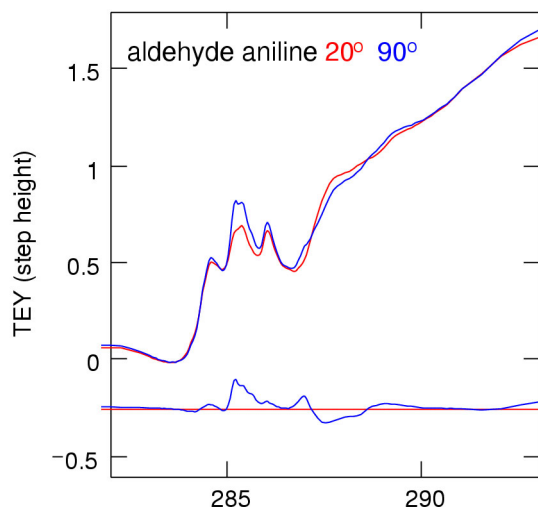


Fig. 8.4. C K-edge spectra of the Near-edge region for the aniline-exposed, aldehyde functionalized surface-attached rotaxane; crown peaks show polarization dependence.

Discussion

The preliminary absorption measurement intensities presented in this study are consistent with the deposition of molecular monolayers. Based on the relative intensities of the pre-edge features and in comparison to results from the previous chapter, an estimated 40-50% of the stopper molecules have a crown ether ring present on the surface.

In the first case, the aldehyde-functionalized rotaxane shows small polarization dependence with anthracene units (position *a*) statistically more upright than the magic angle. This could be a real effect, but could also be due to a higher concentration of anthracene stoppers on the surface, which have been shown to order in an upright manner when deposited without crown ether rings in the previous chapter. In any case, both samples presented here were prepared under the same conditions and have similar relative concentrations of surface-bound rotaxanes and non-rotaxane anthracene

stoppers. Simple energy minimization calculations show the crown ether ring (position *c*) to be in a cup-like shape or an s-like shape with the aromatics (position *b*) on each end[8.3]; this complicates measurement of the conformation of the ring as the aromatics may not lie in the same plane.

In the second case, the aldehyde unit has been exposed to and reacted with aniline in order to attach another phenyl group to an end of the crown ether. The aniline phenyl ring (Fig. 8.2, position *f*) states contribute slightly to the central feature, and a new peak also appears. The ring portion now shows a polarization dependence, but one with highest intensity at normal incidence. This indicates phenyl rings have statistically a more upright orientation. The anthracene units on the stopper portion of the molecules show less polarization dependence indicating a greater tilt towards the surface or at least a more random distribution of orientations. This could be due to interactions between the conjugated π system with the aniline phenyl group, the nitrogen-carbon double bond, and one phenyl ring of the crown ether (Fig. 8.2, positions *b,e,f*) with anthracene portions of molecules (Fig. 8.2, position *a*). This would both pull the anthracene units towards the surface plane and pull the π -conjugated portion of the crown ether upwards. Unfortunately, nitrogen absorption from this system (Fig. 8.2, *e*) are currently inconclusive in this regard, partly due to spectral convolution with the amide group in the backbone of the stopper (Fig. 8.2, *d*).

Further experiments are underway as of the submittal of this dissertation, aimed at determining deposition conditions which consistently lead to molecular monolayers well-bound to the surface.

Conclusions

Aldehyde-functionalized, surface attached rotaxanes have been successfully synthesized and deposited on surfaces. NEXAFS reveals conformational changes when the aldehyde is exposed to aniline, which may show a change in orientation in both the anthracene plane and crown ether orientations. These results demonstrate the feasibility of measuring conformational changes in complex, surface-attached interlocking molecules.

References

- 8.1. A. L. Vance, T. M. Willey, T. van Buuren, et al., *XAS and XPS characterization of a surface-attached rotaxane*. Nano Letters, 2003. **3**(1): p. 81-84.
- 8.2. The synthesis was accomplished by Andy Vance and Brad Hart of Lawrence Livermore National Laboratory, Chemistry and Materials Science Directorate.
- 8.3. A. G. Kolchinski, N. W. Alcock, R. A. Roesner, and D. H. Busch, Chem. Commun., 1998. **17**: p. 1437.

Chapter 9

Conclusions and Outlook

Conclusions

Self-assembled monolayers and surface-attached interlocking molecules are of high current interest for future applications in sensors, molecular electronics, and other devices. However, many questions remain concerning the chemical and molecular structure of SAMs, both immediately after various preparation steps and upon longer exposure to various environments. We have thus quantitatively investigated several SAMs using NEXAFS, XPS, and infrared spectroscopy.

The simplest method for accomplishing surface-attached molecules is through a thiol or disulfide exposed to gold. Although this is the most convenient method for chemical/biological functionalization, these SAMs are not stable in air. Thiolates oxidize readily, and care must be taken to ensure binding and lifetime sufficient for the application. Our results show that simply placing samples in a vial slows the oxidation of the thiolate; these data are consistent with previous results indicating ambient ozone is responsible for the degradation. Alternate methods for preparing SAMs (such as a siloxane attachment to Si or direct carbon silicon bonding) may be the answer for more robust and biologically compatible SAMs, and these options will be further explored in the future.

We also find that carboxyl terminations affect SAM structure. Care must be taken to break carboxyl group dimerizations within initial formation solutions and to ensure the groups remain protonated; otherwise, more-than-monolayer, disordered films form. In particular, adding acetic acid to the formation solutions allows for consistent formation of well-ordered, long-chain, carboxyl-terminated monolayers. The controversy in the literature over the past few years has further been resolved by showing that with acetic acid, alkyl-group interactions are strong enough to form well ordered chains, with NEXAFS obtained tilt angles only slightly larger than with similarly long alkanethiols. These well-ordered carboxyl-terminated SAMs have tilted over endgroups due to hydrogen bonding between neighboring molecules.

Thioctic acid, with a large disulfide containing base and short alkyl-chain which isolates the carboxyl group from strong chain-chain interactions, exhibits a similar tilting of endgroups from hydrogen dimerization. The remaining thioctic acid molecules are also oriented statistically upright. This confirmed recipe for formation of well-ordered monolayers improves consistency in SAMs for use in chemical- and biosensor applications, and may lead to more robust systems due to the added stability of the disulfide precursor vs. a thiol, and greater bonding strength from the additional gold-sulfur bond in each molecule. The strong hydrogen bonding within the functional groups may also impact surface-functionalization performance.

Both carboxyl-terminated monolayers show a strong reorientation – a chemically induced conformational switching – when rinsed in alkali solutions. The carboxylate end group is oriented upright, and in the thioctic case, induces the rest of the molecule to have a more upright orientation. Simple nanomechanical systems such

as these could eventually be utilized in creating molecular scale devices. This chemically induced nanomechanical switching is reversible, but the harsh alkali environment tends to degrade the films with repeated rinsing.

One potential method for creating surface-attached catenanes with both ends of the backbone molecule attached to the surface has been outlined. In a simple case with a dithiol and its structurally related disulfide-containing polyamide, only the polyamide formed the intended surface-attached loops. The dithiol, on the other hand, adsorbed to the surface through a single thiol. A strategy for the formation of surface-attached interlocking molecules may be to form a disulfide-containing polymer precursor before forming spontaneous monolayers.

A simple surface-attached rotaxane has been formed and characterized with NEXAFS for the first time to our knowledge. The molecule requires an analogous strategy as above. This rotaxane consisted of an anthracene stopper, and an amide-containing thiol-terminated axle for attachment to the surface and immobilization of the second component, a crown ether ring. Although when mixed in solution with excess crown ether over 90% of the stopper molecules have a ring present, the bare stopper molecules overwhelmingly adsorb onto the surface. In order to create the intended surface-attached rotaxane, the synthesis must include a “molecular riveting” step to form a precursor molecule with two rings locked into place by two anthracene stopper molecules. Two pseudorotaxane molecules have two thiols that oxidize to form a disulfide. This product now forms surface-attached rotaxane as the crown ether rings are present and locked within the molecule as the disulfide reacts with and adsorbs on

the gold. Additionally, anthracene stopper molecules showed a high degree of polarization dependence, even with a large fraction of unbound thiol.

Both ideas of simple functionalization for conformational switching (as exhibited in the carboxyl terminated SAMs) and the π -stacking in the anthracene stopper units led to the synthesis of a surface-attached rotaxane with switchability through a simple functionalization on its crown ether ring. An aldehyde-functionalized crown ether ring on a surface-attached rotaxane shows similar structure and features as its unfunctionalized counterpart. In this ongoing work, when exposed to aniline, the morphology changes with a slightly more upright orientation of the crown ether aromatics, presumably due to ring-stopper interactions or ring-ring interactions between neighboring molecules.

Outlook

Near-future work includes continuing on the possibility of conformational changes using carboxyl-functionalized, surface-attached rotaxanes(Fig. 9.1) and catenanes(Fig. 9.2). These molecules could be a model system and a precursor to nano-mechanical or molecular electronic devices that depend on conformational switching in interlocking molecules. NEXAFS will continue to be a critical tool in determining the orientation of components within these and other more complex molecular monolayers.

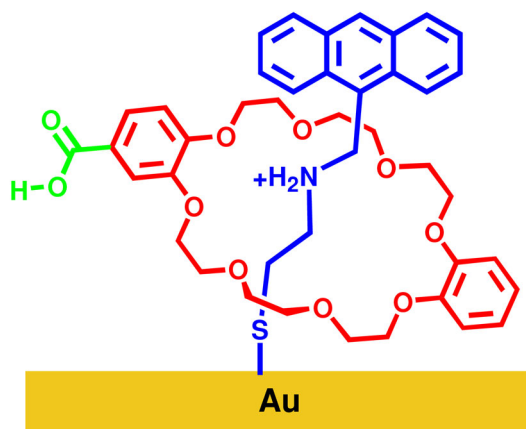


Fig. 9.1. Potential functionalized rotaxane under development.

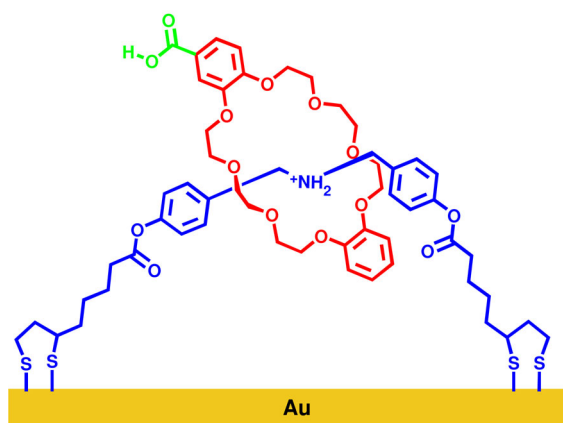


Fig. 9.2. Potential carboxyl-functionalized catenane currently under development.

Alkanethiols on gold will not be suitable or sufficiently stable for many atmospheric or biological environments, therefore we currently are working on forming well-formed monolayers on silicon as depicted in Fig. 9.3. The left depicts siloxane SAMs on silicon oxide, while the right shows a method in which a hydrogen-terminated silicon surface exposed to alkenes and ultraviolet light reacts to form an organic layer

Summary

In summary, we have exposed several new aspects of the chemistry, structure, and stability of some SAMs and surface-attached interlocking molecules that show great promise for future applications. Science and technology of molecular monolayers develop chemically- and biologically- functionalized surfaces, nanomechanical molecular systems for molecular electronics, and certainly other soon-to-be-discovered nanotechnological applications. Often, conformational switching or changes in nanoscopic molecular structure are an integral part of proposed device functionality. The combination of NEXAFS and XPS represents a powerful approach for future studies of these interesting molecular nanostructures by quantitatively and directly measuring chemical composition and molecular orientation.

References

- 9.1. J. M. Buriak, M. P. Stewart, T. W. Geders, et al., *Lewis Acid Mediated Hydrosilylation on Porous Silicon Surfaces*. Journal of the American Chemical Society, 1999. **121**: p. 11491-11502.
- 9.2. S. E. Letant, B. R. Hart, T. van Buuren, and L. J. Terminello, *Functionalized silicon membranes for selective bio-organism capture*. Nature Materials, 2003. **2**: p. 391-395.